Analysis of GNSS raw observations

in PPP solutions

TECHNISCHE
UNIVERSITÄT
DARMSTADT

Erik Schönemann

Analysis of GNSS raw observations in PPP solutions

Analysis of GNSS raw observations in PPP solutions

Vom Fachbereich Bau- und Umweltingenieurwissenschaften
der Technischen Universität Darmstadt
zur Erlangung des akademischen Grades eines
Doktor-Ingenieurs (Dr.-Ing.) genehmigte Dissertation

vorgelegt von
Dipl.-Ing. Erik Schönemann
aus Darmstadt

Referent:	Prof. Dr.-Ing. Matthias Becker
Korreferent:	Prof. Dr.-Ing. Werner Enderle
Tag der Einreichung:	28. Oktober 2013
Tag der mündlichen Prüfung:	14. Januar 2014

Darmstadt, April 2014
D17

Abstract

Global navigation satellite systems (GNSS) are an essential component in many areas of our daily life. They find application in diverse fields of private, commercial and scientific activities and are employed to meet the needs of police and military. Their fundamental importance for industrial countries is not the least the triggering point for the continuing modernisation of the existing and the development of new systems. The global satellite navigation systems are supplemented by regional satellite navigation systems (RNSS) and satellite based augmentation systems (SBAS). The diversity of systems, applied signal modulations and carrier frequencies, in particular in their combination, provide a broad range of opportunities along with new challenges.

The work presented herein focuses on the use of satellite navigation systems for precise positioning and timing applications and scientific analysis. For best and comprehensive results, an equivalent combination of all available systems and signals is a fundamental requirement. For these reasons, relative approaches based on observation differences are rather inappropriate. Hence, this thesis focuses primarily on the method of precise point positioning (PPP) by waiving linear combinations. The objective is the development of a universal PPP analysis approach for standalone PPP and network solutions. Raw observations conserve the physical properties of original observation. This allows a detailed analysis of individual signal characteristics, but leads to the necessity of handling them. The utilisation of raw observations comes along with maximum flexibility. It allows for the application of physical error models as well as individual weighting and edition of all individual observation types. The possibility of a joint processing of all observations and the estimation of all parameters in a single run results in a significant simplification of the processing procedure.

The first part of the thesis provides a general introduction to conventional GNSS analysis and highlights the limitations thereof. The second part introduces the technique of raw observations processing. It highlights the differences from the common ionosphere free processing approach and discusses the challenges. The concept presented for the analysis of GNSS raw observations is flexible and adjustable to any kind of GNSS application. This flexibility is attributed to a variety of different possible interpretations of the raw observation equation. In the frame of this thesis, a selection of different interpretations is introduced and demonstrated. One of the most important parameters for the analysis of raw observations is the so-called uncalibrated signal delays. The work presented exemplarily demonstrates their characteristics and discusses their implications for the analysis.

For maximum stability of the results, it is common practice to resolve and apply integer carrier phase ambiguities. The presented work discusses and demonstrates the feasibility of this methodology for the implemented approach. It shows that the new approach simplifies the resolution of inter-GNSS carrier phase ambiguities and extends the spectrum of resolvable ambiguities.

It is demonstrated that the proposed concept provides an "at least" equivalent alternative to the common processing strategies, applicable for highly precise standalone, as well as network PPP solutions, allowing for the simplified, consistent processing of different numbers of observation, suitable for an optimal, flexible, equivalent, joint processing of arbitrary GNSS observation types. It introduces a new dimension of analysis, with direct access to all individual observations and parameters.

Zusammenfassung

Globale Satellitennavigationssysteme (GNSS) sind ein wesentlicher Bestandteil in vielen Bereichen des täglichen Lebens. Sie finden Anwendung im privaten, gewerblichen und wissenschaftlichen Bereich und dienen zur Erfüllung von polizeilichen und militärischen Aufgaben. Ihre grundlegende Bedeutung für Industrieländer war nicht zuletzt der Auslöser für die vorlaufende Modernisierung der bestehenden und die Entwicklung neuer Systeme. Ergänzt werden die globalen Satellitennavigationssysteme durch regionale Satellitennavigationssysteme (RNSS) und satellitengestützte Erweiterungssysteme (SBAS). Die Vielfalt der Systeme, der angewendeten Signalmodulationen und Trägerfrequenzen, nicht zuletzt auch deren Kombination birgt eine Vielzahl neuer Möglichkeiten und damit verbunden neue Herausforderungen.

Die vorliegende Arbeit konzentriert sich auf die Verwendung von Satellitennavigationssystemen für präzise Positionierungs- und Zeitmessungsanwendungen, sowie für wissenschaftliche Analysen. Eine grundlegende Voraussetzung für optimale und umfassende Ergebnisse ist eine gleichwertige Kombination aller verfügbaren Systeme und Signale. In Anbetracht der Zielsetzung sind relative, auf Beobachtungsdifferenzen basierende Ansätze eher ungeeignet. Aus diesem Grund befasst sich die vorliegende Arbeit in erster Linie mit der Methode der präzisen Punktbestimmung (PPP), allerdings unter dem vollständigen Verzicht auf Linearkombinationen. Die Zielsetzung ist die Entwicklung eines universell einsetzbaren, präzisen Punktbestimmungsansatzes für Einzelpunkt- und Netzwerkanalysen. Die Verwendung von Rohbeobachtungen (raw) hat den Vorteil, dass sie die wahren physikalischen Eigenschaften der Beobachtungen erhält. Dies ermöglicht eine detaillierte Untersuchung aller einzelnen Signaleigenschaften, allerdings mit der Konsequenz, dass diese behandelt werden müssen. Die Verwendung von Rohbeobachtungen macht den Ansatz sehr flexibel. Der Ansatz ermöglicht die Verwendung von physikalischen Modellen und erlaubt eine beobachtungstypbezogene Gewichtung und Bearbeitung. Die gemeinsame Auswertung alle Beobachtungen und die Schätzung aller Parameter in einem Prozess führt zu einer deutlichen Vereinfachung der Verarbeitungsabläufe.

Der erste Teil der Arbeit führt allgemein in die Thematik der GNSS-Analyse ein und hebt die Beschränkungen der herkömmlichen Analyseansätze hervor. Die Technik der Rohdatenverarbeitung wird im zweiten Teil der Arbeit behandelt. Hierbei werden die Unterschiede zu dem gängigen ionosphärenfreien Ansatz dargelegt und die Herausforderungen der Rohdatenverarbeitung diskutiert. Das präsentierte Konzept ist flexibel auf jegliche GNSS-Anwendung anpassbar. Diese Flexibilität basiert auf der Vielzahl an Interpretationsmöglichkeiten der Beobachtungsgleichung. Einer der wichtigsten Parameter für die Auswertung von Rohbeobachtungen sind die sogenannten unkalibrierten Signalverzögerungen. Die vorliegende Arbeit zeigt beispielhaft deren Eigenschaften und diskutiert die Auswirkungen auf die Analyse.

Für eine maximal Stabilität der Ergebnisse ist es gängig, die ganzzahligen Trägerphasenmehrdeutigkeiten zu lösen und in der Lösung zu verwenden. Die vorliegende Arbeit diskutiert und demonstriert die Umsetzbarkeit dieser Methodik für den implementierten Ansatz. Es zeigt sich, dass der neue Ansatz die Auflösung von Trägerphasenmehrdeutigkeiten zwischen GNSS deutlich vereinfacht und das Spektrum der lösbaren Mehrdeutigkeiten erweitert.

Das vorgeschlagene Konzept bietet eine zumindest gleichwertige Alternative zu den herkömmlichen Strategien. Es ist sowohl für hochgenaue Einzelpunktpositionierungen wie auch für Netzwerk-PPP-Lösungen einsetzbar. Weiterhin ermöglicht es eine vereinfachte, konsistente Verarbeitung einer beliebigen Anzahl an Beobachtungen und ist geeignet, um beliebige Beobachtungstypen flexibel und gleichwertig in einem einzigen Durchlauf zu verarbeiten. Damit führt der Ansatz eine neue Dimension der GNSS-Auswertungen mit einem direkten Zugang zu allen individuellen Beobachtungen und Parametern ein.

Contents

1 Introduction

Global Navigation Satellite Systems (GNSS) have become an integral part of daily life. The areas of application range from simple navigation applications with accuracy requirements of several metres and applications that require the best possible integrity, to applications with need for highest accuracy. The increasing importance of GNSS in all fields of applications triggered not only the refurbishment of operational GNSS, as in the Global Positioning System (GPS) and the Global Navigation Satellite System (GLONASS), but also the development of new GNSS, such as Galileo (Galileo), the BeiDou Navigation System (BeiDou) and the Indian Global Navigational Satellite System (IGNSS). GNSS can be augmented by Satellite Based Augmentation Systems (SBASs) like the Wide Area Augmentation System (WAAS), the Multi-Functional Satellite Augmentation System (MSAS) and the European Geostationary Navigation Overlay Service (EGNOS). Moreover, GNSS can be supplemented by Regional Navigation Satellite Systems (RNSS). There are different existing and new upcoming RNSS, such as the Indian Regional Navigation Satellite System (IRNSS) and the Quasi-Zenith Satellite System (QZSS). Overall, multiplicities of applicable satellite navigation systems apply different signal modulations via a variety of carrier frequencies.

This thesis focuses on the use of satellite navigation systems for precise positioning and timing applications and scientific analysis. It is a fact that the highest accuracy requires as many independent observations as possible. Furthermore, with regard to universal signal analyses, which demands the highest accuracy, a joint and equivalent treatment of all available signals, irrespective their system, is indispensable. The heterogeneity of satellite navigation systems offers great potential to uncover and analyse system-specific systematics but, at the same time, it requires an exact knowledge and a proper handling of these. The restriction to GPS dual-frequency observations of the most up-to-date processing setups does not take these effects into consideration. For this reason, the characteristics of these effects are mostly unknown. Thus, one of the greatest challenges for the future is the characterisation and proper handling of all these effects and biases, in order to allow for an optimal combination of all signals.

The complexity of this topic is one of the reasons that most up-to-date GNSS analyses maintain the well-known processing strategies, which were intentionally developed for dual-frequency GPS observations. Thus, it is still common practice to form linear combinations (LCs) or observation differences for bias mitigation. In fact, these techniques work satisfactorily for a well-defined environment with only two signals. However, as soon as further signals come into play, the situation becomes increasingly complicated. The most prominent example of such complications is the misleadingly called intersystem biases (ISBs). ISBs are commonly used to absorb the receiver-dependent differences between GPS and GLONASS observations. In fact, in contrast to their nomenclature, ISBs are not used to account for intersystem biases. Instead, ISBs are required to absorb the receiver-dependent inter-signal biases. Consequently, the application of ISBs becomes necessary whenever two different observation types with different biases are combined, as also in the case of a third GPS (L5) observation. Moreover, the application of ISBs, at least formally, divides the systems into master and auxiliary systems. Further disadvantages of the utilisation of LC observations are the increased noise, the missing flexibility in terms of signal handling and the loss of the physical observation characteristics. The points raised motivated the development of a new approach to overcome these limitations. The new approach is intended to allow for the joint, equivalent processing of arbitrary GNSS observations and therewith opening of new avenues for detailed analyses of all individual signal components and their characteristics.

To attain these objectives, it is necessary to preserve the true physical characteristics of the measurements in their original magnitude and shape. It is clear that this is only achievable with original (raw) observations. Consequently, relative positioning techniques that make use of double-difference (DD) observations are not an option. The most natural approach for this purpose is precise point positioning (PPP) (Zumberge et al., 1997; Héroux and Kouba, 2001). Commonly, PPP implementations apply ionosphere-free LC observations in order to mitigate the first-order effect of the ionosphere. Admittedly, this practice prevents direct access to the physical observation characteristics. An alternative method, which is the only way to conserve the characteristics of the raw observations, is the estimation of slant total electron content (STEC) parameters (Odijk, 2002). This principle is also adopted in the processing approach presented by Schönemann et al. (2011) and by Li et al. (2013).

The challenge for original (raw) observation-based approaches is the elimination of the rank defect of the normal equation matrix. To this end, Li et al. (2013) applied different ionospheric constraints from external models, as well as temporal and spatial constraints, whereas Schönemann et al. (2011) concentrated on the clock definition, represented by the respective uncalibrated code delays (UCDs). The approach presented in this thesis aims to

provide a basis for a comprehensive GNSS analysis, completely renouncing linear combinations. In contrast, Li et al. (2013) concentrated on the estimation of uncalibrated phase delays (UPDs), requiring a detour via narrow-lane ambiguity fixing, assuming all other parameters to be well known (station coordinates, satellite orbits and clocks are fixed). However, particularly for network PPP solutions estimating the complete set of parameters, the processing of raw observations offers vast potential.

1.1 Objectives of the research

The aim of the research presented in this thesis is the development of a universal PPP analysis approach, applicable for standalone and network PPP solutions. The development aims to allow a joint, equivalent analysis of arbitrary types of GNSS observations, regardless of their number, system, modulation or frequency. One essential point for a comprehensive analysis of all biases is the conservation of the original physical observation characteristics. The joint processing of all observations in their original (raw) form, allowing a free adjustment between all parameters and observations, is vital in order to ensure the comparability of the analysis results.

The development and parameterisation of the analysis approach requires at least a basic knowledge regarding the expected bias characteristics. For that reason, a crucial point of the presented research is the analysis of the most relevant bias characteristics.

The requirements of the new analysis approach can be summarised as follows:

- Development of a processing scheme applicable for standalone and global network PPP solutions.
- Unified treatment and joint processing of arbitrary GNSS observations.
- Processing and estimation of all observations and parameters in a single step.
- Capability to allow a separate weighting of all individual signal components.
- Conservation of physical observation characteristics.

1.2 External reference solutions

It is common practice to validate newly-implemented processing schemes against external reference solutions. Different commercial and scientific products are available for the comparison of local and global GNSS products. In fact, highly accurate scientific solutions are often the reference of choice for satellite orbits, clocks and earth rotation parameters. As is well known, numerous scientific nonprofit organisations, such as the International Earth Rotation and Reference Systems Service (IERS), the International DORIS Service (IDS), the International Laser Ranging Service (ILRS) and the International GNSS Service (IGS) generate global reference solutions on a routine basis. In most cases, in addition to the final products, the raw observations are also made available free of charge. The most important service in the frame of this thesis is the IGS, covering all areas of GNSS processing and the IERS, providing data on Earth orientation and a detailed description of conventional models, constants and standards.

1.2.1 The International Earth Rotation and Reference Systems Service

The International Earth Rotation and Reference Systems Service (IERS) (IERS, 2013; Boucher et al., 1988) was set up to fulfil the need for celestial and terrestrial reference frames for Earth orientation monitoring. It was established by the International Astronomical Union and the International Union of Geodesy and Geophysics as the International Earth Rotation Service in 1987. The IERS started operations on the 1st January 1988. In 2003, its name was expanded to the International Earth Rotation and Reference Systems Service. The IERS consists of different components like technique centres, product centres, International Terrestrial Reference System (ITRS) combination centres, research centres, analysis coordinator, the central bureau, the board of directors and different working groups. Numerous organisations contribute to the IERS, either directly or indirectly, via different, autonomous, independent services. One example is the IGS, which will be described next. It cooperates with the IERS in the form of a technique centre.

The IERS provides different products, such as:

- Earth orientation data.
- IERS conventions.
- International Celestial Reference Frame (ICRF).
- International Celestial Reference System (ICRS).
- International Terrestrial Reference Frame (ITRF).
- International Terrestrial Reference System (ITRS).
- Geophysical fluids data.

The most relevant products for this thesis are the earth rotation parameters (polar motion, universal time, precession/nutation) and the IERS conventions. The IERS conventions describe the conventional models, constants and standards and define the standard reference systems (Petit and Luzum, 2010). For a detailed description of services and products, refer to IERS (2013).

1.2.2 The International GNSS Service

The International GNSS Service (IGS) is a joint international activity, involving more than 200 participating organisations in over 80 countries. It was initiated in order to understand GPS and to make it applicable to earth sciences. Another objective of the IGS was the generation of precise GPS satellite orbits, clocks and additional by-products, such as the earth rotation parameter (ERP) (Mueller, 1993). The initiative started with a test campaign in 1992, which was followed by a pilot project, bridging the time from the test campaign until the official start of the service on the 1st of January 1994 (Beutler et al., 1999). The standardisation of equipment, site selection and preparation, data handling and analyses is a fundamental requirement for the scientific use of GPS products. The objective of the IGS has not changed significantly up to the present day. According to the 2008 - 2012 IGS Strategic Plan (IGS, 2008), the first long-term goal of the IGS is to serve "as the premier source of the highest-quality GNSS data, products and related standards and conventions, openly available to all user communities". IGS products, such as GPS orbit and clock solutions, serve as the de facto world standard for high-precision GNSS applications (IGS, 2008). A selection of the available IGS products is presented in table 1.1. This shows the different IGS orbit and clock products and their accuracy (IGS, 2014). The orbit accuracies are expressed by 1D mean rms values for comparison against independent satellite orbits, based on Satellite Laser Ranging (SLR). Note, the clock rms does not consider instrumental delays.

Products		Accuracy	Latency	Updates	Sampling Interval
Broadcast	orbits	$\approx 100\,cm$	real time	–	daily
	sat. clocks	$\approx 5\,ns$ rms $\approx 2.5\,ns$ std			
Ultra-Rapid (pred.)	orbits	$\approx 5\,cm$	real time	at 03, 09, 15, 21 UTC	$15\,min$
	sat. clocks	$\approx 3\,ns$ rms $\approx 1.5\,ns$ std			
Ultra-Rapid (obs.)	orbits	$\approx 3\,cm$	3 - 9 h	at 03, 09, 15, 21 UTC	$15\,min$
	sat. clocks	$\approx 150\,ps$ rms $\approx 50\,ps$ std			
Rapid	orbits	$\approx 2.5\,cm$	17 - 41 h	at 17 UTC daily	$15\,min$
	sat. + stat. clocks	$\approx 75\,ps$ rms $\approx 25\,ps$ std			$5\,min$
Final	orbits	$\approx 2.5\,cm$	12 - 18 days	every Thursday	$15\,min$
	sat. clocks	$\approx 75\,ps$ rms $\approx 20\,ps$ std			sat.: $30\,s$ stat.: $5\,min$

Table 1.1: Extract from the full IGS product list (IGS, 2014).

In addition to the actual products, the IGS defines and provides standards for GNSS-related file formats and processing strategies (Kouba, 2009). Furthermore, it freely makes available GNSS observation data from hundreds of globally distributed GNSS tracking stations (IGS, 2013). The IGS has established several working groups (antenna, bias and calibration, data centre, etc.) and pilot projects (IGS Multi-GNSS Experiment (MGEX), etc.) in order to be in line with the ongoing changes in the GNSS environment and to further develop and improve the standards and products, thus ultimately maintaining its role as the world leader. One example is the antenna working group, which coordinates the IGS research activities in the field of GNSS receiver and satellite antenna phase centre characterisation and maintains the official IGS antenna file (Schmidt, 2013). The knowledge gained and the outcomes of these working groups are an indispensable part of high accuracy GNSS analyses. From the perspective of this thesis, the MGEX (Rizos et al., 2013) is the most important pilot project. MGEX provides and analyses multi-GNSS, multi-signal, multi-frequency observation data from a set of globally distributed tracking stations. The observation data provided by MGEX not only includes data from native IGS stations, fulfilling the IGS requirements for tracking stations, but also from experimental stations, providing occasional data of variable quality. However, for the task of this thesis, the data is fully sufficient.

1.3 Outline of this thesis

This thesis consists of eight chapters. The individual chapters are outlined as follows:

- Chapter 2 provides a general description of the principles of global positioning satellite systems, as well as the required geodetic reference systems and timescales.

- Chapter 3 outlines the conventional analysis of GNSS observations. It describes the general observation equation and the common strategy for its solution. This chapter introduces the required physical models and introduces the common strategy of ambiguity resolutions.

- Chapter 4 introduces the analysis of raw observations. It highlights the differences from the common processing strategies and the resulting challenges thereof. The major challenge is the removal of matrix rank defects resulting from the correlations of the unknown parameters. It discusses the sources of the matrix singularities and outlines different solution approaches.

- Chapter 5 explains the implementation of the raw observation processing approach and outlines the applied processing strategy.

- Chapter 6 analyses and discusses the sources and the impact of receiver-sited, uncalibrated signal delays for the processing of raw observations and the implications for possible ambiguity resolution procedures.

- Chapter 7 demonstrates the applicability of the proposed approach for standalone and network PPP solutions. It gives a first insight into the analysis capabilities of the implementation and demonstrates the applicability of raw observation DD for ambiguity resolution.

- Chapter 8 concludes the thesis. It summarises the findings and provides certain recommendations for future research.

2 Principles of Global Navigation Satellite Systems

This chapter provides an overview of up-to-date GNSS and the processing of GNSS observations. In order to account for the variety of operational and upcoming GNSS, the description waives the description of individual systems and concentrates instead on a general overview of the basics of GNSS and the processing of GNSS observations. Special focus is given to the models and equations, which are of particular importance for this thesis. As this thesis concentrates on the processing of raw observations, relative approaches are not considered. Instead, the introduction focuses on the PPP related models and techniques. A comprehensive description of GNSS and their processing can be found in Hofmann-Wellenhof et al. (2008); Kaplan (2005); Misra and Enge (2006).

2.1 General architecture

Global Navigation Satellite Systems (GNSS) consist of a ground, a space and a user segment.

2.1.1 Ground segment

The main responsibilities of a GNSS ground segment are mission and satellite control (Galileo, 2002). Satellite control, or constellation management, consists of the monitoring and control of the satellite constellation. Mission control denotes the global control of core functions of the navigation mission. This includes orbit determination, clock synchronisation and the broadcasting of orbits, clock corrections and for individual GNSS integrity information. GNSS ground segments consist of a control centre and a network of globally distributed sensor and uplink stations.

2.1.2 Space segment

GNSS space segments are usually formed by 24 - 30 Medium Earth Orbits (MEOs) satellites. BeiDou extends the constellation with five geostationary High Earth Orbit (HEO) satellites. The GNSS satellites are distributed over different orbital planes, six in the case of GPS and three for GLONASS and Galileo. In addition to the number of orbital planes, the inclination ($55° - 64°8'$), the satellite altitude and the period of revolution also varies among the different GNSS.

However, more relevant to the research presented in this thesis is the performance of the different satellites and, the signal performance in particular. In fact, different satellite types for the GPS, such as Block IIA, Block IIR, Block IIR-M and Block IIF are active and further types, like the Block IIIA, are in preparation. The situation becomes even more complicated when considering all active and upcoming GNSS. It is well known that at least every satellite type, and in some cases even individual satellites, show their own characteristics. For this reason, it is not expedient to discuss the structure of individual satellite types. Figure 2.1 exemplarily explains the different components, based on the payload implemented in the first Galileo In Orbit Validation (IOV) satellites. It shows a modification of the Galileo IOV satellite payload diagram presented in Burbidge (2007).

The backbone of any GNSS signal payload is the reference clock section. This consists of highly stable atomic clocks, such as caesium, Rubidium Atomic Frequency Standards (RAFSs), Passive Hydrogen Masers (PHMs) and a Clock Monitoring and Control Unit (CMCU). Based on the input from the atomic frequency standard, it generates a basis frequency of $10.23\,MHz$. The Frequency Generator and Upconverter Unit (FGUU) receive the reference frequency from the CMCU and synthesises a frequency of $122.76\,MHz$. Based on this frequency, the Navigation Signal Generation Unit (NSGU) generates the navigation signals. These are again upconverted by the FGUU to the desired frequency on the L-band. Different, dedicated output chains are implemented in order to transmit the signals, each at the required power level. The amplified signals are finally transmitted by an L-band antenna. Certainly, only in a perfectly designed and calibrated system all signals are synchronous. It is clear that any lack in synchronicity between the different signals results in delays between the signals. The phase biases, related to the transmitting antenna, are referred to as phase centre offsets (PCOs) and phase centre variations (PCVs), whereas
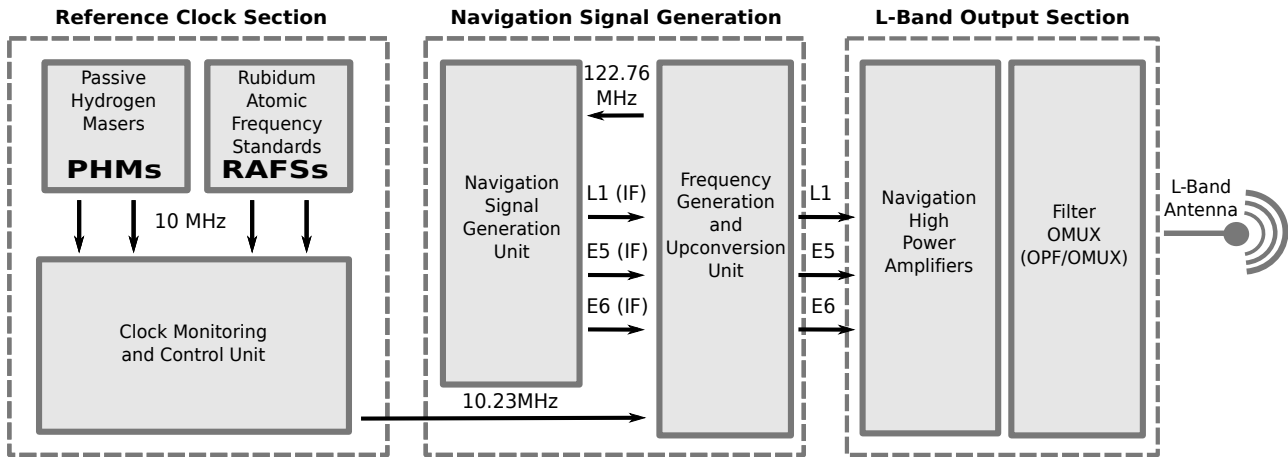
Figure 2.1: Modification of the Galileo IOV satellite payload diagram, presented by Burbidge (2007).

all remaining biases are commonly condensed to the so-called uncalibrated signal delays (USDs), to be divided into UCDs and UPDs. Because of the similarity of satellite and receiver USDs and because the uncalibrated delays also include delays coming from the interaction of satellite and receiver effects, these biases are discussed jointly in section 3.1.2.

2.1.3 User segment

The user segment is formed by the totality of user receivers (Galileo, 2002). However, since the user segment is not an integral part of the system itself and due to its importance for this thesis, it will be discussed later in section 3.1.

2.2 Geodetic reference systems and timescales

Reference and time systems are the basis for describing positions and time. The optimal description of the physical processes, related to geodetic tasks, requires different reference and time systems.

2.2.1 Relevant reference systems and realisations

In essence, reference systems can be divided into the celestial reference system (CRS) and the terrestrial reference system (TRS). TRS are optimally suited to the description of terrestrial processes, positions and time. CRS are most convenient for the description of non-terrestrial phenomena and motions, such as relativity effects on satellites or their equations of motions.

The most important reference systems in the frame of this thesis are the International Terrestrial Reference System (ITRS) and the Geocentric Celestial Reference System (GCRS). ITRS and GCRS are linked via the earth orientation parameters (EOPs). The transformation at the epoch t can be written as per Petit and Luzum (2010):

$$[GCRS] = Q(t)R(t)W(t)[ITRS], \tag{2.1}$$

where the transformation matrices originate from the

$\quad Q(t)$ celestial pole in the celestial reference system.
$\quad R(t)$ rotation of the earth around the axis associated with the pole.
$\quad W(t)$ polar motion, respectively.

The ITRS is realised by coordinate and velocity estimates of a selected set of stations. The stations are observed via different, complementary geodetic techniques like Very Long Baseline Interferometry (VLBI), Lunar Laser Ranging (LLR), Global Navigation Satellite Systems (GNSS), Satellite Laser Ranging (SLR) and Doppler Orbitography and Radiopositioning Integrated by Satellite (DORIS). The latest realisation of the ITRS is the International Terrestrial Reference Frame (ITRF)08 (Altamimi et al., 2011).

However, this realisation is not applicable for institutions that are missing access to the full set of observations. Consequently, each institution generates its own realisation of the ITRF08 on the basis of the applicable observations. Relevant realisations are the IGS realisation IGS08 (Rebischung et al., 2012) and the realisations of the different GNSS providers, such as the World Geodetic System 84 (WGS84) (GPS, 2012a) for GPS, the Earth Parameters 1990 - Parametry Zemli 1990 (PZ-90) (GLONASS, 2008) for GLONASS, the Galileo Terrestrial Reference Frame (GTRF) (Galileo, 2010) for Galileo and the China Geodetic Coordinate System 2000 (CGCS2000) (BeiDou, 2011) for BeiDou.

It is essential to use satellite positions in a common reference frame for the combination of observations from different GNSS. In the case of precise IGS combined GNSS orbit products, currently GPS + GLONASS, this requirement is satisfied. More challenging is the situation when using orbits from different providers, as in the case of broadcast orbits. In this case, the different satellite positions and clock offsets need to be transformed into a single common reference frame. In fact, the latest realisations of the respective terrestrial reference frames (TRFs) for GPS, GLONASS, BeiDou, QZSS and Galileo are all aligned to ITRF08 (Altamimi et al., 2012). However, it has to be noted that this alignment is performed at different accuracy levels (decimetres for GPS and millimetres for Galileo), for different sets of stations and at a particular date. Consequently, it can be expected that the different TRFs will still show significant systematic discrepancies.

2.2.2 Relevant timescales

Different timescales exist. The most basic timescale defined by the earth's rotation is Universal Time (UT). Its observation, corrected for polar wander, is Universal Time 1 (UT1). However, this timescale is not applicable in operations. A continuous applicable timescale is International Atomic Time (TAI), realised by the Bureau International des Poids et Mesures (BIPM). It is based on a combination of more than 200 atomic clocks worldwide. The most common timescale and the basis for civil time is Universal Time Coordinated (UTC). UTC is based on TAI and is aligned to UT1 by the application of leap seconds. Leap seconds are introduced to keep the difference between UT1 and UTC below $0.9\,s$.

Further relevant timescales for GNSS applications are the realisations of the different GNSS, GPS time (GPST) (GPS, 2012a), GLONASS time (GLONASST) (GLONASS, 2008), the Galileo system time (GST) (Galileo, 2010) and BeiDou time (BDT) (BeiDou, 2011). The different system times are realised by a single or an assembly of atomic clocks steered to UTC. Even though the timescales are aligned to UTC, the time still needs to be transformed to UTC, accounting for the UTC time zone and the different number of leap seconds (Δ_{LS}). The transformation can be written as follows:

$$
\begin{aligned}
UTC &= GPST + \Delta_{LS(GPS)} \\
UTC &= GLONASST - 3\,hours \\
UTC &= GST + \Delta_{LS(Galileo)} \\
UTC &= BDT + \Delta_{LS(BeiDou)}
\end{aligned}
\tag{2.2}
$$

In fact, even if all the timescales are steered to UTC, the variable time differences (specs: GPS $< 1\,ms$, Galileo $< 50\,ns$, BeiDou $< 100\,ns$) are still far above the position accuracy, preventing a direct combination of clocks from the different systems. Therefore, in order to improve the interoperability with GPS, Galileo (Galileo, 2010) and GLONASS (GLONASS, 2008) provide the offset to GPST, allowing for the transformation to GPST and vice versa.

2.3 Navigation signals

This section gives a general overview of GNSS signals. For a detailed description of individual signals, consult the respective Interface Control Documents (ICDs)/Interface Specifications (ISs); GPS (2012a,b,c) for GPS, GLONASS (2008) for GLONASS, Galileo (2010) for Galileo and BeiDou (2011) for BeiDou.

GNSS signals are composed of electromagnetic (EM) waves. EM waves are defined as self-propagating waves of energy, consisting of electric and magnetic fields oscillating at the correct angle ratio. Both the magnetic ($\vec{H}$) and the electric fields ($\vec{E}$) are perpendicular to the propagation direction and to each other. Figure 2.2 shows a linearly polarised EM wave. In order to minimise the impact of the so-called Faraday rotation (Hall et al., 1996), GNSS signals are right hand circularly polarised (RHCP), as shown in figure 2.3. This means the electric and the magnetic fields are describing a spiral movement around the transmission path. EM-waves propagate spherically. Spherical waves can be approximated by wave fronts for long distances, such as in between GNSS satellites and the earth's surface. For distances of $25,000\,km$, the curvature is about $4.0e^{-8}\,1/m$. The plane wave front describes a plane, perpendicular to the propagation direction, with a constant phase at a certain time.
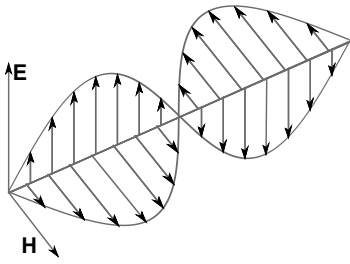
Figure 2.2: Linearly polarised wave.
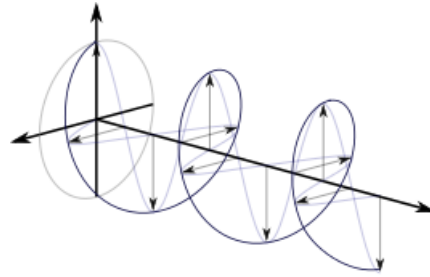
Figure 2.3: RHCP wave.

In the literature the term signal is used ambiguously. It is either used for the composition of carrier and code components, exclusively for the code modulation, or alternatively for either a carrier or a code component. In the interests of clarity and in coincidence with the understanding of Galileo (2010), this thesis defines the term signal as follows:

Signal:
A signal is a composition of individual, trackable signal components, the code and carrier phases.

Hence, GNSS signals are a superposition of different components. The EM waves described earlier act as a carrier for the ranging codes and optional for codes and data. Optional means that some GNSS provide dataless signals in order to improve the correlation performance and, consequently, the signal tracking. This topic is addressed more in detail in section 3.1.1.

2.3.1 Carrier phases

GNSS satellites transmit signals on different carrier frequencies. The restriction to beam antennae for frequencies above $2\,GHz$ and to keep the atmospheric impact as low as possible (the impact of the ionosphere is significantly higher for frequencies below $100\,GHz$ and above $10\,GHz$), GNSS uses carrier frequencies in the L-band ($1\,GHz$ - $2\,GHz$). For GPS, these frequencies are designated as L1, L2 and L5, for Galileo as E1, E5a, E5, E5b, E6 and for GLONASS as G1, G2 and G3.

No matter which of the GNSS, all carrier frequencies are derived from a single atomic frequency standard on board the satellites, as demonstrated in figure 2.1. The nominal frequency for GPS and Galileo, as it appears to the observer on the ground, is $f_o = 10.23\,MHz$ (GPS, 2012a; Galileo, 2010). To account for relativistic effects, the true frequency as it would appear to an observer on board the satellite is set minimally below ($\delta f / f = -4.4647e^{-10}$) the nominal frequency. Table 2.1 shows the multipliers for GPS and Galileo.

Frequency	Multiplier x f_0	Center Frequency
L1/E1	154.0 x $10.23\,MHz$	$1575.420\,MHz$
L2	120.0 x $10.23\,MHz$	$1227.600\,MHz$
L5/E5a	115.0 x $10.23\,MHz$	$1176.450\,MHz$
E5a+E5b (E5)	116.5 x $10.23\,MHz$	$1191.795\,MHz$
E5b	118.0 x $10.23\,MHz$	$1207.140\,MHz$
E6	125.0 x $10.23\,MHz$	$1278.700\,MHz$

Table 2.1: GPS, Galileo carrier phase frequencies.

The signals transmitted by the different GNSS are widely spread over the L-Band. Figure 2.4 shows a modification of the figure presented by Hein and Pany (2002). It visualises the frequency allocation for GPS, GLONASS and Galileo and shows that different signals use the same frequency. On one hand, this has the advantage of better interoperability, but also has the disadvantage of interference in the case of poorly designed signal modulations. The limited frequency range inevitably leads to overlapping areas.
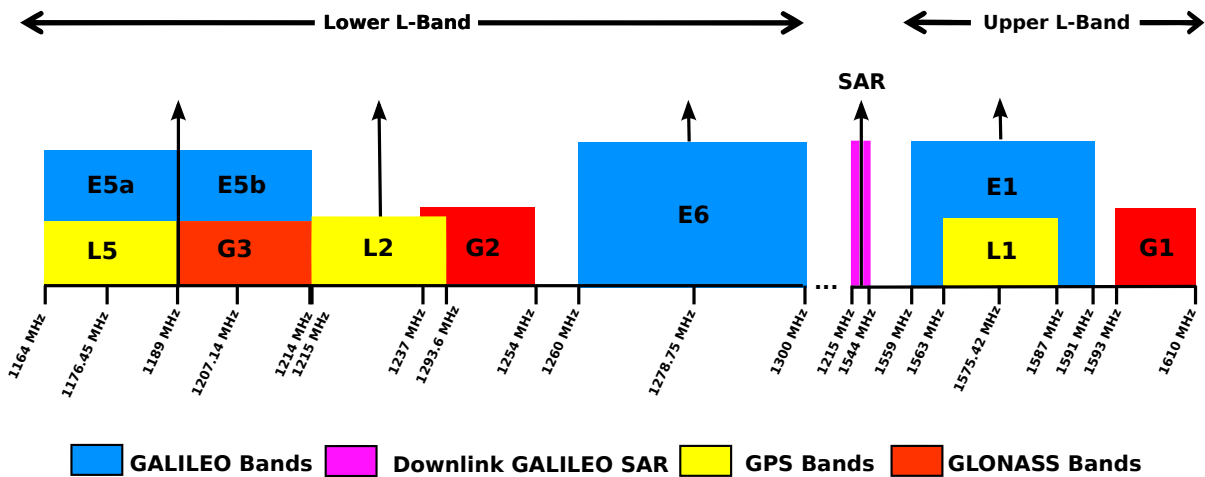
Figure 2.4: Modification of the frequency band allocations for GPS, GLONASS and Galileo, presented by Hein and Pany (2002).

In fact, it is not only the signals of different GNSS that are on the same frequency and need to be distinguished. Since all satellites belonging to the same GNSS transmit at the same time on the same carrier frequency, providing the same data, a technique for unequivocal identification of the satellites is needed. This applied technique is called multiplexing.

2.3.2 Multiplexing

Multiplexing describes the method of transporting multiple signals at the same time, on the same carrier, in the form of a single, complex signal (Ohm and Lüke, 2010; Maral et al., 2009). The procedure for recovering the original signals is called demultiplexing. Since all GNSS satellites are continuously transmitting GNSS signals on the same carrier frequency, multiplexing becomes necessary. Different multiplexing techniques exist, although only two of them are applied by GNSS, namely the Code Division Multiple Access (CDMA) technique, used in most GNSS, and the Frequency Division Multiple Access (FDMA) technique, applied exclusively by GLONASS. The FDMA technique assigns each signal to a dedicated frequency and thus allows a distinction between the individual signals. In future, it is most likely that all GNSS will make use of the CDMA technique. Therefore, FDMA is not further considered in this thesis. In contrast to FDMA, CDMA distinguishes the different signals by the utilisation of so-called spreading codes.

2.3.3 Spreading codes

Spreading codes are a fundamental component of any system applying the CDMA multiplexing technique or more generally spread spectrum communications, and hence also for GNSS. Spreading codes are used to spread the signal frequency spectrum, with the result that the signal power is evenly distributed over the entire spectrum afterwards. This has a positive effect in that the signal becomes more robust against interference, interception and multipath (Hein et al., 2006a). The resulting signals show characteristics similar to radio frequency (RF) noise. Such signal characteristics can be obtained perfectly by the utilisation of random codes. However, the recovery of the original signal requires knowledge of the code sequence, which again necessitates the reproducibility of the spreading codes. Furthermore, the best separation of signals can be achieved if the spreading codes are orthogonal with each other. The solution to this problem is the so-called Pseudo Random Noise (PRN) codes. PRN codes are

optimised to be as random as possible, while at the same time fulfilling the requirements of reproducibility and best possible orthogonality. Different code families have been developed. A famous example is the Gold codes, named after the mathematician Dr Robert Gold, which are applied to the GPS Coarse/Acquisition code (C/A).

In addition to their role in the multiplexing procedure, PRN codes are used for distance measurements between satellite and receiver. As a result of their characteristics, some PRN sequences are more suitable than others, allowing measurements that are more accurate and which are less sensitive to disturbances. It also seems natural that longer codes provide better characteristics than do shorter codes, but certainly at the expense of longer integration times in the receiver. It is obvious that finding an optimal PRN is not an easy task. Nevertheless, in the context of GPS modernisation and the development of new GNSS like Galileo, new advanced PRN code sequences optimised for the needs of up-to-date GNSS have been designed. Table 2.2 shows the code families currently used by GPS and Galileo (Hein et al., 2006a). A detailed description of the applied PRN codes can be found in the respective ICDs/ISs.

Signal	GPS	Galileo
L1/E1	Gold codes (C/A) Weil codes	Random codes (E1 open service (OS))
L2	m-sequences	—
L5/E5	m-sequences	m-sequences
E6	—	Random codes

Table 2.2: PRN codes for GPS and Galileo (Hein et al., 2006a).

2.3.4 Signal modulation

Phase Shift Keying (PSK) is a method of modulating digital information onto a sinusoidal carrier wave. A simple digital PSK modulation technique is Binary Phase Shift Keying (BPSK). BPSK is used as basis modulation for GNSS signals. It is often referred to as BPSK-R or BPSK-R(n), which stands for a rectangular (R) BPSK with a chip rate at n x 1.023 MHz. Figure 2.5 demonstrates the procedure for generating a BPSK signal from two components, the carrier wave and the data wave. The phase of the carrier wave is modulated according to the data wave; thus, in the case of a zero in the data wave, the carrier wave remains unchanged, whereas for a one, it is shifted by 180°.
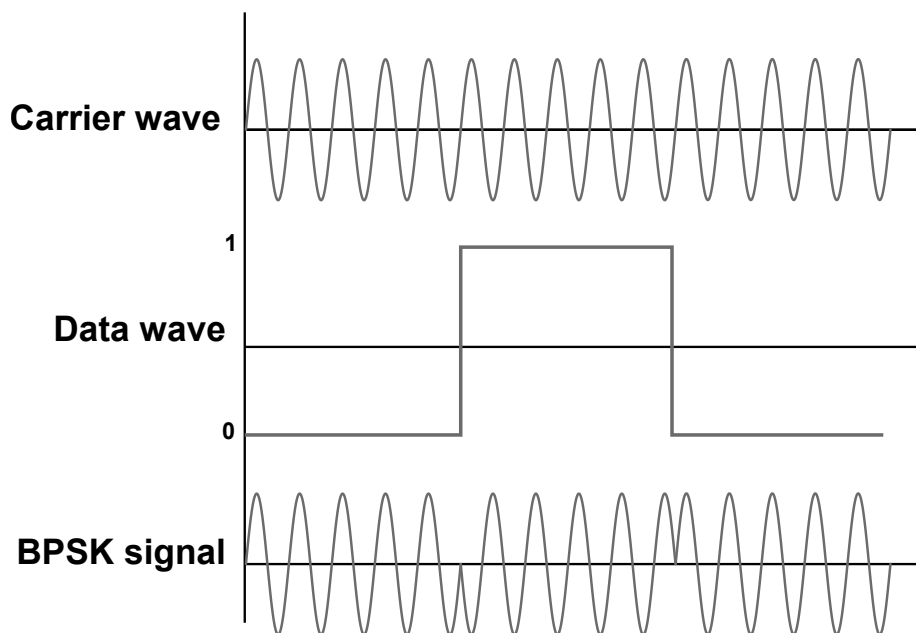
Figure 2.5: BPSK signal modulation.

Applying the spread spectrum technique, the data wave is a combination of the spreading code and the navigation message for GNSS. Exceptions are the dataless signals, for which the data wave is exclusively given by the PRN. The combination of the two waves is carried out using a modulo-2 addition. A modulo-2 addition means that a zero is set if the code chip and the data bit are identical (both zero or both one); if they are different, the result is one. The term chip is used for a bit in a spreading code. Finally, the modulo-2 added code waves are modulated onto the carrier wave using the BPSK technique.

A crucial point for the signal performance, in terms of robustness and tracking accuracy, is given by its power (R) and autocorrelation (S) function. For a BPSK-R signal with a chip period of T_c and a spreading code frequency f_c this can be expressed according to Kaplan (2005) as:

$$
\begin{aligned}
R_{BPSK} - R(\tau) &= \quad \left(1 - \frac{|\tau|}{T_c}\right) \qquad \quad for\ |\tau| \leq T_c \\
S_{BPSK} - R(f_c) &= \quad T_c sinc^2\left(\pi f_c T_c\right)
\end{aligned}
\tag{2.3}
$$

where τ denotes the time lag.

In the frame of the GPS modernisation and the development of new GNSS, numerous analyses on signal modulation techniques have been run. The results are new more robust modulation schemes, such as the Binary Offset Carrier (BOC), the Multiplexed Binary Offset Carrier (MBOC) or the Alternative Binary Offset Carrier (AltBOC). The BOC modulation technique, initially proposed as a baseline modulation for Galileo and GPS, is an extension of the BPSK modulation. A BOC signal can be described as a BPSK spreading symbol (g) multiplied by the signum function (-1 if arguments < 0, else 1) ($sign$) of the subcarrier with a square modulation frequency f_s:

$$
g_{BOC}(t^t) = g_{BPSK-R}(t^t)\, sign\left[sin\left(\pi t^t 2 f_s + \psi\right)\right]
\tag{2.4}
$$

The phase angle (ψ) is commonly used to generate either sine phase ($\psi = 0°$) or cosine phase ($\psi = 90°$) BOC signals. BOC signals are described as BOC(m,n), which means the signal is generated using a subcarrier with a frequency (f_s) of m x $1.023\ MHz$ and a chipping rate of n x $1.023\ MHz$. The goal of this modulation is better tracking performance due to better-optimised power spectrum and autocorrelation function. The power spectrum for a sinus phase BOC modulation can be written according to Kaplan (2005) as:

$$
S_{BOC}(f_c) =
\begin{cases}
T_c sinc^2\left(\pi f_c T_c\right) & tan^2\left(\frac{\pi f_c}{2 f_s}\right) & if\ T_c/T_s\ even \\[2ex]
T_c \frac{cos^2\left(\pi f_c T_c\right)}{\left(\pi f_c T_c\right)} & tan^2\left(\frac{\pi f_c}{2 f_s}\right) & if\ T_c/T_s\ odd
\end{cases}
\tag{2.5}
$$

Figure 2.6 compares the power spectrum of a BPSK-R(1) and a BOC(1,1), showing that the square wave divides the power spectrum into two peaks. The displacement of the peaks represents the square modulation frequency (f_s) and their width represents spreading code frequency (f_c).

Finally, a variation of the BOC modulation, the MBOC, or rather its implementations the Composite Binary Offset Carrier (CBOC) for Galileo and the Time-Multiplexed Binary Offset Carrier (TMBOC) for GPS, are agreed to be the baseline modulation (Fantino et al., 2008; Lestarquit et al., 2008; Avila-Rodriguez et al., 2007). MBOC is the result of multiplexing two different BOC signals (Hein et al., 2006b), with the consequent power split between both. This fact is reflected in the MBOC notation which, in addition to the BOC notation, also specifies the power split between the two BOC modulations. For example, the Galileo OS signal on E1 is specified as CBOC(6,1,1/11), which stands for BOC(6,1) multiplexed with BOC(1,1). The multiplexing is carried out as such that the 1/11 of the power is allocated to the high frequency component (BOC(6,1)).
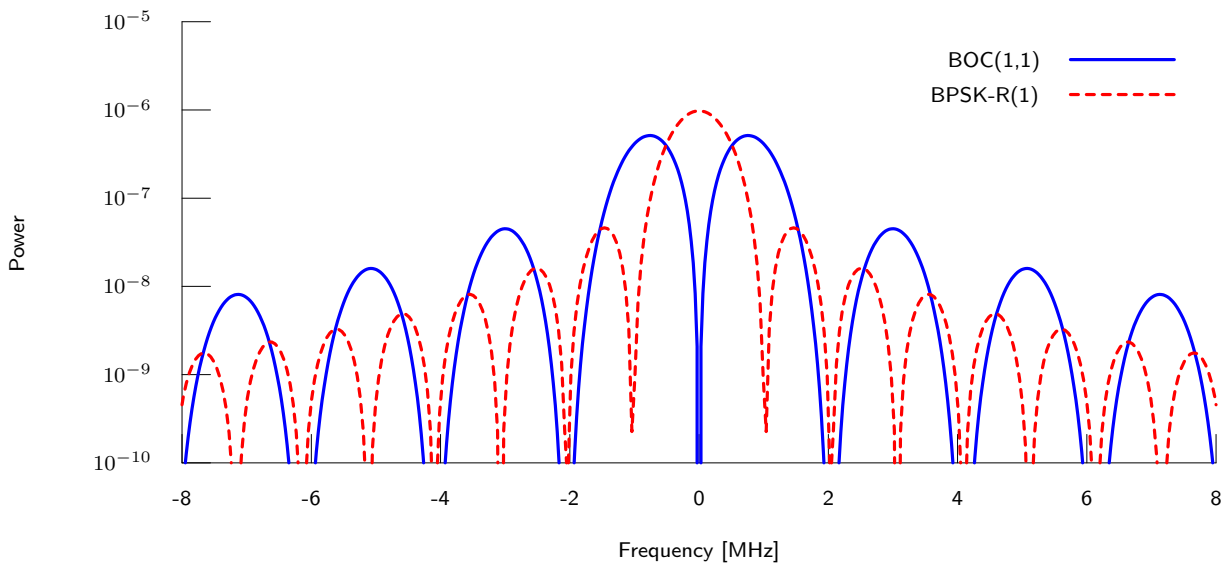
Figure 2.6: Comparison of a BPSK-R(1) and a BOC(1,1) power spectrum.

The most advanced signal modulation, foreseen for the first Galileo generation, is the AltBOC. Similarly to the MBOC modulation, the AltBOC modulation is also a combination of two modulated signals. In contrast to the MBOC modulation, the power spectrum of the AltBOC basis signals still has full power, moreover, they can still be treated as individual signals (Lestarquit et al., 2008; Ries et al., 2002). Detailed information on signal modulation techniques can be found in the respective ICDs and ISs, as well as in Kaplan (2005); Hein et al. (2002, 2006b).

An overview on the new GPS and Galileo signals is given in Avila-Rodriguez et al. (2007). As outlined in the section above, GNSS signals are the result of the superposition of a low frequency group of waves (code) centered on the high frequency carrier. Depending on the characteristics of the passed media, the group velocity may differ from the velocity of the carrier wave. This is an important feature of GNSS signals, requiring a special consideration in GNSS signal analyses. GNSS waves are transmitted in two directions, the prime direction, called the in-phase (data signal) (I), and the perpendicular direction, known as the quadrature (pilot signal) (Q) component. I and Q signals might be identical, but can also be different, as in the case of GPS where the C/A code is transmitted as I and the Q component is used for the encrypted Y-code. In modern GNSS, the quadrature channel is often used for the dataless signals.

2.3.5 Synthetic signal degradation and access control

GNSS makes use of different techniques to prevent unwanted use. The reasons may not only be military, political or police safety concerns, but also commercial reasons. The GPS, for example, makes use of two different techniques, so-called Anti-Spoofing (AS), which is an encryption of the precise military code and Selective Availability (SA), which is implemented to degrade the GPS signals. The SA was deactivated on the 2nd of May 2000 pursuant to a Presidential order. According to a news release by the US Department of Defense (DoD) on the 18th of September 2007 (Office of the Assistant Secretary of Defense (Public Affairs), 2007), SA will be discontinued in the next generation of GPS (GPS-III) satellites. Also, other GNSS like Galileo are able to restrict the use of dedicated signals. Nevertheless, since these restrictions are permanent, which means dedicated signals are assigned to military/authority or commercial use, these are not available to the standard user and, consequently, neither to the scientific community. For this reason, the impact of these techniques and the meaning of such signals are not further considered in this thesis.

3 Conventional GNSS analysis

This chapter is intended to outline the basics of the conventional GNSS analyses. A first, important processing of GNSS signals is performed in the receiver system, generating GNSS observations in the Receiver Independent Exchange Format (RINEX) (Gurtner and Estey, 2009). Nevertheless, RINEX observations files are seen as the starting point of most GNSS analyses. The most important steps in such analyses are observation modelling and the subsequent parameter estimation. The last step for precise GNSS analyses is the recovery of the integer phase ambiguities.

3.1 Receiver system

Highly optimised receiver-systems are used for the best possible recovery of the information modulated on the GNSS signal and, consequently, in order to use this information to measure the distance between the satellite and the receiver. The term "receiver system" is used for the entire system needed to receive, acquire and track the signals. The most important components of a receiver-system are the GNSS antenna and the receiver itself. Various optimised receiver-systems exist to optimally fulfil different applications and tasks. It is inevitable or even intentional that the various systems show different characteristics. From the users' point of view, GNSS antennae are the interface to the outside world, establishing the link to the GNSS, or more specifically, to the space segment. Since all received signals interfere with each other, resulting in undesirable effects, antennae are optimised to reduce the influence of undesired signals to a minimum. At the same time, antennae are designed to allow the optimal passage and amplification of the desired signals. Various antenna types exist to meet the requirements of different applications, tasks and signals. These differ in purpose (rover, reference station, satellite), type (patch, helix, design (shape, shielding) and electronics (filter, amplifier), resulting in different outputs. The antenna output is pre-processed by the receiver frontend. The frontend is designed to prepare the incoming signals for the final signal processing. It filters and amplifies the received signals to suppress out-of-band interference and down-converts it into an intermediate frequency. In the next step, the I and Q signals are converted to the baseband by multiplication with two tones, displaced by $\pi/2$. The final pre-processing step, in order to allow digital signal processing, is the quantification of the baseband signal, which is performed by an analog digital converter (ADC). However, the results differ, depending on various components, their characteristics and settings. Since different results are not satisfactory for highly precise applications, the different measurements have to be corrected properly. However, the most challenging biases for the processing of raw GNSS observations are those, resulting from the signal generation and tracking process. Therefore, the topic of signal acquisition and processing will be discussed in more detail.

3.1.1 Signal acquisition and processing

Signals transmitted by GNSS satellites appear to the user as part of the mixture of various signals coming from countless different sources. As a result of the spread spectrum technique, the signals appear to be RF noise. Consequently, the first step is the capturing of the individual satellite signals. Therefore, the receiver, or more precisely the replica generator, generates a replica of the a priori known PRN code for a satellite expected to be visible. This replica is now compared, using cross-correlation, against the incoming mixture of signals. If the corresponding satellite signal is included in the incoming mixture of signals, the cross-correlation function exhibits a sharp peak for the point of accordance, as shown in figure 3.1 (right). The left part of this figure shows the flat power spectrum in the case of a non-matching PRN replica.

In order to determine if the replica matches the incoming signal, the so-called spreading code lock detector is implemented. The spreading code lock detector analyses the correlation function and examines if this exhibits a peak of maximum power for the current code alignment. If the code is not yet locked, the code replica is shifted and again correlated with the incoming signals. This procedure, referred to as the delay-lock loop (DLL), is repeated until the code lock detector indicates a match of both signals with a confidence of $\pm\,1$ chip. A discriminator function is used to determine the required code shift for the alignment of replica and incoming signal. Typically, the discriminator correlates different versions of the replica with the incoming signal and computes the required
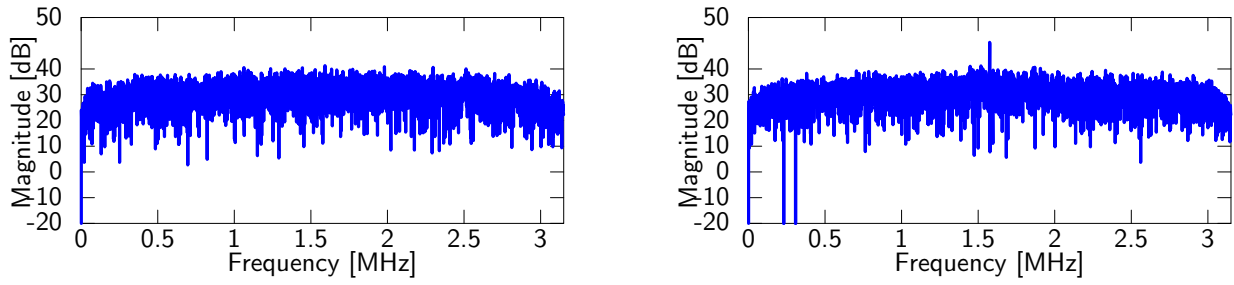
Figure 3.1: Cross-correlation without (left) / with (right) included signal.

code shift. A simple example of a discriminator implementation with two correlation functions is given in the following. Figure 3.2 shows an early cross-correlation function ($R_E(\tau)$), making use of a PRN replica shifted by $-d/2$ and a late cross-correlation function ($R_L(\tau)$), based on a PRN replica shifted by $d/2$, whereas $d \leq 1$. The discriminator function ($D(\tau)$) is now formed as a difference between early and late cross-correlation functions (Figure 3.3). The discriminator output is used to steer the replica generator.
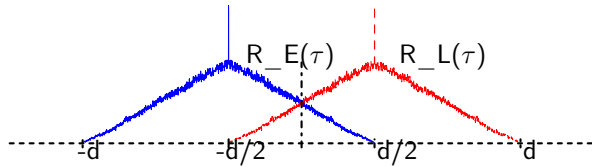
Figure 3.2: Cross-correlation function between received and replicated code.
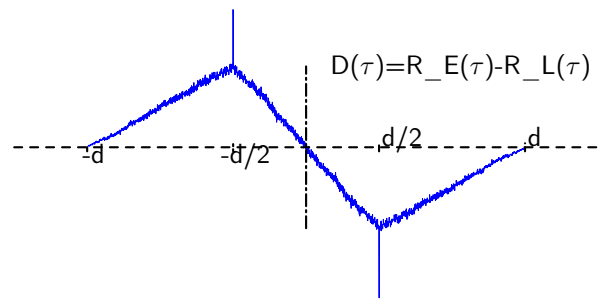
Figure 3.3: Code-discriminator (D_E) formed as a difference of early (S_E) and late (S_L) correlation functions.

The so-called observed carrier frequency ($f_{doppler}$) is required, to account for the fact, that the transmitter moves relative to the receiver. This movement causes the observed carrier frequency (f_{obs}) to differ from the nominal frequency (f_0) by ($f_{doppler} = f_{obs} - f_0$). For GNSS carrier waves, the Doppler frequency can be approximated according to Braasch et al. (1999) as a function of the relative velocity in the line of sight (v_{LOS}):

$$f_{doppler} \approx v_{LOS} \frac{f_0}{c} \tag{3.1}$$

The generation of a proper replica for the received signal requires the consideration of the Doppler frequency. Since the Doppler frequency is unknown, at least in the beginning of the acquisition process, a simultaneous search for PRN code shift and carrier frequency is performed. The frequency or phase lock can be obtained either by a frequency-lock loop (FLL) or a phase-lock loop (PLL) implementation. After a successful code lock, the signal can be despreaded. In addition, if the carrier is locked, the navigation message can be easily derived by removing the carrier wave. Detailed information on the decoding procedure of the navigation message can be found in the respective ICDs/ISs.

The measurement of the desired satellite-receiver distance is, at least in theory, quite a simple task. The distance can be computed by a multiplication of the time lag (τ) between signal transmission and reception time with the speed of light (c = 299,792,458 m/s). For perfectly aligned receiver and satellite clocks, and under the assumption of undisturbed signal propagation, this is given by the time shift needed to align the replica with the received signal. Since this is never the case, the distance so derived is called pseudo range (Pr). In addition to the less accurate pseudo range measurement, the integrated Doppler or carrier phase (in cycles) measurement is derived. Carrier phase (in cycles) observations are relative measurements, but are accurate to millimetre level. The meaning and treatment of pseudo range and carrier phase measurements for positioning and timing applications are discussed in section 3.2.

It is well known that signals are affected by numerous different effects that cause the signals to delay, advance or to change their shape. Furthermore, it is also clear that the signal performance depends on the correlation properties, and thus on their characteristics, such as frequency, power, power distribution or signal shape. Hence, it is obvious that different signals show different performance in terms of sensitivity to disturbances and measurement accuracy. Numerous analyses studying the performance of different carrier frequencies, PRNs and signal modulations have been run. Due the multitude of different signals, and since the user has to cope with whatever is available, the following section focuses less on the performance of individual signals and more on the implications of signal disturbances for positioning and timing. For the performance of individual signals, refer to the respective analyses by Avila-Rodriguez et al. (2004); Eissfeller et al. (2007); Fantino et al. (2008); Simsky et al. (2008a,b) and others.

The sources of signal disturbances are manifold, as is their impact on the signals. The impact extends from simple signal delays to the complex problem of signal deformations. Stable signal delays, assignable to a specific source, such as the satellite or receiver, can be easily handled by a priori corrections or by estimation. Signal delays common to all signals are absorbed by the respective estimate of the clock offset, either the satellite or the receiver. Consequently, they do not affect the positioning solutions. For timing applications interested in the "absolute" clock, those effects are more critical. Therefore, different approaches for the calibration of receiver-dependent delays have been developed and presented (Plumb et al., 2005; Proia et al., 2011). The most challenging biases for the processing of original (raw) observations, which are generally not considered in the calibration methods, are signal delays caused by signal deformation, thus producing different results for different PRNs (Phelts and Akos, 2006).

The following paragraph exemplarily explains the impact of signal deformations on the signal recovery and tracking process. A disturbed code sequence, as might be received by the user, is shown at the top of figure 3.4 (red). Underneath the disturbed signal, this figure shows differently shifted code replicas, starting from 0.5 chips early (E5), to the 0.5 chips late (L5). The cross-correlation functions of the undisturbed (blue) and correlation function of the disturbed (red) signal with the different replicas (E5, E4, . . . , I (In phase), . . . , L4, L5) are presented in figure 3.5. This shows as a response to disturbances in the signal and the resulting deformation of its shape; also, the correlation function is distorted. Taking into account that different discriminator functions sense different points in the correlation function, it becomes obvious that different implementations, for example different correlator spacings, give different results. The result of different discriminator functions (D1, D2, D3, D4, D5), applied on the correlation function presented in figure 3.5, is shown in figure 3.6.
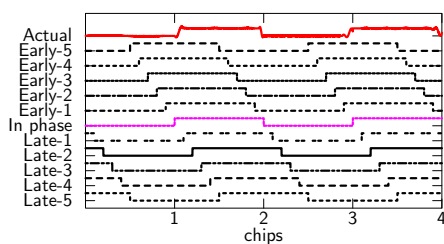
Figure 3.4: Early, in phase and late code sequence replica.
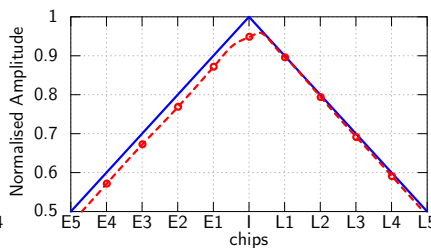
Figure 3.5: Correlation peaks; ideal (blue) disturbed (red).
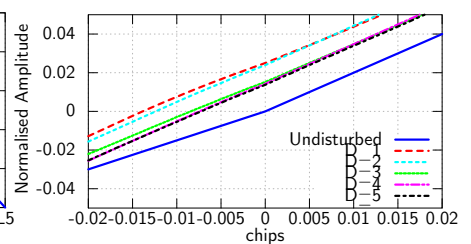
Figure 3.6: Impact of disturbances on discriminator results.

It becomes obvious that, in the case of a nominal input signal (undisturbed), all discriminators provide the same, correct result, in that the function shows no shift between input and replica. For the distorted signals, the different discriminator functions show different displacements, unequal to zero. These pseudo range displacements are referred to as uncalibrated code delays (UCDs). The comparable delays for carrier phase measurements are the so-called uncalibrated phase delay (UPDs). Apart from the correlator induced effects, the code and phase signal components are exposed to a number of further disturbances with similar characteristics. The similarity of these effects prevents the separation of the individual effects. Consequently, the common understanding of uncalibrated signal delays (UCDs, UPDs), often referred to as hardware delays, is not comprehensive. Instead, the corresponding parameters can be described as follows:

Uncalibrated signal delays:
Uncalibrated signal delays (USDs), namely UCDs and UPDs, are a conglomerate of numerous different signal-dependent effects. Such effects include hardware delays, unmodelled atmospheric delays, model inaccuracies, such as for PCOs/PCVs, and multipath. Strictly speaking, USDs are receiver-satellite-signal dependent. For reasons of simplification, uncalibrated signal delays are commonly assumed to be divisible into satellite-signal and receiver-signal portions.

This description already exposes the issue or the challenge with those parameters. UCDs and UPDs condense all uncalibrated and unmodelled signal-component-specific delays. Hence, among others, multipath and model errors. It is easy to imagine that these parameters are difficult to describe by physical models. In addition, due to the interaction of signal and correlator, that are different signals affected by the same disturbances lead to different correlator responses. Hence, strictly speaking, a definite assignment of the delay to a receiver or satellite is not possible. Different analyses, for example, Phelts (2004, 2007), confirmed the PRN - PRN variability of these biases. A detailed analysis of this topic, showing the interaction of PRN codes and correlators, can be found in Wong et al. (2011). As a result, the biases have to be seen as more satellite-receiver-signal dependent than satellite-signal and receiver-signal dependent. Nevertheless, for practical reasons, up-to-date processing strategies assume the separability of satellite and receiver components. The IGS, for example, provides so-called differential code bias (DCB) corrections. DCBs represent a bias between two code signal components referred to an individual satellite or receiver. Against the backdrop of the upcoming variety of different signals, the utilisation of signal differences significantly complicates the bias representations. A simplification, or at least a clearer representation, is given by the apparently "absolute" or better individual biases, referred to as UCDs and UPDs. The term "absolute" is misleading, since it is only "absolute" against the clock definition. A discussion on the handling of uncalibrated signal delays for the common processing, making use of LCs and observation differences, can be found in section 3.2.1, whereas the impact on the processing of raw observations is discussed in chapter 4.

A further significant error source is reflected signals. These signals, known as multipath signals, interfere with the original signals and cause virtual signal delays. In GNSS antennae, different mechanisms for the mitigation of multipath signals, such as electromagnetic-wave attenuation shields or polarisation filters, are already implemented. In fact, a complete removal of multipath signals is not possible. Thus, different receiver-sited techniques for multipath mitigation have been developed and are implemented in different receiver types. A comparison of different multipath mitigation techniques is presented in Irsigler and Eissfeller (2003), as well as in Bhuiyan and Lohan (2010). Actually, none of the implemented approaches removes the impact of multipath signals completely. However, it is also clear that the application of multipath mitigation techniques affects the resulting observations, their characteristics and biases. An example of the impact of multipath mitigation techniques on the code biases can be found in chapter 6.

3.2 GNSS observation modelling

No matter if, for timing, standalone or network PPP applications, the goal is the description of the physical background of the GNSS observation and the recovery of the true geometric range $(\rho(t)_{rec}^{sat})$ between the satellite at the transmission time (t^t) and the receiver at the reception time. The reception time (t) is defined in the time-frame of the analyses.

A common exchange format for GNSS raw observations is the RINEX. According to its format description (Gurtner and Estey, 2009), all observations belonging to a single epoch are measured at the same time. It is important to note that all observations, regardless their belonging to a GNSS, are provided in a single time system, indicated in the file header. This requires a receiver sited-correction of the measurements for the offsets of the respective GNSS system times versus the time system used for the representation of the receiver time.

Since the receiver time cannot be assumed to be accurate, the estimation of a receiver clock offset becomes necessary. The relationship between observation and true geometric range is expressed by the so-called observation equation. To account for the fact that code, often referred to as pseudo range and carrier phase observations, have different characteristics, two separate observation equations, one for the pseudo range (Pr) and one for the carrier phase observations (Ph) are used. As outlined previously, all signals, starting with the generation process and moving through the signal transmission and the travel path, all the way to the signal reception and tracking processes, are affected by a variety of interference effects. In order to describe the observations accurately, all these effects

need to be modelled and/or estimated. Thus, all individual effects are part of the observation equation. In the following representation of the observation equation, for reasons of clarity the different effects are grouped according to their characteristics, such as relativistic effects (rel), clock errors (clk), the propagation path related effects, split in atmospheric (atm) and multipath (mp) delays, site displacements ($site$), antenna dependent delays (ant) and uncalibrated signal delays (USDs). Conventionally, if necessary, USDs or to be more precise uncalibrated code (ucd) and phase delays (upd) are treated by the so-called inter-system bias (isb) parameters. For carrier phase observations the phase wind-up (pwu) and the unknown number of ambiguities (N) need to be considered in addition. All insufficiently modelled disturbances are finally absorbed by the measurement error (ϵ). Accordingly, the observations can be expressed as a sum of the true geometric range ($\rho(t)_{rec}^{sat}$) and all modelled and estimated disturbances, mapped to the line of sight (LOS):

$$Pr(t) = \rho(t)_{rec}^{sat} + rel(t) + clk(t) + atm_{Pr}(t) + site(t) + ant_{Pr}(t) + \cancel{ucd(t)} + isb(t) + mp_{Pr}(t) + \epsilon_{Pr}(t)$$

$$Ph(t) * \lambda = \rho(t)_{rec}^{sat} + rel(t) + clk(t) + atm_{Ph}(t) + site(t) + ant_{Ph}(t) + \cancel{upd(t)} + isb(t) + mp_{Ph}(t) + \epsilon_{Ph}(t) \qquad (3.2)$$
$$+ pwu(t) + N\lambda$$

With reference to the latest description of the Antenna Exchange Format (ANTEX) (Rothacher and Schmid, 2010) where the true geometric range describes the distance between the satellite position (centre of mass) (GCRS) ($\vec{X}_{gcrs}^{sat}$) at transmission time ($t^t = t - \tau$) and the receiver position (antenna reference point) (ECEF) ($\vec{X}_{rec}$) at the reception time (t). τ stands for the time lag between the transmission time and the reception time. Since in most cases, at least the receiver position is unknown, the true geometric range cannot be computed immediately. In the case of precise orbit determination (POD), the satellite position is also unknown. This problem is typically solved by an iterative least squares (LSQ) or filter implementation, estimating either exclusive receiver or receiver and satellite positions in earth centred earth fixed (ECEF) coordinates. Satellite positions are commonly described by a set of orbital parameters as explained in section 3.2.3.

3.2.1 Error sources, unknowns and the handling thereof

According to up-to-date accuracy requirements, the majority of disturbing effects can be modelled sufficiently. In the case of insufficient modelling capabilities, the parameters are estimated. This section briefly introduces the disturbances and describes their typical handling in GNSS analyses. For reasons of clarity, the inter-system bias (isb) is discussed jointly with the uncalibrated signal delays. Special focus is placed on the parameter most relevant for PPP applications. A detailed, overall description of high-precision PPP applications is given by Kouba (2009). Note that not all formulas presented in the following directly output the corrections in metres and the direction of LOS. Consequently, a mapping in LOS becomes necessary for some corrections. For the mapping of ECEF coordinate differences ($\delta\vec{X}_{ecef}(t)$) to δLOS, the following formula can be used:

$$\delta LOS(t) = \frac{\Delta\vec{X}_{ecef\ rec}^{\ \ sat}}{|\Delta\vec{X}_{ecef\ rec}^{\ \ sat}|} \cdot \delta\vec{X}_{ecef}(t) \qquad (3.3)$$

GCRS coordinates require a prior transformation to ECEF (see section 2.2, Petit and Luzum, 2010).

Relativistic effects (rel)

According to Einstein's relativity theory, clocks run at different frequencies if they are either moving relative to each other, described by the special relativity (SR) theory, or if they are located at different gravitational potentials, described by the general relativity (GR) theory. Navigation satellites operate at altitudes of $19{,}000\ km$ (GLONASS), up to $24{,}000\ km$ (Galileo) and even in highly elliptical orbits up to $35{,}000\ km$ (QZSS). Since the isotropic light frame in the case of GNSS is earth centred inertial (ECI), these satellites are affected by both theories.

According to Petit and Luzum (2010), for artificial earth satellites the general relativistic correction for the space-time curvature, caused by the earth's gravity field, can be computed in the geocentric celestial reference system (CRS) as follows:

$$
\delta\ddot{\vec{X}}_{gcrs} = \frac{GM_E}{c^2|\vec{X}_{gcrs}^{sat}|^3} \left\{ \left[2\left(\beta+\gamma\right)\frac{GM_E}{|\vec{X}_{gcrs}^{sat}|} - \gamma\dot{\vec{X}}_{gcrs}^{sat}\cdot\dot{\vec{X}}_{gcrs}^{sat} \right]\vec{X}_{gcrs}^{sat} + 2\left(1+\gamma\right)\left(\vec{X}_{gcrs}^{sat}\cdot\dot{\vec{X}}_{gcrs}^{sat}\right)\dot{\vec{X}}_{gcrs}^{sat} \right\} +
$$

$$
\left(1+\gamma\right)\frac{GM_E}{c^2|\vec{X}_{gcrs}^{sat}|^3}\left[\frac{3}{|\vec{X}_{gcrs}^{sat}|^2}\left(\vec{X}_{gcrs}^{sat}\times\dot{\vec{X}}_{gcrs}^{sat}\right)\left(\vec{X}_{gcrs}^{sat}\cdot\vec{J}\right)+\left(\dot{\vec{X}}_{gcrs}^{sat}\times\vec{J}\right)\right] +
$$

$$
\left\{\left(1+2\gamma\right)\left[\dot{\vec{R}}\times\left(\frac{-GM_S\vec{R}}{c^2\vec{R}^3}\right)\right]\times\dot{\vec{X}}_{gcrs}^{sat}\right\} \tag{3.4}
$$

where:

c	is the speed of light (c = 299,792,458 m/s)
β,γ	are PPN (parameterised post-Newtonian) parameters, equal to 1 in general relativity
$\vec{R}$	is the position of the earth with respect to the sun
$\vec{J}$	is the earth's angular momentum per unit mass
GM_E, GM_S	are the gravitational constants of the earth and the sun

Note the second and the third line in the equation, known as Lense-Thirring or frame-dragging precession, and the geodetic or de Sitter precession are neglected in the up-to-date GNSS processing. Consequently, with β and γ equal to one, the equation can be rewritten as:

$$
\delta\ddot{\vec{X}}_{gcrs} = \frac{GM_E}{c^2|\vec{X}_{gcrs}^{sat}|^3}\left\{\left[4\frac{GM_E}{|\vec{X}_{gcrs}^{sat}|}-\dot{\vec{X}}_{gcrs}^{sat}\cdot\dot{\vec{X}}_{gcrs}^{sat}\right]\vec{X}_{gcrs}^{sat}+4\left(\vec{X}_{gcrs}^{sat}\cdot\dot{\vec{X}}_{gcrs}^{sat}\right)\dot{\vec{X}}_{gcrs}^{sat}\right\} \tag{3.5}
$$

Following the general theory of relativity the EM wave is influenced by the gravitational potential along its path. The so-called Shapiro effect can reach values up to $19\,mm$ (Zhu and Groten, 1988) for a single measurement. It can be computed as depicted in Zhu and Groten (1988):

$$
\delta_{shapiro} = \frac{2GM_E}{c^3}\cdot ln\left[\frac{R^{sat}+R_{rec}+r_{rec}^{sat}}{R^{sat}+R_{rec}-r_{rec}^{sat}}\right] \tag{3.6}
$$

where:

R^{sat}	is the geocentric distance of the satellite
R_{rec}	is the geocentric distance of the receiver
r_{rec}^{sat}	is the distance between satellite and receiver

The atomic clocks in the satellites are affected by both general (gravitational potential difference) and special (velocity difference) relativistic effects (Ashby, 2003). The principally constant satellite altitude causes the predominant portion of the relativistic effects to be constant. This constant part is corrected by a shift of the nominal satellite frequency standard (GPS $\delta f/f$ = -4.4647 E-10 Hz; see GPS (2012a)). The variable part of the relativistic effect, often referred to as the periodic relativistic effect, is caused by the eccentricity of the satellite orbit. This effect may reach up to approximately 50 ns (ESOC, 2009). According to Spilker Jr (1996), a first-order approximation of this effect can be computed as:

$$\delta t_{rel} = -2 \frac{\sqrt{GM_E}}{c^2} \cdot e\sqrt{A} sin(E)$$
$$= -2 \frac{\vec{X}_{gcrs}^{sat} \cdot \vec{X}_{gcrs}^{sat}}{c^2}$$

(3.7)

where:

e is the eccentricity of the satellite orbit
E is the eccentric anomaly of the satellite orbit
A is the coefficient matrix

Clock errors (clk)

The signal generation, in addition to the signal tracking, is referred to the satellite and receiver clock. For this reason, an clock offset (δt) in either satellite (sat) or receiver (rec) clocks causes measurements that are too short or too long. The impact on the measurements in metres can be written as the difference in the clock offsets multiplied by the speed of light:

$$clk = (\delta t_{rec} - \delta t^{sat}) \cdot c$$

(3.8)

In global network PPP and POD solutions, both clock terms, the receiver as well as the satellite clock offset, are estimated. The largely unpredictable behaviour of the receiver clock makes it necessary to estimate its offset per epoch. However, the behaviour of most up-to-date GNSS satellite clocks can also not be modelled with sufficient accuracy. For this reason, it is also usual to estimate the satellite clock offsets per epoch. Certainly, various analyses, such as those by Montenbruck et al. (2012); Waller et al. (2010), demonstrate the high stability of modern GNSS clocks. It is most likely that such clocks can be described by functional models, as demonstrated to some extent in Hugentobler et al. (2010); Svehla et al. (2010). However, the final proof in an operational environment is still pending.

An estimation of satellite clocks is not possible for standalone PPP solutions. As a result, satellite clock corrections need to be taken from an external source. Precise applications require clock corrections of the highest accuracy, as offered by different commercial providers or the IGS. However, for applications with accuracy requirements at a decimetre-metre level, the clock information broadcast by the GNSS itself is sufficient. One important requirement for the use of clock correction is belonging to the same timescale. In the case of combined clock products, as is the case with IGS final GPS-GLONASS clock corrections, this requirement is fulfilled by nature. However, in the case of broadcast clocks, it is important to ensure a common timescale (see section 2.2).

A further issue with the conventional ionosphere free processing is the neglected handling of UCDs. The negligence of UCDs causes the clock offsets to be exclusively valid for a dedicated signal or signal combination. This requires a special consideration, particularly for multi-GNSS, signal analyses (see section 3.2.1).

Propagation path related effects ($prop$)

On its propagation path, the signal is exposed to a number of disturbances, resulting in signal deformation, refraction (multipath) and reflection. Since the capabilities for the modelling of signal degradation and multipath are somewhat limited within the processing, the following description concentrates on the delays caused by the refraction of the earth's atmosphere (atm). The topic of signal degradation and multipath was previously discussed in section 3.1.2.

Refraction of the earth's atmosphere (atm)

The signal delay caused by a medium depends on the propagation speed of the radio wave in the medium (v) in relation to its propagation speed in free space (c). This relationship, known as the refraction index (n), can be expressed as:

$$n = \frac{c}{v} \tag{3.9}$$

The main distorting atmospheric layers for GNSS signals are the ionosphere and the troposphere. Consequently, the total atmospheric delay can be described by an integral from the satellite (sat) to the receiver (rec) along the signal propagation-path (pp). Usually, since the deviations of the refractive index from 1 (no delay in vacuum) are very small, the refractivity N = (n - 1) $\cdot 10^6$ is used.

$$prop_{atm} = \int_{sat}^{rec} N(pp)\,\mathrm{d}pp = \delta trop + \delta ion \tag{3.10}$$

In fact, the propagation path of the individual signals differs due to the different refraction indices, but the propagation-path is usually assumed to be identical for all signals of the same link.

The troposphere ($\delta trop$) is the lowest part of the earth's atmosphere. It ranges from the earth's surface up to a height of $12\,km$. For GNSS analyses, it is common practice to consider the troposphere jointly with the next higher atmospheric layer, the stratosphere. The stratosphere ranges from up to a height of $50\,km$ above the earth's surface. For electromagnetic waves, both layers, subsequently referred to as the troposphere, have non-dispersive characteristics. This means the refraction index is frequency independent. Consequently, all GNSS signals are equally delayed (Seeber, 2003).

The tropospheric path delay is commonly expressed as a product of the zenith path delay (ZPD) and a mapping function (M), relating the slant tropospheric delay to the ZPD. A simple mapping function, depending on the cosine (cos) of the zenith angle (z), is given by:

$$M = \frac{1}{cos(z)} \tag{3.11}$$

Modern mapping functions are built on continued fractions, as presented by Herring (1992):

$$\delta trop = \frac{1 + \dfrac{a}{1 + \dfrac{b}{1+c}}}{sin(\epsilon) + \dfrac{a}{sin(\epsilon) + \dfrac{b}{sin(\epsilon)+c}}} \cdot ZPD \tag{3.12}$$

a, b, c are the coefficients of the mapping function. Examples of different mapping functions are given by Niell (1996, 2000); Boehm et al. (2006).

The tropospheric delay can be divided into a predominant, well-predictable hydrostatic component ($\delta trop_{hyd}$) and a significantly smaller wet portion ($\delta trop_{wet}$). Logically, the total tropospheric delay is described by the sum of both:

$$\delta trop = \delta trop_{hyd} + \delta trop_{wet} \tag{3.13}$$

The total zenith delay is in the order of 2.5 m, whereas 90 % of this effect can be assigned to the hydrostatic component. Because of the unpredictable variations of the wet troposphere, a complete modelling of the tropospheric delay for precise applications is not applicable. Therefore, it is usual that a priori models are exclusively used for the modelling of the hydrostatic part, whereas the portion of the wet troposphere delay is estimated. The two most famous troposphere models for GNSS observation are the ones proposed by Hopfield (1969); Saastamoinen (1973). The model by Saastamoinen uses the atmospheric pressure (p), the partial water vapour pressure (e) (both in millibars) and the temperature (T) in Kelvin.

The equation for the zenith delay can be written as:

$$\delta trop_{saast} = 0.002277 \cdot \left[p + \left(\frac{1255}{T} + 0.05 \right) \cdot e \right] \tag{3.14}$$

In case of an exclusively hydrostatic modelling, the water vapour pressure (e) is set to zero, resulting in the following equation:

$$\delta trop_{saast} = 0.002277 \cdot p \tag{3.15}$$

In the case of a lack of continuous meteorological measurements, the required parameter can be estimated based on the models presented in Berg (1948). As outlined earlier, the models are not sufficient to describe the total tropospheric delay. For that reason, in order to compensate for the modelling deficiencies and to account for the unmodelled portions of the wet delay, it is common that tropospheric delay parameters are also estimated.

The ionosphere (δion) is the atmospheric layer reaching from $50\,km$ to $1000\,km$ above the earth's surface (Klobuchar, 1991). The ultraviolet radiation of the sun ionises gas molecules, causing them to release electrons. The free electrons influence the microwave signals in terms of speed, direction and polarisation. In reality, the largest effect is the change in the propagation speed of the GNSS signals. The ionospheric condition is specified by the electron density (n_e). Consequently, the impact on the propagation speed of microwaves is characterised by the total electron content (TEC), where:

$$TEC = \int_{sat}^{rec} n_e(pp)\,\mathrm{d}pp \tag{3.16}$$

The integral counts the total number of free electrons in a cross-section of $1m^2$ along the propagation-path (pp). According to Seeber (2003), a first-order approximation of the ionospheric refraction index is given by:

$$n = 1 - \frac{A \cdot n_e}{f^2} \tag{3.17}$$

A is the ionospheric constant ($A = 40.28\,m^3/s^2$). Considering the opposing refraction index for the pseudo range (group delay) (+) and phase observations (-), the actual propagation speed for the pseudo range (v_{Pr}) and the carrier phase (in metres) (v_L) can be written as follows:

$$v_L = \frac{c}{1 - \frac{A}{f^2}} \qquad v_{Pr} = \frac{c}{1 + \frac{A}{f^2}} \tag{3.18}$$

A comparison of the group and phase delays shows that they are comparable in magnitude, but have a different sign. For reasons of simplicity, the propagation-path is generally assumed to follow the geometric range. The TEC along this path is known as slant total electron content (STEC). Based on this assumption, the equations for the ionospheric phase (δion_L) and code (δion_{Pr}) delays can be simplified, according to Seeber (2003), as:

$$\delta ion_L = -\frac{A \cdot STEC}{f^2} \qquad \delta ion_{Pr} = \frac{A \cdot STEC}{f^2} \tag{3.19}$$

The formulation presented so far concentrated on the first-order term of the ionospheric delay, being the baseline implementation. In addition to the presented corrections, there exist further correction models for higher order terms of the ionospheric delay, although these are not yet standard. However, formulations for the second and third order ionospheric effects can be found in Petit and Luzum (2010); Kedar et al. (2003); Fritsche et al. (2005). In common GNSS processing strategies, the first-order term of the ionospheric delay is eliminated by forming the

so-called ionosphere-free linear combination (LC), as discussed in section 3.2.2. An alternative strategy applied in various undifferenced approaches such as those of De Jonge (1998); Odijk (2002); Schönemann et al. (2011); Li et al. (2013), is the utilisation of original (raw) observations and the direct estimation of the total electron content. A detailed description of this procedure is provided in chapter 4 of this thesis.

In order to make different TEC estimates comparable and to allow the application of global ionosphere models, the STEC values can be transformed into the so-called vertical total electron content (VTEC). The VTEC representation condenses the impact of the ionosphere to a single global layer, as demonstrated in figure 3.7.
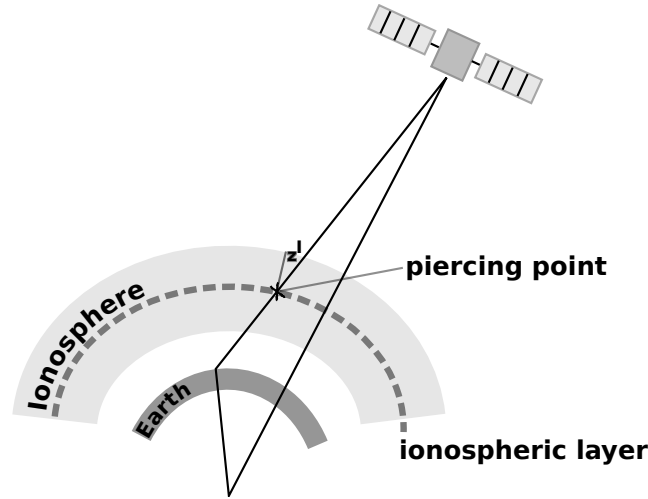
Figure 3.7: Ionospheric single layer model.

This shows the ionospheric layer pierced by the GNSS signal. The value at the piercing point represents the impact of the ionosphere along the signal propagation path. The equation for the transformation from VTEC to STEC and vice versa is given according to Schaer (1999), as:

$$VTEC = \frac{1}{M} \cdot TEC \tag{3.20}$$

with the mapping function:

$$M = \frac{1}{cos(z^I)} \tag{3.21}$$

z^I is the zenith angle of the propagation-path with the ionospheric layer in the piercing point.

Site displacements ($site$)

Because of tectonic, gravitational, rotational forces and loading effects, the site coordinates are variable in time. In order to obtain a single set of coordinates, or in other words to separate the apparent motion from the true motion, these effects need to be modelled and removed from the observation equations. The relative coordinate offset ($site(t)$) at the reception time (t) can be expressed as the sum of the individually coordinated offsets, namely tectonic movement with respect to the reference epoch t_0 ($\delta\vec{x}(t-t_0)$), solid earth tide ($\delta\vec{x}_{set}$), pole tide ($\delta\vec{x}_{pt}$), ocean loading ($\delta\vec{x}_{oc}$) and atmospheric loading ($\delta\vec{x}_{al}$).

$$\delta\vec{X}_{ecef\,site} = \delta\vec{x}(t-t_0) + \delta\vec{x}_{set} + \delta\vec{x}_{pt} + \delta\vec{x}_{oc} + \delta\vec{x}_{al} \tag{3.22}$$

The solid crust and the upper mantle of the earth together called the lithosphere is divided into separate plates that move relative to each other. For most applications aiming to derive instantaneous coordinates, the rather long-periodic effects of tectonic movements can be neglected. However, if longer time-periods are covered in the processing, these effects need to be considered. If necessary, the velocities can be taken from reference frames like the ITRF (Altamimi et al., 2002, 2012). Alternatively, in the case of unknown station velocities, these can be derived from a plate motion model such as NUVEL-1, or from the recalibrated plate motion model NUVEL-1A (DeMets et al., 1994).

The most important reasons for time variable coordinate changes are gravitational forces. The gravitational attraction of celestial bodies, mainly the sun and the moon, causes deformations and changes in the mass distribution of the earth. The most critical tidal effect is the ocean tide, causing ocean loading effects (Scherneck, 1991). It is easy to imagine that the greatest impact of this effect can be found in stations close to the coast. This effect can cause coordinate displacements of up to several centimetres. Like the ocean, the solid body of the earth is also affected by tidal effects. The impact of solid earth tides on the station coordinates can reach up to $40\,cm$ in the radial direction and several centimetres in the horizontal components. The third gravitational impact is the effect of the so-called pole tide. The pole tide is caused by changes to the earth's rotational axis due to polar motion, which causes coordinate changes of up to $25\,mm$ in the radial and $7\,mm$ in the horizontal direction. A summary of up-to-date formulas for the modelling of these effects can be found in the IERS conventions (Petit and Luzum, 2010). In contrast to ocean loadings, that primarily affect stations in coastal regions, atmospheric loadings mainly affect stations on the continental plates. As with the ocean, the atmospheric loading mainly affects the height component. This can result in height displacements of several centimetres (Boy, 2013). Grids of atmospheric corrections are provided by the IERS Special Bureau for Loading (Boy, 2013), see also Van Dam and Wahr (1987); Boy (2011).

Antenna dependent delays (ant)

It is well known that antennae, depending on their purpose (rover, reference station, satellite), type (patch, helix), design (shape, shielding), electronics (filter, amplifier), show different characteristics. In order to gain equipment independent, reliable and comparable results, accounting for these differences is unavoidable. Thus, it is common practice to apply antenna calibration tables for the analysis of phase observations. Even though the antennae also introduce static and variable code/group delays, these are not considered in most applications. Different analyses, such as those by Wübbena et al., demonstrated the existence of group delay variations and the applicability of common antenna (phase) calibration techniques for the calibration of group delays. In addition, Kersten et al. (2012) demonstrated that, in the case of calibrated group delays, the pseudo range rms could be reduced by approximately $6\,\%$. However, since the calibration of group delays is not yet fully developed and established, the following description concentrates on the antenna phase characteristics. Nevertheless, it is most likely that the antenna model and the calibration procedure for phase and pseudo range measurements are almost identical.

In an ideal case, all GNSS signals or, to be more accurate, signal components are received at a single point. For phase measurements, this point is known as the antenna phase centre (APC). The APC is a virtual point, usually in or above the antenna thus; it cannot be used to link the measurement with the measurement point on the ground. For this reason, the antenna reference point (ARP) has been introduced. According to general understanding, the ARP of receiver antennae is described as the crossing point of the antenna centre line and the bottom side of the antenna (Campbell et al., 2004). The situation is different for satellite antennae. Due to a lack regarding information concerning the offset between the antenna mounting point and the satellite's centre of mass (COM), the satellite antenna offsets are directly referred to the COM (Rothacher and Schmid, 2010). In both cases, the link between ARP/COM and APC is described by the so-called phase centre offsets (PCOs).

Up to now, a perfect antenna has been assumed. However, a perfect antenna is equally sensitive to all signals, regardless of their direction, frequency and polarisation. However, considering the impact of the multipath, interferences and so on, these kinds of antennae are not desirable. Therefore, in order to reduce such effects, the antennae are built in such a way as to have maximum sensitivity in the direction of the receiver or transmitter. Figure 3.8 clearly shows the gain pattern of a receiver patch antenna.

This shows that the antenna gain is optimised for the zenith direction, whereas for signals below the horizon, the gain decreases significantly. This antenna optimisation entails the loss of a unique APC. Instead, the APC varies depending on the elevation, azimuth and frequency of the incoming or outgoing signals. Figure 3.9 shows the elevation and azimuth-dependent variation of the L1 PCVs.
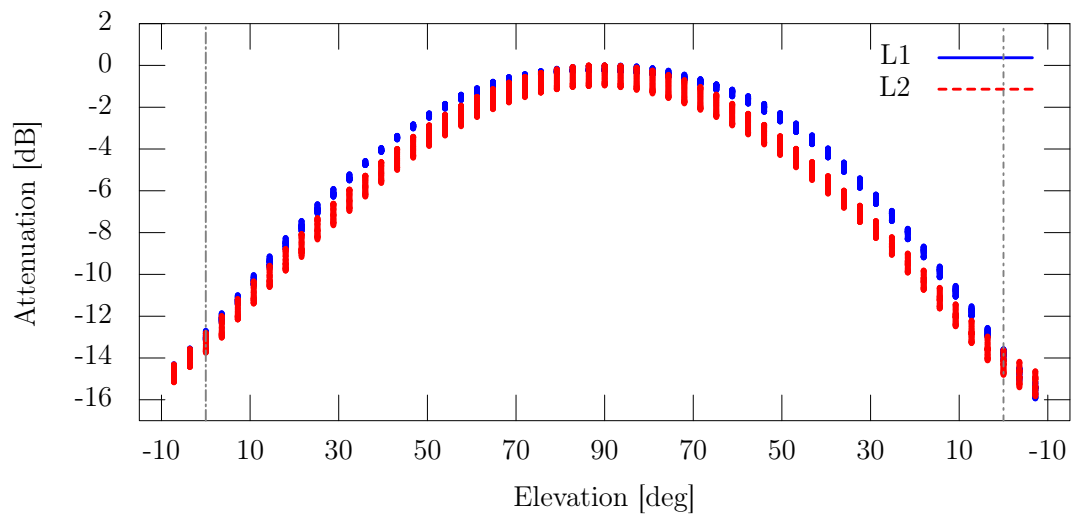
Figure 3.8: Exemplary gain pattern of reference station antenna.
Results of anechoic chamber calibration (Technische Universität Darmstadt / Universität Bonn)
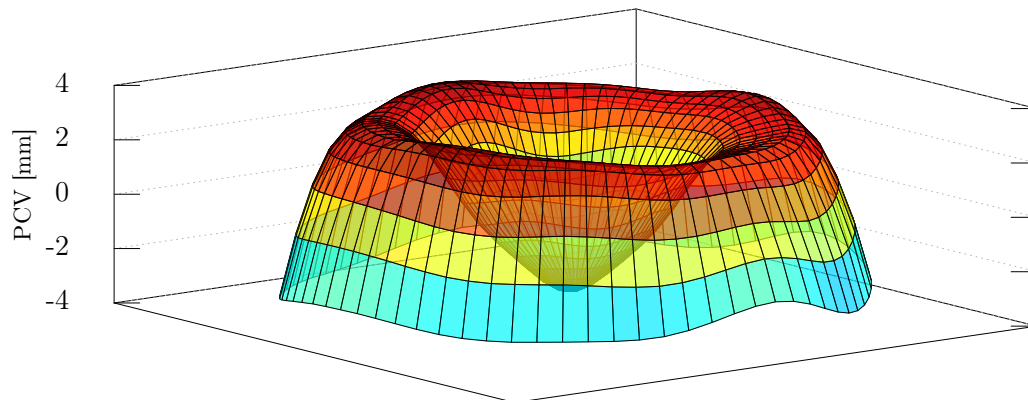
Figure 3.9: Exemplary GPS L1 PCVs of a reference station antenna.
Results of anechoic chamber calibration (Technische Universität Darmstadt / Universität Bonn)

For this reason, the antenna model considers PCVs in addition to the PCOs. Figure 3.10 shows the general antenna model as presented in Campbell et al. (2004).
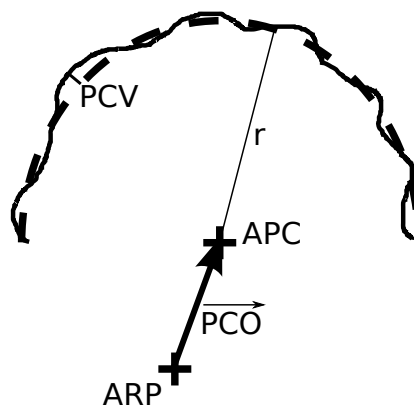
Figure 3.10: General GNSS antenna model.

This shows the ARP to which all measurements need to be referred. The PCO, defined as a three-dimensional vector (north, east, up), establishes the link with the mean APC. Furthermore, the graphic shows the optimal (spherical) wavefront, depicted by a broken line, in contrast the deviation of the true wavefront. The radius of the sphere essentially does not exist, since it is part of the distance measurement and is absorbed by the estimated clock offset. Consequently, the PCV is defined as being different from the optimal spherical wavefront.

Different approaches for the calibration of receiver antennae have been developed and established. Essentially, there are three different approaches; relative field calibrations (Breuer et al., 1995; Rothacher et al., 1996; Mader, 1999), absolute field calibrations (Wübbena et al., 1996) and absolute chamber calibrations (Schupler and Clark, 1991; Zeimetz, 2010). In contrast to the field calibrations, the chamber calibrations make use of artificial signals, usually unmodulated carrier frequencies. All three methods provide reasonable results, whereas for reasons of consistency, the mixing of relative and absolute calibrations is not reasonable. The IGS relative antenna calibrations were the method of choice until November 2005 (Gendt, 2006). Relative antenna calibration makes use of a reference antenna, commonly the AOADM_T (Allen Osborne Associates Dorne Margolin T), assuming its PCVs to be zero. This assumption, together with various other limitations of this technique, lead to systematic errors (Schmid et al., 2005). Since then, the IGS has made use of absolute calibrations.

The calibration of satellite antennae is obviously more difficult. Therefore, apart from a few exceptions (Mader and Czopek, 2002; Wübbena et al., 2007), satellite antennae are not available for ground calibrations. However, Schmid and Rothacher (2003) demonstrated a method for the estimation of elevation-dependent satellite antenna PCVs.

The antenna working group of the IGS provides a consistent set of antenna calibrations for satellite antennae, as well as for all common geodetic receiver antennae. The calibration values of the receiver antennae are type mean values from an absolute field calibration (Wübbena et al., 1996), whereas the satellite antenna calibrations are the result of a global LSQ, making use of the receiver antenna calibration tables. A comprehensive overview of the topic of antenna calibration can be found in Schmid et al. (2007).

Apart from the type mean values as provided by IGS, there is also the option of using individual antenna calibrations. However, it should be noted that even individual antenna calibration does not fully represent the antenna characteristics, particularly since the antenna itself might change its characteristics based on the near field (mounting, etc.). Different analyses demonstrated that, for the ionosphere-free signal combination, the impact of the near field can reach up to a centimetre for the horizontal and up to several centimetres for the height component (Wübbena et al., 2006; Dilssner et al., 2008; Schönemann et al., 2007b). This actually shows that the selection of a suitable location and mounting is more important than are individually calibrated antennae.

Uncalibrated signal delays (DCBs, UCDs, UPDs)

Uncalibrated signal delays, namely UPDs and UCDs as described in section 3.1.2, are a conglomerate of a variety of inseparable effects, such as hardware delays, model inaccuracies, multipath, etc.

It is well known that, in the case of a single GNSS and dual frequency observations, the USDs can be absorbed by the clock estimates and do not need any further consideration. Furthermore, in the case of DDs observations (see section 3.4), the impact of the USDs is mitigated. However, the situation changes as soon as a third signal type comes into play. For this reason, it is common practice to estimate so-called intersystem biases (ISBs). The name ISB has its origin in the joint processing of GPS and GLONASS, where the users faced this issue for the first time. Here, the ISBs were introduced to adapt the GLONASS observations to the "master system", in this case GPS. In fact, the name ISB is not correct. Strictly speaking, it is not a bias between the systems, but is rather a question of receiver dependent USDs. Certainly, the situation is even more complex for GLONASS than for the other GNSS (Wanninger, 2012). Considering the specialty of the multiplexing procedure applied in up-to-date GLONASS satellites (FDMA), each satellite has its own frequency. This again makes it necessary to estimate one bias per satellite. According to Sleewaegen et al. (2012), the different frequency biases can be traced back to a single receiver dependent GLONASS bias, at least for GLONASS phase observations.

In contrast to DD observations requiring a network of stations, the USDs are still present in the observations for standalone PPP applications. In the case of float-valued phase ambiguities, neglecting any ambiguity fixing procedure, the UPDs are absorbed by the float-valued phase ambiguities and therefore have no impact on the processing. However, the handling of UPDs is a major challenge for ambiguity resolution techniques. A deeper insight into this topic is given in section 3.4.

Apart from phase biases, UCDs also need to be considered. Strictly speaking, GNSS products, such as orbit and clock estimates, are only valid for the signal or signal combination applied in the generation process. Consequently, IGS, as well as broadcasted orbits and clocks, are exclusively valid for ionosphere-free signal combinations. This again means that the orbits and clocks, or alternatively the observations, need to be corrected for any other signal or signal combination. The required correction is part of the broadcast message (GPS, 2012a). For the application of IGS orbit and clock products, the corrections are provided in the form of differential code biases (DCBs) (Schaer and Dach, 2010). DCBs describe differences between two specified code observations (C1/P1, C1/P2 and so on) and thus effectively the difference between two UCDs. However, due to the variety of already existing and upcoming signals this definition is no longer the definition of choice. For this reason, the code bias description is currently developing from relative (DCBs) to apparently "absolute" delays (UCDs). In fact, UCDs are relative to the clock definition (see section 4.2). Since all unconsidered delays affect the clock estimates, it must be mentioned that UCDs are of major importance for any timing applications.

Phase-wind-up (pwu)

GNSS signals are right circularly polarised (RCP) radio waves. For relative changes in the satellite receiver antenna orientation, the polarised signal leads to different phase measurements. Figure 3.11 depicts this situation.
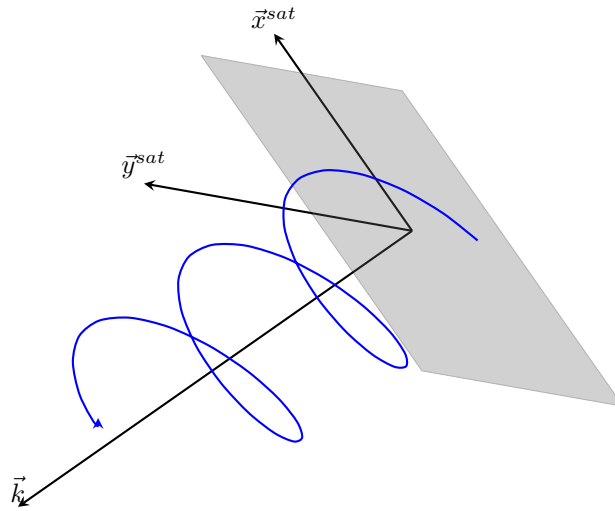
Figure 3.11: Phase-wind-up.

This shows an RHCP radio wave on its way from the transmitter antenna to the receiver antenna. The figure demonstrates that a relative rotation of the transmitting satellite (sat) to receiver (rec) antenna causes the phase to wind up or down. This again means the phase signal is received earlier or later, and therefore results in an apparent change in the satellite receiver distance. According to Wu et al. (1993), the phase wind-up effect (pwu) in radians can be computed from dot($\cdot$) and vector ($\times$) products. For this purpose, each antenna is described by a dipole (D) model:

$$
\begin{aligned}
D^{sat} &= \vec{x}^{sat} - \vec{k}\left(k \cdot \vec{x}_{sat}\right) - \vec{k} \times \vec{y}^{sat} \\
D_{rec} &= \vec{x}_{rec} - \vec{k}\left(k \cdot \vec{x}_{rec}\right) + \vec{k} \times \vec{y}_{rec}
\end{aligned}
\tag{3.23}
$$

where $\vec{k}$ is the satellite to receiver unit vector and $\vec{x}^{sat}, \vec{y}^{sat}, \vec{x}^{rec}, \vec{y}^{rec}$ are the unit vectors of satellite and receiver antennae, pointing in local north and east direction. The phase wind-up correction can then be computed as:

$$
pwu = sign(\zeta)\, arccos\left(\frac{D^{sat} \cdot D_{rec}}{|D^{sat}| \cdot |D_{rec}|}\right) with\ \zeta = \vec{k}\left(D^{sat} \times D_{rec}\right)
\tag{3.24}
$$

To keep the phase continuity between consecutive cycles, a full cycle term (2π) needs to be added to the correction for the transition from one cycle to the next cycle.

Due to the minor wavelength of the carrier phase ($\lambda = c/f \approx 0.18\,m - 0.27\,m$) compared to the receiver-satellite distances, the carrier phase measurements are ambiguous. Consequently, the absolute number of integer phase cycles cannot be measured. For this reason, carrier phases are measured relative to the so-called initial phase ambiguity, containing an unknown number of phase cycles (Remondi, 1985). In order to make the phase measurement absolute, it is necessary to recover the original number of phase ambiguities. According to the physical understanding, the number of carrier phase ambiguities is an integer (N). However, for numerous reasons discussed later in section 3.4, the recovery of this integer number is not an easy task. Therefore, it is common practice to estimate float valued phase ambiguities (Nf), at least as a first approximation.

3.2.2 Error mitigation by observation differences and combinations

As outlined in the previous section, not all disturbances and biases can be sufficiently modelled. As a result, different techniques such as linear combinations (LCs) and observation differences have been developed to mitigate the remaining biases. The target of these techniques is the design of new observations that optimise the observation characteristics. However, the negative aspect of combinations and differences is the loss of the original (raw) observations and, consequently their physical characteristics. This again means that the impact of disturbances on the observations is not one-to-one explainable by physical models. In the following, the most relevant linear combinations and signal differences are briefly introduced.

Linear combinations

Linear combinations (LCs) are combinations of measurements belonging to the same link and to the same epoch. LCs are designed to optimise the observation characteristics for specific tasks. Nevertheless, there are two main objectives for the formation of LCs. The first objective is the mitigation of errors, such as the ionospheric delay, or the highlighting of selected effects, such as the ionospheric delay or multipath. The second objective is the generation of observations with different wavelengths, required to facilitate the recovery of the integer ambiguities.

It is possible to generate observations with different wavelength (λ) or different sensitivities to atmospheric and environmental disturbances. However, the advantages of LCs are accompanied by increased noise and a loss of the physical observation characteristics. LCs can be formed by two, three or multiple different observations. Linear combinations making use of more than two frequencies have been proposed and demonstrated in three carrier ambiguity resolution (TCAR) and multi carrier ambiguity resolution (MCAR) methods (Vollath et al., 1998; Han and Rizos, 1999; Eissfeller et al., 2007; Odijk et al., 2002; Richert and El-Sheimy, 2007). Since the number of possible LCs is enormous and cannot be completely covered, the following overview concentrates on the most common dual-frequency LC combinations, which are also of importance for further discussions. For reasons of clarity, in the following, the phase observations are expressed in metres described by $L = Ph * \lambda$.

Ionosphere free linear combination

For most applications, the ionospheric delay on signals cannot be sufficiently modelled. Therefore, the so-called ionosphere-free LC is the basis of most GNSS processing approaches. This combination aims to mitigate the impact of the first-order ionospheric delay by the combination of observations on two frequencies. For phase observations, the ionosphere-free LC (L_{IF}) can be expressed as follows (Beutler et al., 2007):

$$L_{IF} = \frac{1}{f_1^2 - f_2^2} \left(f_1^2 L_1 - f_2^2 L_2 \right) \tag{3.25}$$

The indices indicate the first and the second frequency. For code observations, the ionosphere-free LC (Pr_{IF}) can be written as follows:

$$Pr_{IF} = \frac{1}{f_1^2 - f_2^2} \left(f_1^2 Pr_1 - f_2^2 Pr_2 \right) \tag{3.26}$$

Geometry free linear combination

In contrast to the ionosphere-free LC, mitigating the impact of the ionospheric delay, the geometry free LC (L_{GF}, Pr_{GF}) exposes the ionospheric delay. Because of this characteristic, it is often used for the estimation of ionosphere models. The geometry-free LC is formed by the difference between two measurements on different frequencies, with the result that all non-frequency dependent errors, such as satellite, receiver clock and geometry (orbit and station coordinates) are removed. For the phase observation (L_{GF}), the geometry-free LC is given as (Beutler et al., 2007):

$$L_{GF} = L_1 - L_2 \tag{3.27}$$

For code observations (Pr_{GF}) it can be equally written as:

$$Pr_{GF} = Pr_2 - Pr_1 \tag{3.28}$$

Widelane linear combination

The relationship between observation noise and wavelength is of major importance for the recovery of the integer characteristics of the phase ambiguities (see section 3.4). Therefore, the widelane LC (L_{WL}) is used to increase the wavelength of the phase observation. The widelane linear combination is formed as follows (Beutler et al., 2007):

$$L_{WL} = \frac{1}{f_1 - f_2} \left(f_1 L_1 - f_2 L_2 \right) \tag{3.29}$$

Melbourne-Wübbena linear combination

The Melbourne-Wübbena LC (L_{MW}), proposed by Melbourne (1985); Wübbena and Goad (1985), can be seen as an extension to the widelane LC. In addition to the phase observations (L_{WL}) forming the first part of the equation, code observations are used in the second part to mitigate the ionospheric effects. Thus, the L_{MW} is free from ionospheric delays, geometry, clock, and tropospheric effects. The disadvantage of the inclusion of code observations in the LC is the significant increase of the observation noise and the multipath effects. However, in the future, advanced code modulations with significantly improved noise characteristics will considerably reduce the noise of this combination. The Melbourne-Wübbena LC is formed as follows:

$$L_{MW} = \frac{1}{f_1 - f_2} \left(f_1 L_1 - f_2 L_2 \right) - \frac{1}{f_1 + f_2} \left(f_1 Pr_1 + f_2 Pr_2 \right) \tag{3.30}$$

With the exception of the multipath error (mp) and the measurement noise (ϵ), this equation contains only the L_{MW} ambiguities. Consequently, it can be used for cycle slip detection for the original phase observations. In the case of low code noise, low multipath and real-value widelane ambiguities, the L_{MW} can be used for the resolution of widelane ambiguities (see section 3.4).

Characteristics of linear combinations

It is clear that the phase noise, as well as the noise of the pseudo range measurements, depend on different parameters such as the signal to noise ratio, among others. Hence, the comparison of absolute values is almost impossible. Therefore, in the following, the noise of the different carriers and LCs is specified relative to the noise of the carrier of the GPS L1 frequency (L1). According to the theory and as demonstrated in different publications such as those by Simsky et al.; Schönemann et al. (2007a), phase tracking noise is independent from the signal modulation. In the cycle domain it is equal for all carriers, but when converting the measurement into units of length it becomes proportional to the wavelength. Hence, the noise of the carrier measurement relative to L1 can be expressed as $\epsilon_n = \epsilon_{L1} \frac{f_n}{f_{L1}}$. Furthermore, the noise of the different LCs can be determined using the law of error

propagation. Table 3.1 summarises the wavelength and the noise characteristics of the introduced LCs. For reasons of clarity, the summary concentrates on the GPS carriers and the respective dual-frequency LCs.

LC / Carrier	λ [m]	Noise Rel. to L1	Iono. Delay Rel. to L1
L1	0.19	1.00	1.00
L2	0.24	1.28	1.63
L5	0.25	1.34	1.67
L_{IF} (L1 - L2)	0	3.22	0.00
L_{IF} (L1 - L5)	0	2.82	0.00
L_{IF} (L2 - L5)	0	21.78	0.00
L_{GF} (L1 - L2)	∞	1.27	-0.65
L_{GF} (L1 - L5)	∞	1.25	-0.79
L_{GF} (L2 - L5)	∞	1.08	-0.08
L_{WL} (L1 - L2)	0.86	5.74	1.28
L_{WL} (L1 - L5)	0.75	4.93	1.34
L_{WL} (L2 - L5)	5.86	25.39	1.04
L_{MW} (L1 - L2)	0.86		0.00
L_{MW} (L1 - L5)	0.75		0.00
L_{MW} (L2 - L5)	5.86		0.00

Table 3.1: Characteristics of dual-frequency linear combinations based on GPS carrier frequencies.

It is obvious that the advantages gained from LCs, such as longer wavelength or lower impact of the ionosphere, is at the expense of an increased measurement noise. The noise of the Melbourne-Wübbena combinations depends on the quality of the code observations. Therefore, it cannot be easily compared to the carrier noise

Observation differences and their characteristics

Observation differences are a further technique for cancelling error sources in observations. The goal of this technique is the cancelling of common biases by differences. It is well known and described later in chapter 4 that undifferenced observations, often referred to as zero-difference (ZD) observations, contain a number of parameters, being difficult or impossible to model. Examples of these parameters are USD or clock estimates. The simplest observation difference is the single-difference (SD). In fact, SDs are not clearly defined. Depending on the application, there are actually two ways to form SDs. Variant one is the difference in observations originating from one satellite and two receivers:

$$\Delta Ph^1_{1,2} = Ph^{sat1}_{rec1} - Ph^{sat1}_{rec2} \qquad \Delta Pr^1_{1,2} = Pr^{sat1}_{rec1} - Pr^{sat1}_{rec2} \qquad (3.31)$$

Thus, all satellite effects common to both observations, such as satellite clock, orbit errors and satellite USDs are cancelled out. However, the receiver portions remain in the equation. Variant two is the difference of observations originating from two satellites and one receiver:

$$\Delta Ph^{1,2}_1 = Ph^{sat1}_{rec1} - Ph^{sat2}_{rec1} \qquad \Delta Pr^{1,2}_1 = Pr^{sat1}_{rec1} - Pr^{sat2}_{rec1} \qquad (3.32)$$

In this case, all common receiver effects, such as receiver clock and receiver USDs are cancelled out, preserving all satellite-dependent effects. The difference between two equally formed SDs, no matter which variant, is known as double-difference (DD):

$$\nabla\Delta Ph^{1,2}_{1,2} = \Delta Ph^{1,2}_1 - \Delta Ph^{1,2}_2; \qquad \nabla\Delta Pr^{1,2}_{1,2} = \Delta Pr^{1,2}_1 - \Delta Pr^{1,2}_2 \qquad (3.33)$$

This second difference again cancels the common effects, the receiver for variant one and, for variant two, the satellite biases. Therefore, DD observations are free from receiver- and satellite-dependent biases. For this reason, DD observations are optimally suited to ambiguity resolution.

The satellite positions must be known for standalone PPP solutions. For applications aiming for decimetre-metre accuracy, the satellite positions can be derived from the navigation message broadcast by the navigation satellite itself. The required formulas for this computation are given in the respective ISs and ICDs (GPS, 2012; etc.). For precise applications, interested in highest accuracy (millimetre-centimetre) broadcast orbits are not sufficient. Such applications usually make use of precise orbits from external sources, such as commercial providers or the IGS. A common exchange format for precise satellite orbits is the Standard Product 3 (SP3) format (Spofford and Remondi, 2010; Hilla, 2010). SP3 files contain ECEF satellite positions and clock information, usually sampled with a sampling rate of $15\,min$. Different interpolation methods have been proposed in order to compute the satellite positions at the required time. A summary of interpolation methods and the corresponding performance analyses can be found in Schenewerk (2003); Feng and Zheng (2005); Horemuž and Andersson (2006).

In contrast to a standalone PPP solution, precise orbit determination (POD) procedures aim to determine the satellite orbit. However, POD is not the target of this thesis, but is rather a technique to validate the results of the implemented processing scheme. Therefore, in the following, only a broad overview of the basics of orbit determination is given. For a more comprehensive description of POD, refer to Beutler (2005); Vallado (2007); ESOC (2009). It is the aim of a POD to solve the satellite equation of motion, as described by Springer (1999):

$$\ddot{\vec{X}}^{sat}_{gcrs} = -GM_E \cdot \frac{\vec{X}^{sat}_{gcrs}}{|\vec{X}^{sat}_{gcrs}|^3} + \vec{a}(t^t, \vec{X}^{sat}_{gcrs}, \dot{\vec{X}}^{sat}_{gcrs}, q_1, q_2, \ldots, q_n) \tag{3.34}$$

The equation can be divided into two terms, the gravitational forces depending on the gravitational constant of the earth (GM_E) and the total perturbing acceleration ($\vec{a}$), being a function of:

$$
\begin{array}{ll}
t^t & \text{transmission time} \\
\vec{X}^{sat}_{gcrs} & \text{satellite position (centre of mass) (GCRS)} \\
\dot{\vec{X}}^{sat}_{gcrs} & \text{satellite velocity (centre of mass) (GCRS)} \\
q & \text{dynamical parameters}
\end{array}
$$

In addition to the gravitational attraction of the earth described by the first part of the equation, numerous other forces act on the satellite. Examples are the solar radiation pressure, the non-sphericality of the earth's gravity field, gravitational forces of third bodies (the sun, the moon and so on) and the earth and ocean tides. A detailed description of the different force models can be found in Tapley et al. (1996); Agrotis (1984); Rosen and Center (1967).

In order to solve this second order differential equation unequivocally, six initial conditions are required. These are given by the satellite position and the velocity vectors at the starting time. Due to the complexity of the function, the equation of motion (equation 3.34) cannot be solved analytically. For this reason, it is common practice to solve it by numerical integration, as described in Beutler (2005); Vallado (2007); ESOC (2009). Finally, once the satellite state vector and the forces acting on the satellite are known, the satellite position can be computed at any time by integration.

However, in order to account for the fact of model inaccuracies, the estimation of different empirical model parameters is required in addition to the satellite state vector. The most common parameters are the nine parameters of the Center for Orbit Determination in Europe (CODE) solar radiation pressure (SRP) model (Springer, 1999) and the so-called cycle-per-revolution (CPR) (ESOC, 2009) parameters, accounting for gravitational and atmospheric forces.

Earth orientation parameters (EOPs) represent the link between the celestial reference system (CRS), realised by the satellite orbits and the terrestrial reference system (TRS), realised by the coordinates of the tracking stations. EOPs denote the full set of parameters, such as pole coordinates (xp, yp), UT1 and two nutation angles, which are required for the description of the earth's orientation in the inertial frame. The pole coordinates are directly accessible by space geodetic techniques, whereas, due to the correlation of the orbital parameters with UT1 and the nutation angles, these are not observable in an absolute sense. For this reason, space geodesy is often restricted to earth rotation parameters (ERPs) instead of to EOP. ERPs are a subset of the EOP, renouncing nutation angles. However, as presented in Rothacher et al. (1999), the rates of the nutation angles and the length of day (LOD) (LOD = UT1-UTC) can be derived from the first derivatives of the orbital elements. The latest transformation formulas from CRS to TRS can be found in the IERS conventions (Petit and Luzum, 2010).

3.3 Parameter estimation

Once the error models are applied to the right side of the observation equation (see equation 3.2), the equation consists of the observation, the corrected "true" range and a number of unknown parameters, like station coordinates, receiver clock and so on. Established methods for the solution of over-determined GNSS problems are filter or LSQ approaches. The main focus of this thesis is GNSS analyses and highly precise applications. The majority of these applications are run in post-processing, making use of LSQ approaches. For this reason, the basics of LSQs are briefly outlined in the following. A comprehensive description of this approach can be found in Koch (1999) and in Niemeier (2002).

The starting point of an LSQ is an over-determined system of equations. Over-determined means that the number of observations (m) is greater than is unknown parameters (n). Furthermore, the LSQ approach assumes the measurement to be observations (b) of a phenomenon, describable by a linear function. Giving A as the coefficient matrix ($m \times n$) and x the unknown parameter vector of type (n), the observation equation can be expressed as:

$$v = Ax - b \tag{3.35}$$

The vector v (m) comprises the observation corrections (or residuals). The fundamental idea behind the Gauß - Markoff model is the minimisation of the weighted square sum of the observation corrections (or residuals). With the matrix P ($m \times m$) being the symmetric weighting matrix, this condition can be expressed as a function $f(x)$:

$$f(x) = v^T P v = minimum \tag{3.36}$$

The function $f(x)$ reaches its minimum for partial derivatives with respect to x being equal to and the second derivatives greater than zero.

$$A = \frac{\partial f(x)}{\partial x_k} = 0 \qquad \frac{\partial^2 f(x)}{\partial^2 x_k} > 0 \qquad (k = 1, 2, \ldots, n) \tag{3.37}$$

This condition leads to the equation:

$$A^T P A x = A^T P b \tag{3.38}$$

Rearranging this equation gives the estimated values for $\hat{x}$ as :

$$\hat{x} = \left(A^T P A \right)^{-1} A^T P b \tag{3.39}$$

In the case of a non-linear functional model, as in the case of the GNSS observation equation, the parameters can be determined numerically in an iterative process. For this purpose, approximate values (x_0) are used for the unknown parameters. Based on these values, the improvements ($\Delta\hat{x}$) can be computed by the following equation:

$$\Delta\hat{x} = \left(A_0^T P A_0\right)^{-1} A_0^T P w \tag{3.40}$$

with

$$
\begin{aligned}
w &= b - f(x_0) \quad &\text{observed - computed} \\
\Delta\hat{x} &\quad &\text{improvements to starting values}
\end{aligned}
$$

This procedure is repeated, making use of the updated parameters until the prior defined convergence criterion is met. After the last iteration, the unknown parameters can be computed as:

$$\hat{x} = x_0 + \Delta\hat{x} \tag{3.41}$$

3.4 Resolution of carrier phase ambiguities

As previously outlined in section 3.2.1, carrier phase measurements are biased by an unknown number of phase ambiguities. Consequently, the carrier phase measurement is a relative measurement referring to the initial phase ambiguity. In order to transform the carrier phase measurement to an absolute range, it becomes necessary to estimate and apply the unknown carrier phase ambiguity. Following the physical understanding of wave propagation, the number of phase ambiguities is an integer value (Remondi, 1985). A simplified depiction of the situation is presented in figure 3.12. The top part of the figure illustrates the situation for an optimal case, disregarding errors
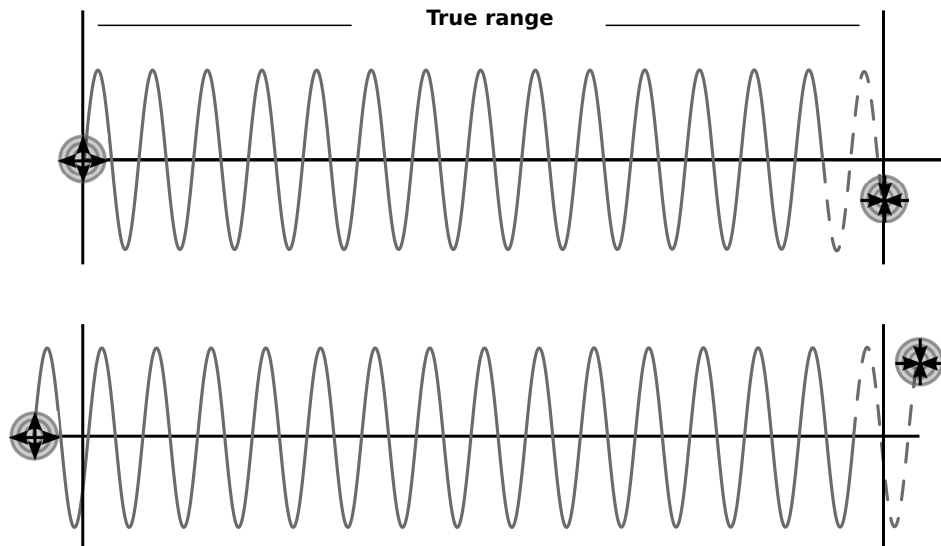
Figure 3.12: Characteristics of phase ambiguities.

and model inaccuracies. In this case, the true range can be described by an integer number of carrier phase ambiguities represented by the solid and the fractional phase measurement by the dashed line. As a result of hard- and software delays, model inaccuracies and numerous other delays jointly referred to as satellite and receiver UPDs (see section 3.2.1), this description is not comprehensive. The lower part of figure 3.12 shows effectively that the point of signal generation and reception is not coincident on the starting and end point of the true geometric distance, corrected by modelled effects. The situation is further complicated by the fact that UPDs are not constant, neither in the satellite (Montenbruck et al., 2011) nor in the receiver (Wübbena et al., 2012). Consequently, at least at the beginning of the process, the carrier phase ambiguity has to be seen as float valued (Nf). It is easy to

imagine that this, in contrast to the application of integer phase ambiguities renouncing the float-valued portions, increases the noise of the adjusted range significantly.

In order to understand the impact of the increased measurement noise on the positioning solution, it is worthwhile to examine the orientation of the satellite orbits. Figure 3.13 clearly shows the satellite ground tracks for the four active Galileo (red) and three arbitrary GPS (green) satellites. It is obvious that, except for high latitudes, the satellite tracks are mostly north-south oriented. The orientation of the ground tracks is caused by a combination of the inclination of the satellite orbits (GPS 55°, Galileo 56°), their speed and the rotation of the earth (Melbourne, 1985). It is clear that, from the geometric point of view, the north-south orientation of the orbits prevents a reasonable distinction of the ranging bias and the east-west component of the receiver coordinate. This fact becomes obvious when analysing the accuracy of the different coordinate estimates. Thus, the east-west component shows a degradation by a factor of 2 - 5 compared to the north-south component (Blewitt, 1989).
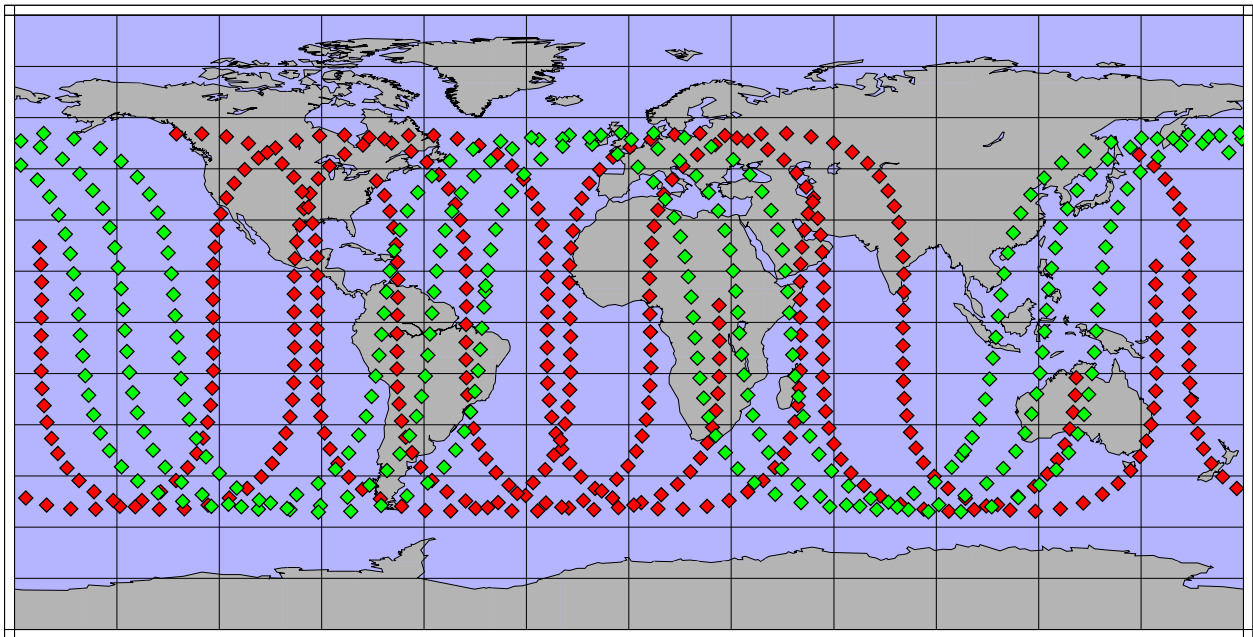
Figure 3.13: Satellite ground tracks for GPS (green) and Galileo (red).

In order to stabilise the absolute estimate of the carrier phase measurement, different techniques for integer ambiguity resolution have been developed. Inevitably, all these techniques are based on the assumption of integer-valued carrier phase ambiguities, no matter how this is realised. The most common and efficient procedure to remove fractional-phase-cycles from the observations is by the differences (see section 3.2.2). Due to the importance of observation differences for ambiguity resolution, a summary of the most important characteristics is given in following table 3.2.

This shows the most important differences and their meaning for bias mitigation. In the case of bias mitigation, the parameter is checked ($\checkmark$). Otherwise, if it remains in the observation, it is crossed ($\times$). It is important to remember that exclusively common error portions cancel out in the differences. This particularly concerns the mitigation capabilities (s) of the tropospheric delay for which, depending on the variability of the regional atmosphere, the impact can only be mitigated for short baselines of a couple of kilometres. In the case of a zero baseline (a baseline between two GNSS receivers, connected to the same antenna), all listed effects are common and cancel out. With increasing baseline length, the atmosphere, the time of transmission, the signal path and consequently the biases become increasingly different. However, when using precise orbits and clock offsets, most of the biases, except the atmospheric delays, can be mitigated sufficiently by observation differences, even for base lines of several thousand kilometres (Blewitt, 1989).

The most conspicuous statements in table 3.2 are the characteristics of undifferenced and DD observations. It becomes obvious that undifferenced observations still contain all biases, whereas for DD observations, with the exception of the atmospheric and multipath effects, all relevant biases are mitigated. Depending on their formation, SD observations contain either satellite or receiver related biases. In fact, no matter which observation difference is

	DD	$SD^{\Delta sat}$	$SD_{\Delta rec}$	ZD
Satellite clock offset (δt^{sat})	✓	✗	✓	✗
Satellite PCO/PCV ($\delta pco^{sat}/\delta pcv^{sat}$)	(✓)	✗	(✓)	✗
Satellite UCD (ucd^{sat})	✓	✗	✓	✗
Satellite UPD (upd^{sat})	✓	✗	✓	✗
Satellite position ($\vec{X}^{sat}_{gcrs}$)	✓	✗	✓	✗
Ionospheric delay (δion)	✗	✗	✗	✗
Tropospheric delay ($\delta trop$)	s	s	✗	✗
Multipath (mp)	✗	✗	✗	✗
Receiver clock offset (δt_{rec})	✓	✓	✗	✗
Receiver PCO/PCV ($\delta pco_{rec}/\delta pcv_{rec}$)	(✓)	(✓)	✗	✗
Receiver UCD (ucd_{rec})	✓	✓	✗	✗
Receiver UPD (upd_{rec})	✓	✓	✗	✗
Receiver position ($\vec{X}_{rec}$)	✓	✓	✗	✗

Table 3.2: Observation differences and their impact on the most important biases.

used, all of them are still affected by the ionospheric delay. However, there are two approaches to the mitigation of ionospheric delays in the observations. The first and most common approach makes use of ionosphere-free LCs as described in section 3.2.2; however, direct estimation of the slant total electron content (STEC), as demonstrated in Odijk (2002); Schönemann et al. (2011); Li et al. (2013), is also possible. The utilisation of the ionosphere-free LC has its advantages in terms of computational burden and the configuration of the normal equations, but also has numerous disadvantages in terms of weighting, flexibility and analysis capabilities. However, this topic is discussed in more detail in chapter 4. After accounting for the ionospheric delays, DD observations are almost free of disturbing biases hampering an integer resolution, with the exception of multipath effects.

However, since DD observations can only be formed in the case of more than one receiver and are triggered by the increasing interest in instantaneous high-precision standalone PPP solutions, SD or even undifferenced ambiguity resolution techniques are currently under development. The challenge for these approaches is the handling of the biases remaining in the equation, such as satellite and/or receiver UPDs, PCOs/PCVs model inaccuracies. The straightforward solution would be an a priori calibration of satellite- and receiver-induced UPDs. However, as outlined at the beginning of this section and as demonstrated in chapter 6, neither the receiver nor the satellite biases can be sufficiently calibrated. Therefore, different approaches for network-based, real-time calibration have been developed. These can be divided into two groups, one making use of fractional-cycle-biases (FCBs) (Ge et al., 2008) and one based on integer-recovery-clocks (IRCs) (Laurichesse et al., 2009; Collins, 2008; Loyer et al., 2012). In general, both approaches apply the same strategy. The main difference can be seen in the procedure to decouple the narrow-lane FCBs from the observations. Ge et al. (2008) estimates float-valued ambiguities, whereas Laurichesse et al. (2009) account for this bias in the so-called IRCs (Geng et al., 2010). The actual difference from the common DD approaches is the estimation of satellite- and receiver-dependent wide- and narrow-lane UPDs. The resulting rank defect in the normal equation matrix is either solved by the application of SD observations (2 satellites + 1 station) or by fixing one UPD per type to zero.

An alternative approach, making use of raw instead of wide- and narrow-lane observations, was demonstrated by Li et al. (2013). He directly estimated L1 and GPS L2 UPDs, whereas the rank defect of the normal equation in this case is solved by a number of constraints. Thus, the network-sided estimation makes use of precise satellite orbits and clocks and fixed station coordinates. The rank defect caused by the correlation of UPD and STEC estimates is solved by different ionospheric constraints, such as external models and temporal and spatial constraints. However, because neither the a priori ionospheric models nor the accuracy of the estimated L1 and L2 ambiguity is sufficient for a direct determination of UPDs, the excursion via wide and narrow-lane ambiguities is again required (Li et al., 2013).

Once all biases, including ionospheric delay and UPDs are handled properly, the integer number of ambiguities can be recovered. Here, it is irrelevant which observation type (DD, SD, ZD) is used. The most well-known procedure for the recovery of integer ambiguities is the Least-squares Ambiguity Decorrelation Adjustment (LAMBDA) method (Teunissen et al., 1995). However, none of the methods is able to resolve all independent ambiguities faultlessly. Due to observation noise and the remaining systematic biases, a unique solution is impossible. The actual success rate depends on different factors, such as the applied functional and stochastic models, the selected fixing method

and, finally, the balancing of the probabilities (Joosten and Tiberius, 2000). In fact, it is all about maximising the probability of finding the correct integer ambiguities. It is clear that integer ambiguity helps to improve the positioning solution, but it is also clear that wrongly-fixed integer ambiguities cause significant positioning errors. A comprehensive overview of integer ambiguity estimation and validation is given in Verhagen (2005).

In order to demonstrate a standard procedure for DD integer ambiguity recovery, the concept applied within this thesis is outlined briefly in the following (ESOC, 2009). The applied method resembles the network method proposed by Blewitt (1989). However, to save computational time and in contrast to the network method, the DD ambiguities are formed per baseline in the first step, neglecting the network geometry. Indeed, the maximal length of baselines is limited ($< 6000\,km$). The procedure starts with the computation of the DD Melbourne-Wübbena widelane ambiguities. In the next step, these are sorted and fixed, based on the value of their probability function. The probability function (P_0) can be written as (ESOC, 2009):

$$P_0 = 1 - \sum_{k=1}^{\infty} erfc\left(\frac{k - (N_{wl} - nInt)}{\sqrt{2}\sigma}\right) - erfc\left(\frac{k + (N_{wl} - nInt)}{\sqrt{2}\sigma}\right) \tag{3.42}$$

with error function ($erfc$):

$$erfc(x) = \frac{2}{\sqrt{\pi}} \int_x^{\infty} e^{-t^2}\,dt \tag{3.43}$$

N_{wl} Widelane DD-ambiguity estimate in cycles
$nInt$ Nearest integer
σ Widelane DD-ambiguity sigma in cycles

Once the widelane ambiguities are fixed successfully, the narrow-lane ambiguities are formed and fixed accordingly. However, it is important to ensure the exclusive fixing of the independent ambiguities. Therefore, in order to obtain an independent set of carrier phase ambiguities, the sorted list of ambiguities is searched from high fixing probability to low. At this point, the independence of the ambiguities is checked using the modified Gram-Schmidt method. Up to this point, all ambiguities, regardless of their network geometry, are handled. For this reason, a second independence check is performed, making sure that the ambiguities are independent from the network point of view as well (ESOC, 2009).

Finally, the information from the independent set of DD ambiguities needs to be applied to the normal equations. For this purpose, the equations describing the DD residual to the nearest integer are given by:

$$DDx_N = \Delta dd \tag{3.44}$$

Being x_N the affected ambiguities and Δdd the DD residuals to the nearest integer, added to the normal equation system (ESOC, 2009):

$$\begin{bmatrix} Q_{11} & Q_{12} \\ Q_{21} & Q_{22} + \frac{DD'DD}{\sigma^2} \end{bmatrix} \begin{bmatrix} x_1 \\ x_2 \end{bmatrix} = \begin{bmatrix} b_1 \\ b_2 + \frac{DD'\Delta dd}{\sigma^2} \end{bmatrix} \tag{3.45}$$

In order to give the DD integer ambiguity conditions a strong weight, close to fixing them, it is important to use a small value for σ. The solution to the normal equation gives the new values for the initial, undifferenced ambiguities. It is easy to imagine that the disturbances on shorter baselines are generally more similar. Consequently, the DD ambiguities of shorter baselines are easier to fix. It is also clear that ambiguity fixing improves the accuracy of the GNSS solution and thus the capabilities for further integer ambiguity fixing. Therefore, the fixing procedure is run in different iterations, with the result that DD ambiguities that are not fixable in the first iteration can be accounted an integer value in the subsequent runs.

4 Analysis of raw GNSS observations

In principle, the most straightforward approach for GNSS analyses is the processing of original (raw) observations. This approach waives any kind of linear combinations (LCs) and observation differences. Accordingly, it applies the observation equation in its original form. As a result, several effects and biases wiped out by linear combinations or observation differences remain in the equation and require an appropriate treatment. Equation 4.1 recalls the GNSS observation equations from the viewpoint of raw observations. For this representation, the term for the atmospheric delays (atm) was replaced by its individual components.

$$
\begin{aligned}
Pr(t) = {} & \rho(t)^{sat}_{rec} + rel(t) + clk(t) + \left(\begin{array}{c} atm(t) \\ trop(t) + \underbrace{ion_{Pr}(t)} \end{array} \right) + site(t) + ant_{Pr}(t) + \underbrace{ucd(t)} + \underbrace{isb(t)} \\
& + mp_{Pr}(t) + \epsilon_{Pr}(t)
\end{aligned}
$$

$$
\begin{aligned}
L(t) = {} & \rho(t)^{sat}_{rec} + rel(t) + clk(t) + \left(\begin{array}{c} trop(t) + \overbrace{ion_{Ph}(t)} \\ atm(t) \end{array} \right) + site(t) + ant_{Ph}(t) + \overbrace{upd(t)} + \overbrace{isb(t)} \\
& + mp_{Ph}(t) + \epsilon_{Ph}(t) + pwu(t) + N\lambda
\end{aligned}
$$

(4.1)

In the case of ionophere free linear combinations mitigated.

In the case of ionophere free linear combinations absorbed by the clock estimates.

In the case of raw observations no longer needed.

This shows that previously mitigated delays, such as the ionospheric delay and the different uncalibrated signal delays UCDs (ucd) and UPDs (upd) remain in the equation. The sources and characteristics of uncalibrated signal delays were discussed in section 3.1.2. Strictly speaking, USDs are a time-variable conglomerate of different inseparable biases, exclusively valid for individual, satellite-receiver signal combinations. However, for reasons of simplicity and to make them treatable for providers of global network products, they are commonly assumed to be time-invariant over 24 hours and satellite-signal and receiver-signal dependent. It is clear that this artificial separation is not necessarily reasonable for all applications. A more in-depth discussion of this aspect can be found in section 5.3.

4.1 Benefits of raw observation analyses

The total renunciation of linear combinations (LCs) and observation differences has numerous advantages. One of the most significant attributes is the conservation of the original physical observation characteristics, which allows for a detailed analysis of all individual effects, biases and components. On one hand, this requires a proper treatment of all these effects and biases but, at the same time, it enables the application of true physical models. An important characteristic of observations is its noise level. For raw observations, in contrast to LCs that are known to amplify the measurement errors, the original error and noise levels are persevered. This fact is demonstrated in figure 4.1. It is generated based on the results of the analysis presented in section 7.1. It shows the standard deviation of the different code and carrier phase residuals of the adjusted observations for one pass of GAL-101 (E11) in Kiruna (KIRU) on day 134 2013. The ionosphere-free LC (E1 - E5a) residuals are derived from a conventional GNSS analysis, whereas all other residuals originate from a single raw observation-based run.
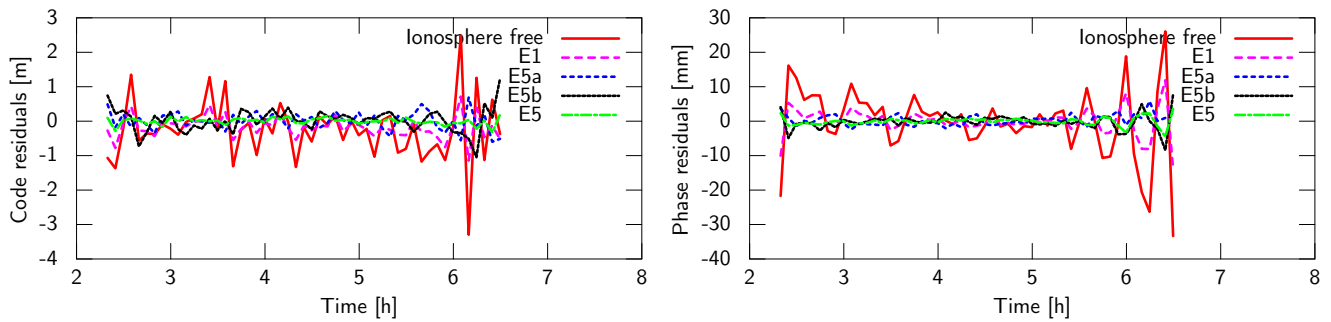
Figure 4.1: Standard deviation of code (left) and phase (right) residuals for different signals (one pass of GAL-101 KIRU, day 134 2013).

At a first glance, the outstanding analytical capabilities of the raw processing approach becomes visible. It shows that effectively all individual signal components can be analysed. The different size of the ionosphere-free LC and the raw observation residual is clearly visible. The magnitude becomes obvious while considering the standard deviation of the residuals, given in table 4.1. In particular, for the phase residuals the difference in the standard deviation is impressive (almost a factor of ten). Another remarkable difference can be found when comparing the code residuals of the AltBOC signal on E5 ($0.09\,m$) against the ionosphere-free LC code observations ($0.67\,m$).

Signal (LC)	Code [m]	Phase [mm]
Iono. free	0.67	10
E1	0.22	1
E5a	0.27	1
E5b	0.27	1
E5	0.09	1

Table 4.1: Standard deviation of code and phase residuals for different signals (one pass of GAL-101 KIRU, day 134 2013).

This, as well as the possibility of combining all observations equally, regardless of their belonging to a GNSS, their signal modulation frequency or number of measurements, predestines this approach for any kind of GNSS analyses. Workarounds, in the form of the misleadingly called intersystem biases (ISBs), are no longer necessary. Under the assumption of identical signal power, the carrier phase noise on L2 is 1.28 times higher than the noise on L1. Considering that the signal power for signals on L2 is lower than on L1 (GPS, 2012a) and that in general carrier phase observations on L2 are less accurate, as demonstrated for antenna calibrations (Zeimetz, 2010), it is clear that a different observation weighting is mandatory. In contrast to the ionosphere free observations, applying a fixed weighting scheme, as for GPS (L1 - L2) a 1.65 times higher weight for observations on the L1 frequency band, the application of raw observations allows an explicit weighting and editing of all individual signal components.

As demonstrated in table 4.1, for pseudo-range observations, the differences among the various signal modulations are even more striking. The ability to process all observations and to estimate all parameters jointly in a single run significantly simplifies the GNSS analysis.

4.2 Challenges of raw observation analyses

The major challenge for the processing of raw observations is the strong correlation of clock offsets, ionospheric delays and USDs. The similarity of the impacts on the observation prevents a clean separation of the individual effects and results in rank deficiencies of the normal equation system.

The treatment of raw observation accompanies a number of strongly correlated unknown parameters, resulting in a rank defect of the normal equation matrix. The following section aims to demonstrate the problems and explains the relationships between the different unknown parameters. The start and the end points for all measurements are the satellite and receiver clocks. For this reason, an accurate knowledge of their offsets versus the "system time" is essential. It should be noted that, in this case, "system time (analysis)" denotes the time realised by a global network analysis, not the system time of an individual GNSS. In a joined analysis of different GNSS, all clocks refer to the same timescale and consequently intersystem time biases no longer exist.

It is a matter of fact that the time offsets of the different clocks cannot be read directly. The only way to access the different clock offsets is estimation, commonly done using GNSS observations. The fact that all GNSS signal components are delayed by an unknown bias (UCDs, UPDs) makes it impossible to estimate the true clock. Furthermore, the correlation of uncalibrated signal delays and the clock estimate causes a rank defect, resulting in a matrix singularity. Figure 4.2 sketches the situation for one GPS and one Galileo satellite, both of which are tracked by the same receiver. It shows the "system time (analysis)" realised by the adjustment, usually the mean
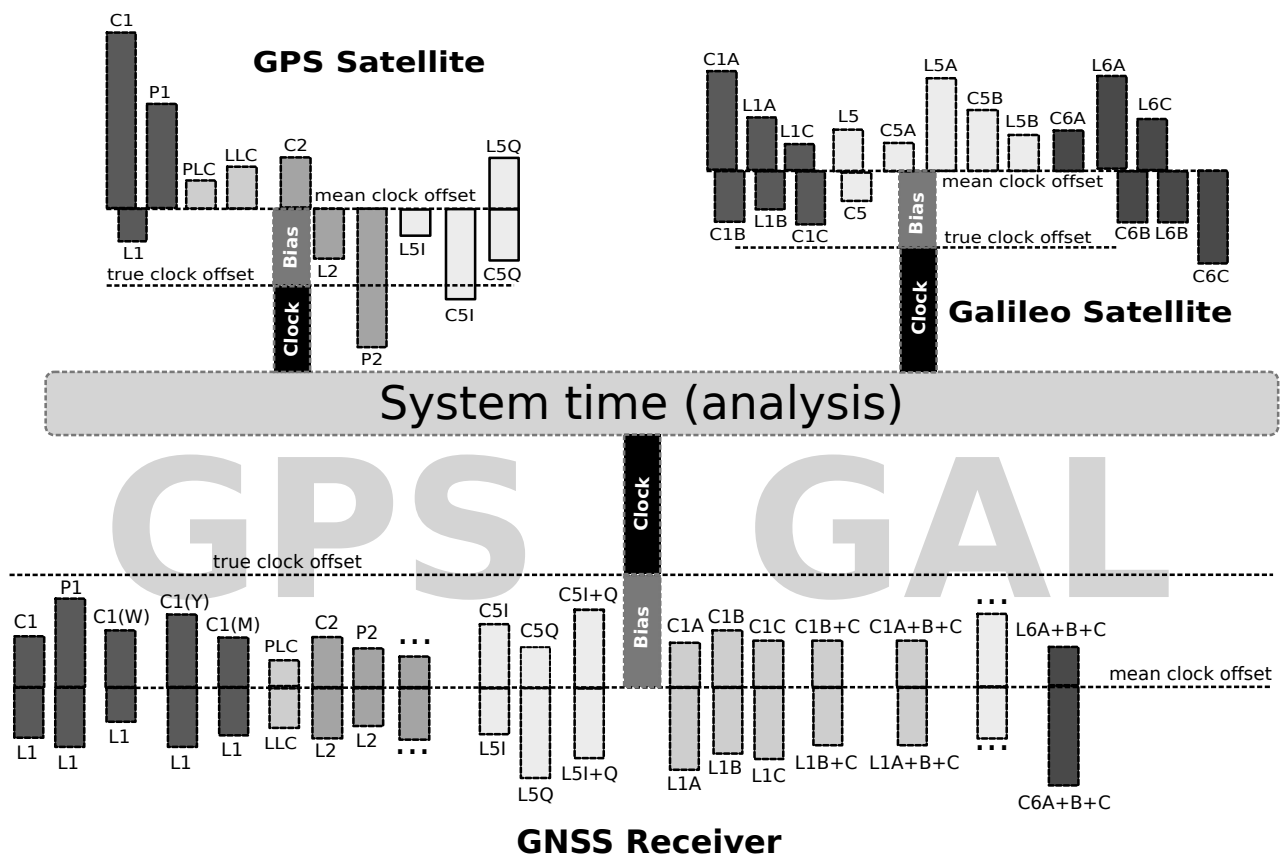
Figure 4.2: Problem of clock definition.

clock of the global network analysis and the individual true clocks, displaced by an unknown, undefinable offset, the clock bias. In order to solve the rank defect, a clock definition or, in other words, an assumption regarding the uncalibrated signal delays is mandatory. However, due to the unknown number of carrier phase ambiguities, carrier phase measurements are not suitable to define the clock.

In general, the most straightforward solution for a clock definition is a zero mean condition per clock, assuming the sum of the UCDs to be zero. In a physical sense, this solution is implausible because it would imply that some code signal components accelerate, whereas others slow down. The advantage of this condition is that it is applicable independent from the type of the transmitted and received signals. The main disadvantage of this solution is the variability of the clock estimate. In fact, any shift in the distribution of code observations between different signals results in changes to the composition of the UCDs and therefore affects the clock estimate. The impact of signal delays on the clock estimates is discussed more in detail in section 7.1.3. From this point of view, the most reasonable solution is the assumption of a single, unbiased signal component per satellite and receiver. The selection of a unique, error-free code signal component that is equally valid for all satellites and receivers is not possible. This becomes apparent when comparing the signals transmitted by the two satellites in figure 4.2. This shows that they have no signal in common. The situation becomes even more complicated when taking into account the different tracking modes (Gurtner and Estey, 2009) and receiver settings, again causing a variety of different delays. It has to be mentioned that figure 4.2 shows the variety of signals in a rudimentary way. In reality, the situation is even more complex. An additional difficulty is the diversity of available receivers like GPS only, GPS + GLONASS and GPS + Galileo, as well as their different configurations. Thus, it is impossible to originate a simple standard for clock definition. Rather, it is essential to know about the problem and to account correctly for the biases.

The different signal delays and the clock definition are no longer an isolated problem for raw observations. For LCs, in figure 4.2 denoted by LLC and PLC, it is increasingly coming into perspective. In the past, for dual-frequency GPS and still today for many up-to-date applications, it is common practice to estimate and provide GPS clocks based on L1-L2 ionosphere-free LC observations. Well-known examples are the IGS products (Kouba, 2009) and the GPS broadcast clock information (GPS, 2012a). As outlined in section 3.2, the situation becomes increasingly complicated. New GNSS modulations on additional frequencies enable the formation of a variety of different ionosphere-free LCs. As a result, there are different methods to correct for discrepancies, such as DCBs (Schaer and Dach, 2010; Romero, 2012). In addition, also workarounds like the misleadingly called intersystem biases (ISBs), which are used to absorb receiver-dependent, inter-frequency biases (see section 3.2.1), have been implemented. In contrast to raw observations, a clean clock definition without a priori observation corrections and or auxiliary parameters as ISBs is almost impossible for LC observations.

For the processing of raw observations, in addition to the clock, the estimates of the ionospheric delay are also correlated with the uncalibrated signal delays. In the case of float-valued carrier phase ambiguities, the UPDs are an integral part of the ambiguity estimates. Consequently, UPDs only apply in cases of ambiguity fixing. For this reason, the following discussion concentrates on the situation for code observations. Section 7.3.2 addresses the topic of UPDs, together with the recovery of the integer ambiguities. Once the first rank defect is solved by a proper clock definition, the situation can be described as shown in figure 4.3. For reasons of simplicity, all effects and measurements are shown in units of time.

Figure 4.3 describes the situation for a standalone PPP, assuming that the code observations are corrected by all biases and delays, with the exception of the receiver clock, the receiver UCDs and the ionospheric delay. In terms of the demonstration of the relationship between the frequency-dependent ionospheric delays, the receiver clock and the UCDs, the code modulation does not matter. Instead, the relevant characteristic is the frequency of the carrier phase. The figure shows different code observations on arbitrary frequencies. The intention of the observation equation is the modelling of all effects, in order to assimilate observations and true range. Firstly, it shows that the clock estimate is the same for all observations, whereas the correction for the ionospheric delay is frequency dependent. Exemplarily different potential ionospheric delay corrections, represented by solid lines are shown. The remaining discrepancies needs to equalised by UCDs. It becomes obvious that there is no unique solution for this problem. Thus, the same true range can be reconstructed by making use of different TEC estimates and the corresponding UCDs. This fact results in a further rank defect of the normal equation (NEQ). As a result, the rank defect for a dual-frequency standalone PPP solution increases to two. The rank defect for dual-frequency network PPP solutions consists of one defect for the realisation of the absolute clock level and two defects per clock for the definition of the clock and the TEC level.
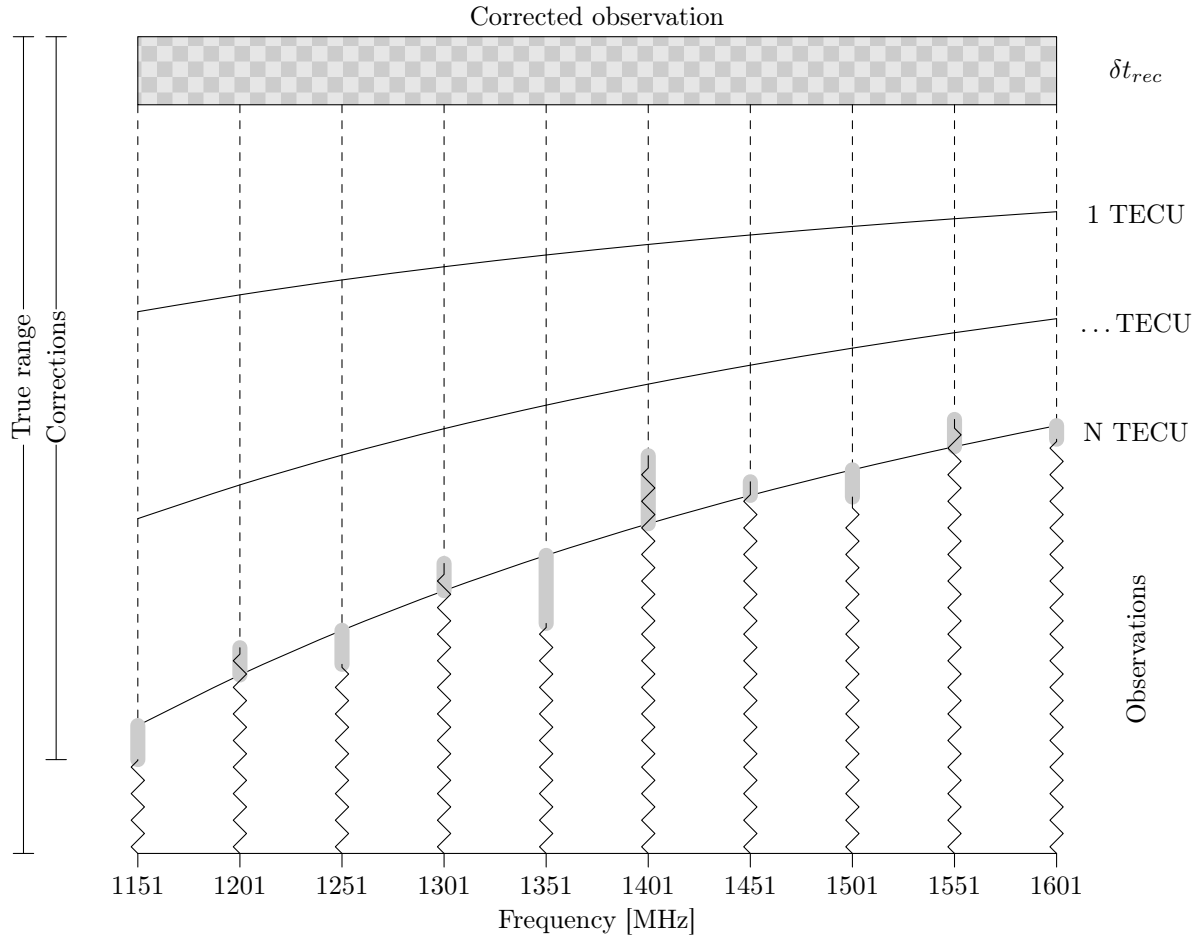
Figure 4.3: Correlation between UCDs and STEC estimates in units of time.

As previously indicated, there are different possible solutions for the removal of rank defects. The respective optimal solution depends strongly on the conditions and the requirements of the application. For an easier understanding of the facts, the raw observation equation (see equation 4.1) was rearranged. It is assumed that all effects that can be corrected by well-established procedures, such as those implemented in common ionosphere-free processing setups, were removed from the measurement. As is usual, multipath and measurement noise remain unconsidered. The resulting residuals to the true geometric range (res) per signal and tracking mode ($sig, track$) can be described as follows.

$$res_{Pr}(t,_{sig,track}^{sat}) = \delta\vec{X}_{rec}(t) + \delta\vec{X}^{sat}(t) + clk^{sat}(t) + clk^{rec}(t) + trop(t) + ion_{Pr}(t) + ucd^{sat,sig,track} + ucd_{rec,sig,track}$$

$$res_{Ph}(t,_{sig,track}^{sat}) = \delta\vec{X}_{rec}(t) + \delta\vec{X}^{sat}(t) + clk^{sat}(t) + clk^{rec}(t) + trop(t) + ion_{Ph}(t) + upd^{sat,sig,track} + upd_{rec,sig,track}$$

$$+ N_{sig,track}^{sat} \cdot \lambda_{sig}$$

$$(4.2)$$

Whereas $\delta\vec{X}_{rec}$ and $\delta\vec{X}^{sat}$ are the differences to the a priori receiver and satellite positions. It is important to note that the raw observation equation can be interpreted and implemented in different ways. The implementation of the equation requires a detailed knowledge of the respective application. To make the facts clearer, the situation is demonstrated by a practical example. Table 4.2 depicts the situation for a single receiver and different carrier phase observations from two GPS and one Galileo satellite. The left side of the table shows the residuals, as defined in equation 4.2. The right side shows the respective parameters. Since carrier-phase observations do not contribute to the pseudo-range related parameters, these are not displayed in table 4.2. In contrast, table 4.3 concentrates on the pseudo-range observations and their related parameters. It has to be mentioned that the presented illustration assumes integer-valued carrier phase ambiguities. A separation of ambiguity, receiver and satellite UPDs is not possible in the case of float-valued ambiguities. Consequently, UPDs will not appear in the equation in the event of float-valued carrier phase ambiguities.

Table 4.2: Example for observation - parameter relations (carrier phase).

Column headers (left to right):

$res_{Ph(t_0),L6Z}^{GAL_1}$, ⋯, $res_{Ph(t_0),L1A}^{GAL_1}$, $res_{Ph(t_0),L5X}^{GPS_2}$, $res_{Ph(t_0),L5Q}^{GPS_2}$, $res_{Ph(t_0),L5I}^{GPS_2}$, $res_{Ph(t_0),L2M}^{GPS_2}$, ⋯, $res_{Ph(t_0),L2C}^{GPS_2}$, ⋯, $res_{Ph(t_0),L1C}^{GPS_2}$, $res_{Ph(t_0),L5X}^{GPS_1}$, $res_{Ph(t_0),L5Q}^{GPS_1}$, $res_{Ph(t_0),L5I}^{GPS_1}$, $res_{Ph(t_0),L2M}^{GPS_1}$, ⋯, $res_{Ph(t_0),L2C}^{GPS_1}$, $res_{Ph(t_0),L1N}^{GPS_1}$, ⋯, $res_{Ph(t_0),L1C}^{GPS_1}$

Row labels (top to bottom):

$\delta \vec{X}_{rec}(t)$
$\delta \vec{X}^{GPS_1}(t)$
$\delta \vec{X}^{GPS_2}(t)$
$\delta \vec{X}^{GAL_1}(t)$
clk^{GPS_1}
$clk^{GPS_2}(t)$
$clk^{GAL_1}(t)$
$clk_{rec}(t)$
$trop(t)$
$ion^{GPS_1}(t)$
$ion^{GPS_2}(t)$
$ion^{GAL_1}(t)$
$N_{GPS_1,L1C}$
...
$N_{GPS_1,L1N}$
$N_{GPS_1,L2C}$
...
$N_{GPS_1,L2M}$
$N_{GPS_1,L5I}$
$N_{GPS_1,L5Q}$
$N_{GPS_1,L5X}$
$N_{GPS_2,L1C}$
...
$N_{GPS_2,L1N}$
$N_{GPS_2,L2C}$
...
$N_{GPS_2,L2M}$
$N_{GPS_2,L5I}$
$N_{GPS_2,L5Q}$
$N_{GPS_2,L5X}$
$N_{GAL,L1A}$
...
$N_{GAL,L6Z}$
$upd_{rec:L1C(GPS)}$
...
$upd_{rec:L1N(GPS)}$
$upd_{rec:L2C(GPS)}$
...
$upd_{rec:L2M(GPS)}$
$upd_{rec:L5I(GPS)}$
$upd_{rec:L5Q(GPS)}$
$upd_{rec:L5X(GPS)}$
$upd_{rec:L1A(GAL)}$
...
$upd_{rec:L6Z(GAL)}$
$upd^{GPS_1,L1C}$
...
$upd^{GPS_1,L1N}$
$upd^{GPS_1,L2C}$
...
$upd^{GPS_1,L2M}$
$upd^{GPS_1,L5I}$
$upd^{GPS_1,L5Q}$
$upd^{GPS_1,L5X}$
$upd^{GPS_2,L1C}$
...
$upd^{GPS_2,L1N}$
$upd^{GPS_2,L2C}$
...
$upd^{GPS_2,L2M}$
$upd^{GPS_2,L5I}$
$upd^{GPS_2,L5Q}$
$upd^{GPS_2,L5X}$
$upd^{GAL,L1A}$
...
$upd^{GAL,L6Z}$
⋮

no contribution to pseudo-range related parameters

Table 4.3: Example for observation - parameter relations (pseudo-range).

A first look already shows the flexibility of this approach in selecting observations. Depending upon the implementation all or those that are exclusively selected, observation can be used. This comprises free choice of GNSS observations and the freedom of individual editing and weighting rules. Thus, this approach allows a dedicated selection of observations, regardless of the availability of associated observations on a second frequency. By contrast, the ionosphere-free approach requires a defined set of observations, which are usually pseudo-range/carrier phase measurements on L1 and L2 frequencies.

It becomes obvious that there is effectively no difference for observations of different GNSS. Workarounds such as ISB parameters are no longer needed. Neglecting the impact of the observation weighting shows that, in addition to the carrier phase observations, the pseudo-range observations also contribute to the clock and ionosphere estimates. However, considering the downweighting of the pseudo-range observations, it is clear that the main objective of pseudo-range observations is the realisation of an "absolute" clock and optionally the TEC level. The absolute clock reference can be effectively realised by the pseudo-range observations of a single observation type. As a result, there is no longer a need to combine extremely precise code measurements like the AltBOC (see section 4.1, Simsky et al., 2005) with less accurate observations.

Depending on the type of application, it is not possible to determine the full set of unknown parameters. For example, it is impossible to separate satellite and receiver UCDs/UPDs, STEC and clock estimates for standalone PPP solutions. However, it is questionable whether all applications require a complete separation of all individual effects. For applications exclusively interested in coordinate solutions, it is conceivable to renounce a separation of STEC and satellite receiver UCDs/UPDs. It is easy to imagine that the resulting estimate has nothing to do with the true ionospheric delay. However, it is not a problem if this information is not required. Alternatively, this parameter can be assigned or constrained to a priori values. Furthermore, in terms of a global solution, it is possible to imagine estimating a global ionosphere model instead of constraining the UCDs to a priori values.

To sum up, the raw processing approach is flexible and adaptable to the respective application and its requirements. Consequently, an optimal tuning of observation selection, editing, weighting and parameter setup requires an in-depth knowledge of the available observations, hardware, conditions and requirements of the application.

Dual- versus multi-frequency processing

In addition to the increase in the number of observations, measurements on a third frequency further improve the ionospheric modelling capabilities. It is well known that two observations on different frequencies uniquely define the function of the first-order ionospheric delay. The situation changes as soon as the third frequency comes into the play. Figure 4.3 shows that, in the case of observations on exclusively two frequencies, the STEC and clock estimates can absorb discrepancies between the two observations. The situation changes for observations on a third frequency. In the following, this is demonstrated for an artificial bias between two phase measurements, symbolised by $\Delta L_{1/2}$. As shown in equation 4.3, the difference in the phase observation can be adjusted by changes in the epoch-wise STEC ($\Delta STEC$) and the receiver, satellite clock estimates (Δclk).

$$\Delta L_{1/2} = \frac{A}{f_{L1}^2} * \Delta STEC(t) - \frac{A}{f_{L2}^2} * \Delta STEC(t) + \Delta clk \qquad (4.3)$$

It should be noted that the presented equation includes only the carrier phase section. Strictly speaking, when using the raw processing approach, the code observations also need to be considered. However, the minor weight of pseudo-range observations in the LSQ adjustment prevents them from significantly influencing the observation equation for carrier phases. The analysis presented in chapter 6 confirms this statement. In the event of more than two frequencies, this equation is over-determined. As a result, it no longer allows the absorption of inter-frequency biases. The implication of this for different inter-frequency biases is demonstrated in the following. Figure 4.4 shows the magnitude of the disclosed effects caused by different linearly-frequency dependent biases. For this test, different linearly-frequency dependent biases were simulated. Afterwards, equation 4.3 was best fitted to the different Galileo frequencies, making use of a least squares adjustment.
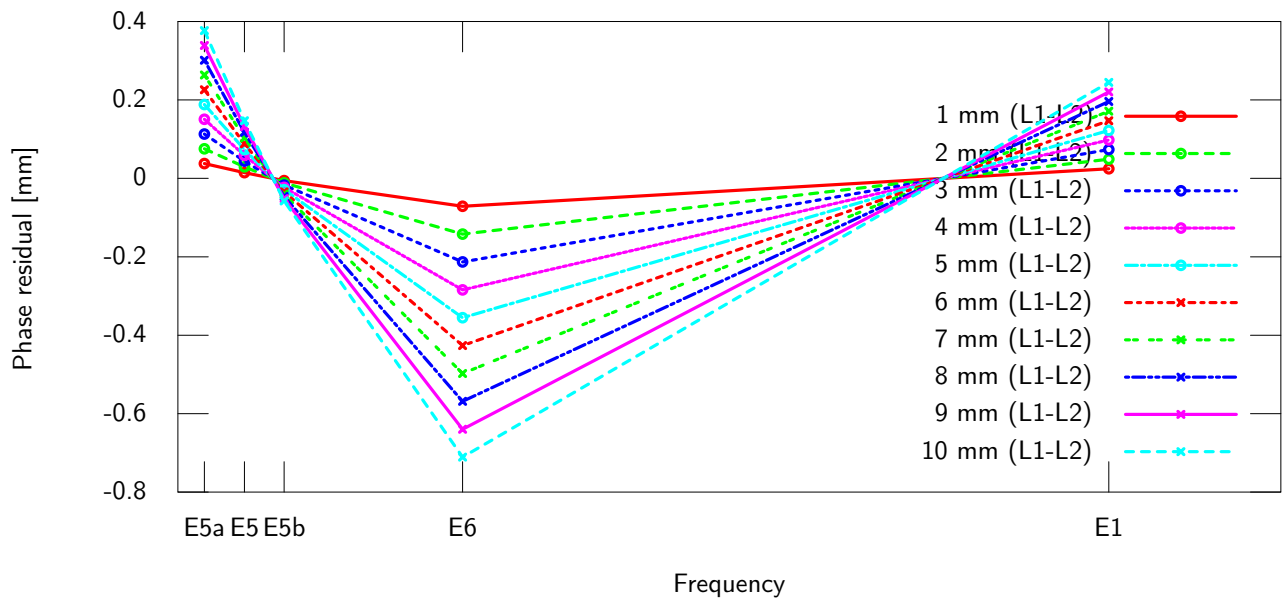
Figure 4.4: Absorbability of linearly frequency-dependent phase differences for multi-frequency processing.

It becomes apparent that linear-frequency dependent phase biases can be about 89 % absorbed by clock and STEC estimates. In fact, the situation looks different for random biases. Figure 4.5 shows the least squares fit as result of ten different random frequency dependent offsets. All randomly generated biases were below one millimetre.
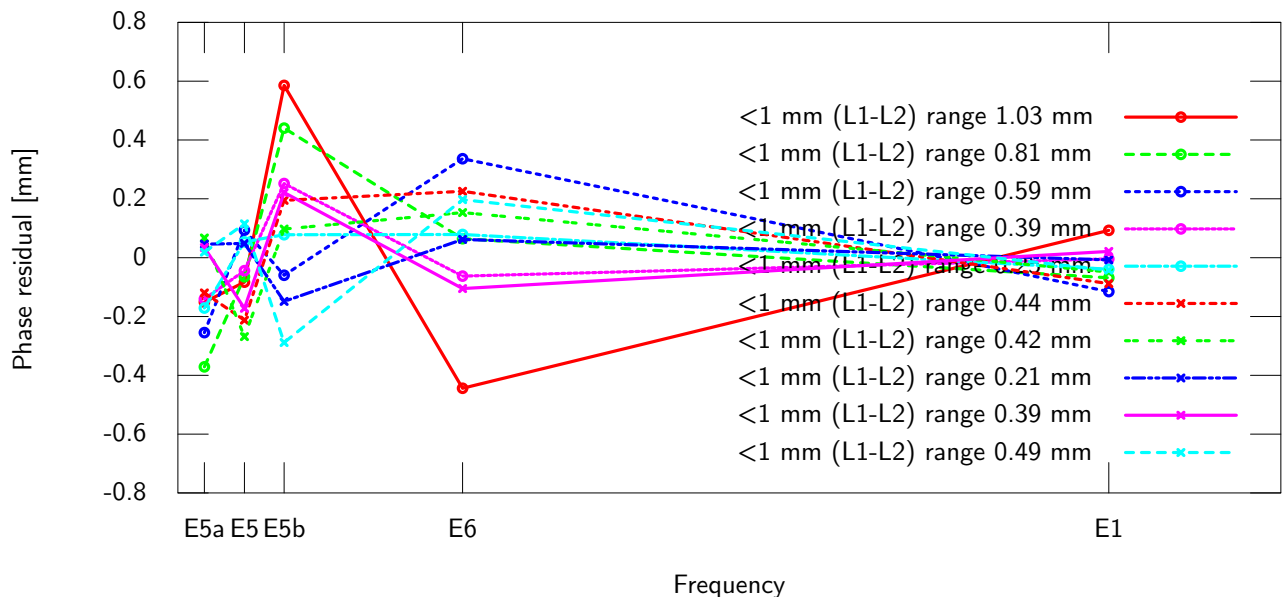
Figure 4.5: Absorbability of random frequency dependent phase differences for multi-frequency processing.

It becomes clear that, for some constellations of random biases, the effects can be absorbed, whereas for others they cannot. Therefore, in general, for random biases and in the case of multiple signals, the absorption of inter-signal biases in terms of STEC and clock estimates is limited. As a result of the low weight of the code observations in the LSQ adjustment, discrepancies between the different code signals have a minor impact on the coordinate and clock solutions. In general, these effects go into the residuals of the code observations. This fact is considerably more critical for phase observations. Considering multipath or systematic model inaccuracies that are frequency dependent, but which are not a function of the frequency, one must deal with systematic biases between the different carrier phases. In principle, this is not a bad feature, since it allows a better separation of the ionospheric

delay and the remaining observation residuals. Constant fractional-cycle-biases per signal and satellite-receiver pair can be absorb by the fractions of the "float" ambiguities. Certainly, when assuming a single fractional-cycle-biases per frequency, as in the case of integer ambiguities, these effects might show up as systematic phase biases. Thus, on one hand, different errors that are hidden for dual-frequency observations show up and allow the analysis of these biases, as well as their handling or an up or down weighting of individual observations. On the other hand, the correct modelling of these effects becomes necessary in order to avoid systematic errors.

4.3 Ambiguity resolution for raw observations

Model errors, signal disturbances and biases still present in undifferentiated raw observations make it very demanding, if not impossible, to recover their true integer ambiguities. Furthermore, it is clear that the application of integer ambiguities without the sufficient modelling of all effects causes systematic discrepancies in the phase observations. The variety of effects and, what is more serious, the lack of or insufficient knowledge regarding numerous biases such as PCOs, PCVs, UPDs, their variability for all components in satellites, receivers and antennae, atmospheric delays and much more prevents a recovery from undifferentiated raw ambiguities. For this reason, all ambiguity-fixing approaches published until now, even those processing raw observations (Li et al., 2013), perform ambiguity-fixing on the basis of wide-lane and narrow-lane combinations.

Since the ambiguity fixing for raw observations is obviously not feasible, it may be reasonable to recall the intention of ambiguity fixing and find alternative ways to achieve the same results. As outlined in section 3.4, this entails improving the east coordinate and stabilising the LSQ adjustment or filter solutions. Common network PPP approaches stabilise the solution by adding DD narrow-lane constraints on the NEQs. Thus, the NEQ still contains the non-integer valued ionosphere-free LC ambiguities. In fact, the same approach is applicable for NEQs containing raw observations. The principal disadvantage of this procedure is the loss of flexibility. Thus, in the case of narrow-lane ambiguities, only identical combinations can be processed jointly. This ultimately prevents the formation of numerous inter-GNSS DDs. Indeed, the use of raw instead of narrow-lane observations is considerably more flexible. This approach allows the formation of DD from observations with the same frequency, regardless of their GNSS and possibly missing second coincident frequency. Possible inter-system combinations for GPS and Galileo are L1/E1 and L5/E5a. Certainly, it is not essential that both of them, L1/E1 and L5/E5a, are available. It is clear that the unprocessed raw observations still contain the impact of the ionosphere, as well as numerous other errors. After the first LSQ run (see section 5.2), these effects are modelled by the designated parameters. As a result the resolution of raw DD ambiguities becomes possible. As is well known, DDs cannot be formed in standalone PPP. However, the standard ambiguity resolution technique, making use of satellite-to-satellite SDs and UPDs, can easily be adapted to raw instead of narrow-lane observations.

In the future, with additional GNSS and improved signal modulations on further frequencies, the parameter estimates are expected to become more stable by themselves. Thus, it is debatable whether ambiguity fixing, which entails the risk of incorrectly fixed ambiguities, will still be the best solution. However, for up-to-date dual-frequency observations, its benefits are undeniable.

5 Implementation and general processing strategy

This section aims to give an overview of the implementation of the raw observation processing approach. It starts with a short introduction to the applied software, followed by a description of the required changes and the newly implemented parameters. In the next step, the general processing scheme applied for the processing of both ionosphere-free linear combinations and raw observations is described.

5.1 Software implementation

The research activities were performed using the Navigation Package for Earth Observation Satellites (NAPEOS) (ESOC, 2009). NAPEOS is developed and maintained by the Navigation Support Office (OPS-GN) of the European Space Agency (ESA) at the European Space Operations Centre (ESOC) in Darmstadt, Germany. It is used on a regular basis for all OPS-GN activities related to the IGS, the IDS and the ILRS, as well as for precise orbit determination (POD) of satellites in Low Earth Orbits (LEOs). NAPEOS is one of the most flexible and accurate software tools available, particularly for GNSS analyses. However, since NAPEOS was developed solely for GPS processing, several software changes have become necessary in order to allow the processing of any type of navigation signal regardless of their origin (GNSS), modulation, frequency or quantity.

The most important improvements implemented in the frame of this thesis are the:

- implementation of an interactive signal selection. This feature is needed in order to select the desired observation types to be processed.
- implementation of processing capabilities for raw observations.
- implementation of ionospheric corrections, making use of ionosphere map exchange (IONEX) files.
- extension of PCO/PCV handling to all frequencies.
- implementation of parameter types and partials for satellite and receiver UPDs and UCDs, as well as epoch-wise STEC (ionosphere) estimates.
- extension of the satellite PCO/PCV estimation to enable the estimation of frequency dependent, instead of ionosphere-free, corrections.
- implementation of ambiguity-fixing for raw observations, making use of DD raw observations.

The most important changes in the scope of the processing of raw observations are the newly implemented parameters, namely UCDs, UPDs and STEC. For this reason, the implementation is briefly discussed in the following.

Uncalibrated code delays (UCDs)

Following the common understanding of UCDs, these can be assumed to be at least constant over the common processing period (one day). Their partial can be written as:

$$\frac{\partial Pr(t)}{\partial ucd} = 1 \tag{5.1}$$

There are two understandings regarding UCDs. The first is designed for providers of global GNSS products, assuming the UCDs to be separable into satellite and receiver portions. The second and more realistic definition assumes UCDs to be satellite-receiver pair related. The software implementation includes both approaches.

Uncalibrated phase delays (UPDs)

UPDs describe the non-integer part of the carrier phase ambiguities. Hence, using integer-valued carrier phase ambiguities in conjunction with satellite-receiver related UPDs, the result is the same as it is for a solution with float-valued ambiguities. UPDs apply exclusively in the case of integer-fixed carrier phase ambiguities. Following the common understanding of UPDs, these are common for all carrier phases on the same frequency, either in the transmitter or the receiver. Due to the lack of better knowledge, these are assumed to be constant throughout the processing period. The partials can be written as:

$$\frac{\partial Ph(t)}{\partial upd} = 1 \tag{5.2}$$

Slant total electron content STEC

While there are a number of different approaches to estimating the ionospheric delay, it has been shown that the estimation of STEC values is the only suitable approach to handling strong ionosphere activities properly. For this reason, the decision was made to implement an epoch-wise STEC estimation. It is well known that dual-frequency measurements can only properly estimate the first-order term of ionospheric delay. Since most satellites are still dual-frequency satellites, the second-order term has been neglected in the implementation. Furthermore, in the case of exclusively estimating the first-order term, the estimated delay corresponds to the delay mitigated by the ionosphere-free linear combination. Consequently, based on equation 3.19, the partial derivative reads as:

$$\frac{\partial Pr(t)}{\partial STEC} = +\frac{A}{f^2}$$

$$\frac{\partial Ph(t)}{\partial STEC} = -\frac{A}{f^2}$$

(5.3)

5.2 GNSS processing strategy applied

The implemented strategy is adapted to the processing scheme described in Kouba (2009). It applies regardless of whether the GNSS analysis makes use of an ionosphere-free linear combination or raw observations. In reality, the only difference is the parameter setup as described in section 5.3. The following paragraph briefly outlines the most important processing steps. The general processing strategy for standalone and network PPP is almost identical. The main difference between them is in the handling of the global parameters, such as ERPs, satellite orbits and clocks, and therefore in the parameter setup as described in section 5.3. Approximate orbit and clocks are sufficient for global network analyses. In contrast, standalone PPP solutions require precise orbits and clocks. In the case of a priori existing orbits and clocks, the processing steps of both scenarios are identical; otherwise, the generation of the a priori orbits requires an additional step. Figure 5.1 gives an overview on the required processing steps.

A full run starts with observation pre-processing, followed by the actual observation processing, performed by least squares parameter estimation. In the case of a solution renouncing integer ambiguity constraints, the processing stops after this step. Otherwise, an additional step for ambiguity resolution and a second least squares parameter estimation, applying the integer constraints, is needed. The following briefly introduces the different steps. For reasons of simplicity, the description concentrates on the purpose of the individual steps. For a detailed description of the models used, refer to the ESOC IGS analysis strategy summary (ESOC, 2011).

Generation of a priori orbits and clocks

Standalone PPP requires precise satellites orbits and clocks. These can either be taken from an external provider like the IGS, or could be a product of prior network analysis. Consequently, this step is not necessary for standalone PPP solutions.
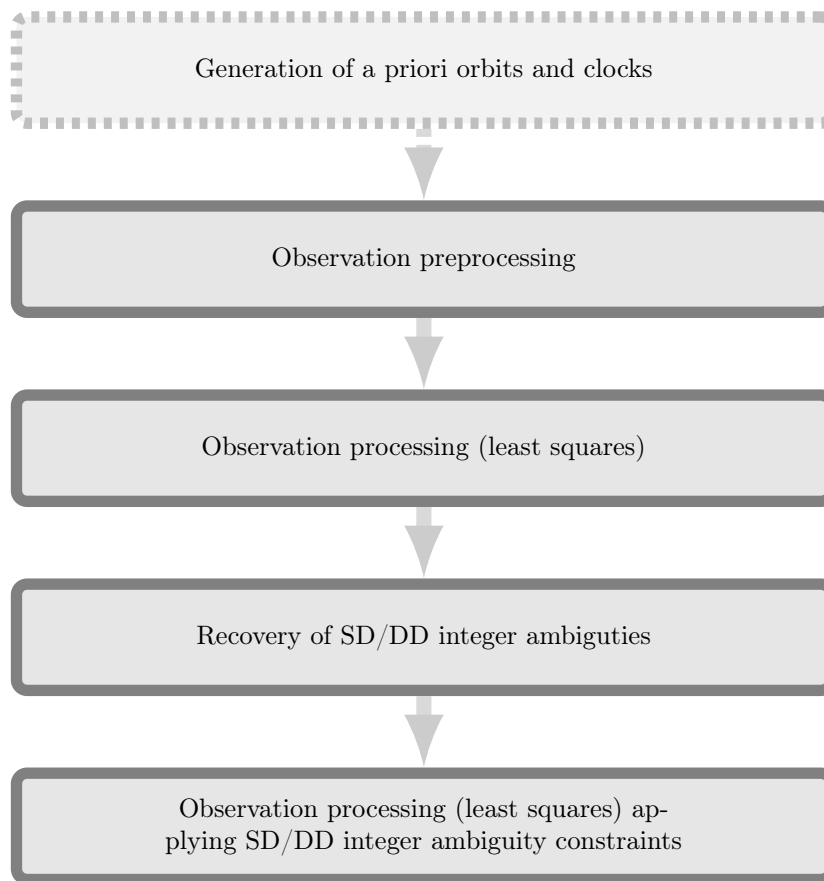
Figure 5.1: Flowchart of a general analysis procedure for GNSS.

A global network analysis aims to determine precise satellite orbits and clocks. Thus, the requirements of the input satellite orbits and clocks are less strict and it is therefore common practice to make use of broadcasted navigation data, being accurate by $1\,m$ (IGS, 2014). The intention of this step is the computation of satellite orbits (ECEF positions) and clock corrections. The required formulas are given in the respective ICDs and ISs of the different GNSS. A further possibility for the generation of a priori orbits and clocks is the extrapolation from previous solutions. In fact, the implemented procedure is a mixture of both methods.

Observation pre-processing

A variety of effects causes signal delays, degradations, outages and cycle slips. Furthermore, in the case of GNSS observations data provided on a "best effort" base as is done by the IGS tracking network, there are significant day-to-day and station-to-station variations in data quality and availability. To ensure a consistent set of clean observations and hence avoiding unwanted effects on the LSQ adjustment, proper observation pre-processing is of primary importance.

The procedure starts with the selection of the desired observations, taking into account the sampling rate and a sorted list of preferred observation types. In the next step, the selected observations are checked for integrity. This check aims to ensure the availability of all required observations. In the case of precise applications, this means at least two pairs of code and phase observations on at least two frequencies.

Once an adequate data set has been selected, the individual observations are screened, making use of different linear combinations (LCs) and statistical tests. The purpose of these tests is the disclosure of outliers and cycle slips. A more detailed description of the different tests and the applied LCs can be found in Beutler et al. (2007); Kouba (2009). One important point for the estimation of precise satellite orbits and clocks is the balancing of the network geometry. In the case of a bad station distribution, the orbits fit best in regions with the highest station density (maximum weight) and absorb the discrepancies in sparsely covered regions. For this reason, in the case of network processing, a further step for the station selection is applied. This step selects a predefined number of stations, based on geometrical and quality properties.

Observation processing (least squares)

As indicated by the name, this step is the most important step in the processing chain. Based on the pre-processed observations, applying all the error models described in ESOC's IGS analysis strategy summary (ESOC, 2011) it generates the normal equation matrix and solves for the unknowns. Since the a priori values cannot be assumed to be accurate enough, it is common practice to run this step using an iterative process. This procedure allows for a stepwise observation screening, with the advantage that observations can be screened based on their residuals to the estimated parameter solution, becoming more and more accurate. The screening criteria are described in section 5.4.

Recovery of SD or DD integer ambiguities

The intention of this step is the recovery of the SD or DD integer ambiguities. The recovered integer ambiguities are used in the next step, the second LSQ adjustment, in order to constraint the normal equation matrix. A description of this procedure for ionosphere-free LC observations is given in section 3.4. In fact, the same procedure can be applied for raw observations. The realisation of ambiguity-fixing for raw observations is discussed and demonstrated in section 7.3.

Observation processing (least squares) applying SD/DD integer ambiguity constraints

The second least squares process generally corresponds to the first run. The major differences are the integer ambiguity constraints. The ambiguity parameters taken from the previous step are added to the normal equation and the iterative least squares process is rerun.

5.3 Parameter estimation setup

The most important criterion for correct analysis results is the setup of the unknown parameters. As explained in section 4.2 regarding raw observation processing, there are different, strongly correlated parameters that cause rank defects in the normal equation matrix. As noted in that section, there are several possible approaches to the solution. The section explains that, theoretically, the rank defects can be removed by adding constraints to the normal equation system. It is clear that any constraint on the normal equation system will affect the parameter estimates. For this reason, it is important to ensure realistic constraints in order to obtain realistic values. However, due to the difficulty of gathering knowledge of the true values, it is worth considering whether it is really important to recover all individual parameters. As already mentioned, for applications exclusively interested in station coordinates, it is irrelevant whether the estimates of atmospheric delays depict the true physics or if they are just parameters to absorb the effects. Based on these considerations, renouncing elaborate and not yet fully sophisticated bias calibrations, necessary for a proper estimation of all parameters, seems to be a feasible option for some applications. In the following section, two possible parameter setups for raw observations are compared to the initial setup for ionosphere-free linear combinations. The discussion begins with the basic parametrisation for a standalone PPP and extends this parametrisation by the parameters needed for global network analyses in a second step.

5.3.1 Parameter setup for standalone PPP

This section describes the parameter setup for two different, raw observation-based standalone PPP solutions. It compares the parameter setups to the common setup for ionosphere-free linear combinations.

The first setup, referred to as raw satellite-receiver pair (link) dependent, describes the situation without a priori knowledge of ionospheric delays or UCDs. This scenario can be used if the separation of clock, UCDs and ionospheric delay is not required. In fact, this separation is essential for timing applications. For this reason, the second scenario, denoted as raw constraint, is introduced. There are again two possible parameter setups, one making use of a priori ionosphere information and the other constraining a priori UCDs. The high variability of the ionosphere

and its lack of predictability makes the application of ionosphere constraints for standalone PPP inefficient. For this reason, only the setup making use of UCD constraints is considered. It is conceivable that either satellite or station UCDs can be used but, for the accurate separation of all effects, a priori information regarding both is required. A summary of the different unknown parameters is given in table 5.1.

	Ionosphere-free LC		Raw link		Raw constraint	
	Validity	Sigma	Validity	Sigma	Validity	Sigma
Station coordinates	epoch/day	$1.0\,km$	epoch/day	$1.0\,km$	epoch/day	$1.0\,km$
Atmospheric zenith delay	$2.0\,h$	$2.0\,m$	$2.0\,h$	$2.0\,m$	$2.0\,h$	$2.0\,m$
Receiver clock error	epoch	$1.0\,\mu s$	epoch	$1.0\,\mu s$	epoch	$1.0\,\mu s$
Carrier phase ambiguity	pass	$1.0\,km$	pass	$1.0\,km$	pass	$1.0\,km$
Inter system bias (GAL/GLO)	day	$1\,s$	-	-	-	-
Slant total electron content	-	-	epoch	$10\,TECU$	epoch	$10\,TECU$
Uncalibrated code delay (link)	-	-	day [a]	$20\,m$	-	-
Uncalibrated code delay (satellite)[a]	-	-	-	-	day	$10\,cm$
Uncalibrated code delay (station)[a]	-	-	-	-	day	$10\,cm$

[a] Uncalibrated code delay for code on L1/E1 set to zero.

Table 5.1: Parameter setup for standalone PPP solutions.

For reasons of completeness, table 5.1 displays all unknown parameters, whereas the following discussion concentrate on the differences between the two approaches. The common parameters, for example station coordinates and tropospheric zenith path delays, are depicted in grey. The first important finding in the table is the handling of the ISBs. Strictly speaking, ISBs divide the involved GNSS into a master system with GPS as the usual clock reference, while secondary systems like GLONASS and Galileo are attached to the master clock via the ISBs. Considering the parameter setup for the two raw observation scenarios, it shows that ISBs are no longer needed. Remembering that one intention of this thesis is the equal treatment of all observations regardless of their GNSS, this criterion is fulfilled. The parameter sigmas given in the table are the ones applied for the analyses that were run in the frame of this thesis. Their values result from a limited number of empirical tests. For this reason, it is most likely that a further optimisation is possible and may even be required. With regard to UCDs, it is possible to fix the parameter to the a priori values instead of constraining it. However, in order to account for calibration inaccuracies and to enable minor adaptions of the parameter, it is preferable to constrain the parameter with an appropriate weight.

5.3.2 Parameter setup for network PPP with precise orbit determination

This section describes the parameter setup for network PPP approaches using precise orbit determination (POD). The parameter setup for global networks is based on the setup for standalone PPP solutions described previously. It extends the setup by additional global parameters like ERPs, satellite orbits and clocks. For well-balanced global networks, it is possible to estimate ERPs in relation to the a priori values and thereby improve the solution. Furthermore, the application of POD entails different, unknown satellite-related parameters, such as the satellite state vector and different model parameter describing the disturbances in the satellite orbit. The implemented analysis estimates six parameters of the CODE SRP (Springer, 1999) model and three along the track components of the CPRs. As is true for standalone PPP, different parameter setups for raw observations are also possible for network PPP solutions. The first setup, referred to as raw free, leaves the UCD parameters as unconstrained as possible. For this purpose, it applies zero mean conditions instead of individual UCD constraints. The second scenario, referred to as raw constraint, constrains the a priori UCD values. Thus, the UCDs on at least two frequencies can be fixed/constrained to zero, but also to values resulting from a priori calibrations. Indeed, similar matrix constraints are obtainable by using a priori ionosphere models or by estimating global spherical harmonics for the ionospheric delay. However, these variants were not analysed in the scope of this thesis. Nevertheless, the estimation of STEC parameters cannot be waived, even though the magnitude of the STEC parameters can be reduced by estimated or a priori global ionosphere models. Thus, apart from the parameter sigmas, the actual parameter setup is almost identical to the raw free parametrisation. For this reason, it is not explicitly depicted in the summary. Table 5.2 summarises the unknown parameters for the different setups.

	Iono. free LC		Raw free		Raw constraint	
	Duration	Sigma	Duration	Sigma	Duration	Sigma
UT1-UTC	day	$1.0\,ns$	day	$1.0\,ns$	day	$1.0\,ns$
Pole coordinates	day	$1\,mas$	day	$1\,mas$	day	$1\,mas$
Pole coordinates rate	day	$1\,mas/day$	day	$1\,mas/day$	day	$1\,mas/day$
Length of day	day	$1.0\,ms$	day	$1.0\,ms$	day	$1.0\,ms$
State vector	day	$1.0\,km$	day	$1.0\,km$	day	$1.0\,km$
CODE SRP (D0, Y0, B0, BC, BS)	day	$1.0\,km/s^2$	day	$1.0\,km/s^2$	day	$1.0\,km/s^2$
CPR along track (const., cos, sin)	day	$1.0\,E^{10}\,m$	day	$1.0\,E^{10}\,m$	day	$1.0\,E^{10}\,m$
Station coordinates	epoch/day	$1.0\,cm$	epoch/day	$1.0\,cm$	epoch/day	$1.0\,cm$
Atmospheric zenith delay	$1.0\,h$	$2.0\,m$	$1.0\,h$	$2.0\,m$	$1.0\,h$	$2.0\,m$
Atmospheric grad. (east/west)	day	$2.0\,m$	day	$2.0\,m$	day	$2.0\,m$
Satellite clock error	epoch	$1.0\,\mu s$	epoch	$1.0\,\mu s$	epoch	$1.0\,\mu s$
Receiver clock error	epoch	$1.0\,\mu s$	epoch	$1.0\,\mu s$	epoch	$1.0\,\mu s$
Carrier phase ambiguity	pass	$1.0\,km$	pass	$1.0\,km$	pass	$1.0\,km$
Inter system bias (GAL / GLO)	day	$1\,s$	-	-	-	-
Slant total electron content	-	-	epoch	50 TECU	epoch	50 TECU
Uncalibrated code delay (satellite)	-	-	day	$1.0\,km$ [a,b]	day	$10\,cm$ [a]
Uncalibrated code delay (station)	-	-	day	$1.0\,km$ [a,b]	day	$10\,cm$ [a]

[a] Uncalibrated code delay for code on L1/E1 set to zero. [b] Zero mean condition on L2/E5a.

Table 5.2: Parameter setup for network PPP solutions.

5.4 Observation weighting and screening criteria

In addition to the parameter setup, one of the most important criteria for achieving precise analyses results are the settings for the observation weighting and screening. The analyses that were run in the frame of this thesis performs an observation screening using a threshold of twice the observation sigma. For the ionosphere-free linear combination, the a priori assumption regarding the observation accuracy, as applied in ESAs IGS processing (ESOC, 2011), has been used. For raw observations, the situation is less clear. Thus, for the raw phase observations, an accuracy of 0.01 cycles (Simsky et al.; Schönemann et al., 2007a) has been assumed. The lack of knowledge regarding the actual performance of the individual pseudo-range measurements depending on modulation, receiver, correlator type and so on, and because of to the missing discriminability of these parameters in the software, all pseudo-range observations were treated equally. The applied value was determined by empirical tests. Considering the high quality of modern GNSS modulations like the AltBOC, it is worth considering the different pseudo-range accuracies. Note, for the observation weighting, in addition to the actual observation noise, it is important to consider the frequency dependent influence of the ionosphere. Table 5.3 shows an overview of the assumed observation accuracies.

	Frequency	Cut off	Pr	L
ionosphere-free LC	-	10°	$1.0\,m$	$10.00\,mm$
raw observations	L1	10°	$0.5\,m$	$1.70\,mm$
raw observations	L2	10°	$0.5\,m$	$2.18\,mm$
raw observations	L5	10°	$0.5\,m$	$2.28\,mm$
raw observations	E1	10°	$0.5\,m$	$1.70\,mm$
raw observations	E6	10°	$0.5\,m$	$2.09\,mm$
raw observations	E5a	10°	$0.5\,m$	$2.28\,mm$
raw observations	E5	10°	$0.5\,m$	$2.25\,mm$
raw observations	E5b	10°	$0.5\,m$	$2.22\,mm$

Table 5.3: Screening properties for pseuderange and phase observations.

It shows that there is only one value for the ionosphere-free LC, but that there are individual values for each raw observation. Taking into account the importance of observation screening and weighting for the quality of the results, this clearly indicates the advantages of processing the raw observations.

6 Analysis of uncalibrated signal delays

As outlined in the previous sections, the understanding and handling of uncalibrated signal delays is one of the most relevant points for the accurate processing of raw observations. For this reason, this section aims to analyse the characteristics of UCDs and UPDs. Without a priori knowledge of the receiver biases, the analysis of satellite dependent delays is not possible. Therefore, this section begins with analyses of the receiver-dependent delays, followed by a discussion of the characteristics of the satellite-dependent delays. As explained in section 3.1.2, signal delays are a conglomeration of numerous different effects. One important characteristic is the interaction of signal and tracking methodology. Consequently, it is necessary to depict this fact in the observation description for the analysis of these biases. A description well suited to the different observation types is given by the RINEX 3.01 observation notation. According to Gurtner and Estey (2009), the different observation types used in the following analysis can be assigned to the original signals, as described in table 6.1.

System	Frequency Band	Channel or Code	Observation Codes	
			Pr	*Ph*
GPS	L1	C/A	C1C	L1C
		L1C (M+L)	C1X	L1X
		Z-tracking and similar (AS on)	C1W	L1W
	L2	L2C (L)	C2L	L2L
		L2C (M+L)	C2X	L2X
		Z-tracking and similar (AS on)	C2W	L2W
	L5	Q	C5Q	L5Q
		I+Q	C5X	L5X
Galileo	E1	C	C1C	L1C
		B+C	C1X	L1X
	E5a	Q	C5Q	L5Q
		$I+Q$	C5X	L5X
	E5b	Q	C7Q	L7Q
		$I+Q$	C7X	L7X
	E5	Q	C8Q	L8Q
		$I+Q$	C8X	L8X

Table 6.1: RINEX 3.01 observation codes used in this analysis (Gurtner and Estey, 2009).

6.1 Receiver-dependent signal delays

In a real environment, a separation of ionospheric delay, clock estimates and uncalibrated signal delays is difficult due to the strong correlation of the different effects. It is possible to analyse the relative behaviour of UPDs but, at the accuracy level of phase observations, a reasonable separation of model inaccuracies, ionospheric effects and UPDs is impossible. For this reason, the analysis of the receiver-dependent delays was split into two parts. The first part makes use of a GNSS signal generator. This allows the analysis of the different signals with a reduced error budget and without atmospheric delays. The second part is based on real observations. In addition to the actual characteristics of the different delays, it is necessary to understand the relative behaviour of different receiver types and the impact of different receiver settings and antennae. An optimal configuration for the comparison of observations from different receivers is the zero-baseline setup.

Zero-baseline setup

A zero-baseline is a common setup for the analysis and comparison of different receivers. In a zero-baseline, all receivers are connected to the same source via a signal splitter. This setup ensures that all receivers receive the same signals and are affected by the same external errors. In the case of freely running receiver clocks, the measurement points can differ and thus the external errors, delays and distance to the satellites. For this reason and in order to mitigate such effects, the receiver clocks were synchronised. However, due to missing capabilities of one of the test receivers (C005), its clock was not synchronised. Figure 6.1 shows the zero-baseline setup.
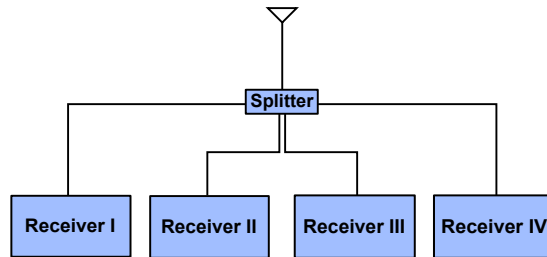
Figure 6.1: Zero-baseline receiver setup.

The signal source for the following analyses is given either by true signals received by an antenna or, alternatively, the GNSS signal generator. In order to ensure similar effects for all receivers, the connections between splitter and the individual receivers were implemented using cables from the same manufacturer and of the same length.

The test receivers

The selected test receivers consist of two pairs of identically constructed receivers that are running the same firmware. In the following section, the receivers are referred to as A001/A002 and B003/B004. In the first instance, this selection allows for the comparison of receivers of the same type. Once it is proven that receivers of the same type show similar performance, it is possible to use one receiver of each type as a reference, while the other receiver can be used for testing. To increase the diversity, a third type of receiver (C005) was added. The different receiver types applies different tracking methods and therefore generates different types of RINEX observations. Table 6.2 gives an overview of the code observation types tracked by the various receivers.

Receiver	GPS								Galileo							
	C1C	C1W	C1X	C2L	C2W	C2X	C5Q	C5X	C1C	C1X	C5Q	C5X	C7Q	C7X	C8Q	C8X
A001/A002	✓	✓		✓	✓		✓		✓		✓		✓		✓	
B003/B004	✓				✓	✓		✓		✓		✓		✓		✓
C005	✓				✓	✓		✓		✓		✓		✓		✓

Table 6.2: Code observations tracked by the test receivers.

It becomes obvious particularly for GPS L5 and Galileo observations that no consistent set of observation types exists on all receivers. Instead, some receivers (A001/A002) track the dataless components, whereas others apply X-tracking (data + pilot).

6.1.1 Approaches to analyses

The application of a zero-baseline setup allows the application of different approaches to analyses. Without doubt, a standalone raw observation PPP is optimally suited to all kinds of signal analyses. Nevertheless, since the proper functionality of the implemented approach has not yet been proven, it is reasonable to use a second, parallel approach in order to confirm the results. The most straightforward approach for zero-baseline analysis is the direct

comparison of signal components, since all receivers track the same signals at the same time. In the following section, this method is referred to as signal difference analysis (SDA). The corresponding signal difference analysis observation (SDAO), formed from two code components, is defined as:

$$SDAO_{Pr}(t) = Pr_1 - Pr_2 \tag{6.1}$$

for a code and a phase signal component as:

$$SDAO_{mix}(t) = Ph_1 + \lambda_1 N_1 - Pr_1 \tag{6.2}$$

and for two phase signal components as:

$$SDAO_{Ph}(t) = Ph_1 + \lambda_1 N_1 - Ph_2 - \lambda_2 N_2 \tag{6.3}$$

For SDAOs including an unknown number of carrier phase ambiguities (N), the relative bias behaviour (stability, trend, etc.) can be analysed by removing the mean value. Care should be taken that this method is only applied for periods without cycle slips.

6.1.2 Simulator analyses

GNSS simulators are designed to generate artificial GNSS signals. They are able to generate unbiased signals, as well as signals that are influenced by predefined error sources. Once again, this allows for a detailed analysis of the biases and the corresponding receiver response. The main goal of the analysis presented in the following is the characterisation of the different receiver delays for pseudo-range and carrier phase measurements.

In order to analyse the characteristics of UCDs and UPDs, various scenarios that made use of different simulator settings were run. Even though it was necessary to run the simulation with different settings, an attempt was made to keep the settings for the different scenarios as similar as possible. Consequently, all simulations were run for the same day (December 7, 2012). Since the simulator was restricted to two GNSS at the same time, the decision was made to concentrate on GPS and Galileo. One of the requirements for the intended analysis is the availability of observation data on more than two frequencies. This requirement is fulfilled by Galileo and by modernised GPS satellites. However, the Galileo satellite constellation that is currently being developed is not yet sufficient for the intended analyses. Furthermore, the number of modernised GPS satellites transmitting on three frequencies is limited. For this reason, the simulations made use of the artificial GPS and Galileo satellite constellations provided by the simulator itself.

The use of the simulator-integrated noise generator was mandatory, even if one intention of the simulator analysis was the analysis of undisturbed signals. However, the receiver requires a realistic noise floor in order to prevent it from oversteering.

Simulator-side limitations and workarounds

The simulator analyses presented in the following section were affected by different limitations. One restriction was the limited loan period of the simulator, which was available for just two weeks. The second limitation concerns the fact that the simulator used for the analyses was still in the development phase. These restrictions affect both the testing capability and the quality of the results. The following paragraph briefly describes the most significant issues and the workarounds applied.

Firstly, due to the limited availability of the simulator, it was not possible to perform a full system calibration, including software, hardware, cables, splitters and the like. However, since the analysis aims to analyse the bias characteristics rather than the absolute bias values, the missing absolute calibration of the simulator system was not a problem. A more critical point was the missing or insufficiently accurate information available regarding simulated disturbances. This concerns the applied models, as well as the satellite orbits and clocks. The consequence

of the lack of information or the existence of inaccurate information prevents a complete recovery of the generated signals and therefore an analysis on the millimetre level. Since this problem affects all recorded observations equally no matter from which receiver they originate, as well as the observation file recorded at the simulator itself, a simple workaround for this problem was found. The workaround is based on the assumption that the observation file recorded at the simulator is error free. Hence, performing a PPP run waiving any correction modelling and bias estimation, the residuals expose the errors coming from differences in models. However, in order to correct the observations of the remaining receivers in terms of these errors, it was necessary to store this information, preferably as LOS correction. Since almost all the parameters in this PPP run could be fixed, this was easily done by estimating satellite clock offsets. Using the estimated satellite clocks as input for the analysis of the true receiver data mitigates the model differences and errors. An additional benefit of this method is the simple densification of satellite clock estimates to a sampling rate of one second.

Investigations and analyses

A number of different investigations and analyses to characterise the behaviour of the receiver-dependent uncalibrated signal delays were run. Among others, these were analyses regarding the influence of different multipath, atmospheric and temperature effects and the impact of different noise and damping levels. For these tests, five receivers were connected alternately to the simulator, whereas four receivers were always connected at the same time. The connection to the receivers was achieved by the previously described zero-baseline setup.

The differences between real and artificial GNSS signals, particularly in the case of undisturbed signals, make it necessary to adjust the standard PPP scenario for raw observations according to the requirements of the respective tests. It is clear that if no atmosphere is modelled on the simulated signals, the application of a priori atmosphere models will significantly falsify the solution. Notwithstanding the number of different setups and the multitude of different effects analysed, the most informative experiments were the ones making use of undisturbed GNSS signals. "Undisturbed" means not adding artificial disturbances to the signals. Consequently, any abnormal behaviour and/or increased observation residuals can be assigned to the receiver itself. In order to force all delays to remain in the observation and show up as residuals, the parameter estimation concentrates on as few parameters as possible. In the event of a PPP making use of undisturbed signals, the most significant changes to the standard modelling and parametrisation can be described as shown in table 6.3. The differences from the initial setup are indicated in grey.

$trop$	STEC	δt_{rec}	ucd_{rec} ucd^{sat}	N	CRD
modelled/estimated	estimated	estimated	estimated per link	estimated	estimated

Table 6.3: Modified parameter setup for simulator PPP analyses.

The analysis addressed two aspects, namely the repeatability of the constant daily delay estimates and their sub-daily variability. The unknown number of carrier phase ambiguities makes the carrier phase measurement ambiguous. As a result, the determination of absolute delays is impossible. In the case of a known number of full phase cycles, the UPDs can be estimated relative to this number. A more detailed description of this topic is given in section 7.3.2. For this reason, the first part of the analysis concentrates on the repeatability of the daily uncalibrated signal delays and deals exclusively with the pseudo-range related delays, namely UCDs. With regard to the pseudo-ranges, "absolute" values can only be derived under the assumption of an unbiased environment. However, since this is never the case, an absolute calibration of the pseudo-ranges is also impossible. For this reason, all delays are referred to the first observed code signal on the L1 frequency band, where "first" is related to the order in table 6.1. For the following analysis, the SDA observations were composed of two pseudo-range observations as per equation 6.1. Table 6.4 shows selected results of the daily USD estimates for receiver A001. The test scenario is indicated by its ID, given in the first column. The second column describes the analysis method used for the estimation of the UCDs. The third column specifies whether the multipath mitigation technique was applied or not. Besides the simulated effects described in column four, environmental effects (column five) such as strong temperature (temp.) variations or signal damping, were also analysed.

ID	Method	MP Mitigation	Simulated Delay	External Effects	GPS					Galileo			
					C1C	C1W	C2W	C2L	C5Q	C1C	C5Q	C7Q	C8Q
05	SDA	on	-	-	0.00	-0.02	0.07	0.07	2.49	0.00	0.06	-2.83	-1.46
05	PPP	on	-	-	0.00			0.07	2.49	0.00	0.06	-2.82	-1.30
06	SDA	on	-	temp.	0.00	-0.02	0.03	0.02	2.43	0.00	-0.01	-2.85	-1.40
06	PPP	on	-	temp.	0.00			0.03	2.42	0.00	0.00	-2.85	-1.77
07	SDA	on	-	-	0.00	-0.02	0.04	0.03	2.51	0.00	0.07	-2.83	-1.33
07	PPP	on	-	-	0.00			0.03	2.51	0.00	0.07	-2.84	-1.11
08	SDA	on	MP	-	0.00	-0.05	-0.16	-0.11	2.52	0.00	0.08	-2.84	-1.16
08	PPP	on	MP	-	0.00			0.03	2.55	0.00	0.05	-2.86	-1.32
11	SDA	off	-	-	0.00	-0.02	0.00	0.00	2.51	0.00	0.07	-2.83	-1.38
11	PPP	off	-	-	0.00			0.00	2.51	0.00	0.07	-2.83	-1.21
12	SDA	off	-	temp.	0.00	-0.02	0.00	0.00	2.50	0.00	0.06	-2.83	-1.72
12	PPP	off	-	temp.	0.00			0.01	2.50	0.00	0.07	-2.83	-1.77
13	SDA	off	-	-30dB	0.00	-0.03	0.23	0.22	2.62	0.00	0.19	-2.76	-1.25
13	PPP	off	-	-30dB	0.00			0.21	2.61	0.00	0.18	-2.76	-0.29

Table 6.4: Sensitivity of uncalibrated code delays (A001) [m].

The comparison of the two analysis methods, SDA versus PPP, shows that both approaches produce comparable results. For the first time, this confirms the correctness of the newly implemented approach and its functionality. The comparison of daily UCD estimates for the different signals and the tracking methods show significant differences. However, considering observations on the same frequency band shows that these are almost comparable.

The next point of interest is the sensitivity of the daily UCD estimates to different effects. Here, it shows that certain effects, such as a strong signal damping or multipath, are able to change UCDs by several decimetres. However, temperature changes and the application of multipath mitigation techniques have no impact on the daily UCD estimates of this receiver (A001). In the case of a constant receiver environment, receiver A001 shows repeatable daily UCD estimates. However, this is not the case for all receivers. Table 6.5 shows a comparable analysis for a receiver from a different manufacturer (B004):

ID	Method	MP Mitigation	Simulated Delay	External Effects	GPS			Galileo			
					C1C	C2W	C2X	C1X	C5X	C7X	C8X
05	SDA	on	-	-	0.00	7.14	6.52	0.00	-0.80	-0.63	-0.15
05	PPP	on	-	-	0.00	7.08		0.00	-0.80	-0.63	-0.02
07	SDA	on	-	-	0.00	7.38	6.64	0.00	-0.56	-0.29	-0.33
07	PPP	on	-	-	0.00	7.14		0.00	-0.59	-0.25	-0.60
08	SDA	on	MP	-	0.00	7.36	6.78	0.00	-0.54	-0.04	0.47
08	PPP	on	MP	-	0.00	7.93		0.00	-0.53	-0.07	1.35
11	SDA	off	-	-	0.00	3.48	2.80	0.00	-1.22	-0.82	-1.20
11	PPP	off	-	-	0.00	3.19		0.00	-1.22	-0.82	-0.90
12	SDA	off	-	temp.	0.00	3.97	3.29	0.00	-1.28	-1.03	-0.89
12	PPP	off	-	temp.	0.00	3.61		0.00	-1.28	-1.04	-1.06

Table 6.5: Stability of uncalibrated code delays (B004) [m].

In comparison with the first receiver, this receiver type shows a significantly stronger variability in the daily UCD estimates. This concerns the stability of the UCDs for unchanged setups, as well as the sensitivity of UCDs to different effects. It becomes obvious that the application of multipath mitigation techniques offset the pseudo-range observations in L2 with respect to L1 by about $3.9\,m$. On closer inspection, significant offsets between differently tracked code signals on the same frequency band become obvious. For example, the code measurements of C2W differ from those of C2X observations by approximately $0.6\,m$. The presented analysis demonstrated that the SDA results were comparable to the results gained from the PPP analysis. Therefore, the SDA was no longer considered in the following analyses.

As shown in table 6.2, there is no consistent set of observation types available at all receivers. Therefore, in order to make the UCDs of the different receiver types comparable, a single pseudo-range observation per frequency was

considered. The information regarding the tracking procedure was neglected and the UCDs were named according to their carrier frequency instead of by the type of observation. A summary of the most relevant results from the analysis of the daily UCD estimates is given in table 6.6.

	UCD	L1		L2		L5		E1		E5a		E5b		E5	
	Rec.\MP	On	Off	On	Off	On	Off	On	Off	On	Off	On	Off	On	Off
E1 BOC	A001	0.00	-	-0.08	-	2.28	-	-0.03	-	2.27	-	-0.57	-	0.47	-
	A002	0.00	-	0.01	-	2.51	-	-0.03	-	2.50	-	-0.52	-	1.38	-
	B003	0.00	-	7.27	-	-	-	-1.79	-	-0.08	-	0.26	-	0.50	-
	B004	0.00	-	7.32	-	-	-	-1.90	-	-0.36	-	0.13	-	4.51	-
	C005	0.00	-	-3.39	-	-	-	16.76	-	15.80	-	35.77	-	36.22	-
E1 CBOC	A001	0.00	0.00	0.05	0.01	2.50	2.51	2.42	2.42	2.48	2.49	-0.42	-0.41	1.21	1.21
	A002	0.00	0.00	0.14	0.13	2.76	2.74	2.42	2.42	2.73	2.71	-0.37	-0.36	0.70	0.82
	B003	-	0.00	-	4.04	-	-	-	2.43	-	2.00	-	2.57	-	2.50
	B004	0.00	0.00	7.11	3.19	-	-	0.38	2.08	-0.32	0.86	-0.06	1.26	0.07	1.18
	C005	0.00	-	-3.26	-	-	-	19.19	-	16.12	-	35.96	-	36.13	-

Table 6.6: Summary of UCDs for different receivers with and without multipath mitigation [m].

The second header line of this table indicates whether or not the multipath mitigation technique was used. The table is split into two parts, divided by a horizontal line. The upper part shows the UCDs in the case of a BOC modulation to the E1 signal and the lower part shows the case of CBOC. As expected, the tracking of signals applying different modulations results in different UCDs. The almost equal UCD difference at all four test receivers is conspicuous. Since the simulator itself was not calibrated, the possibility that this shift was induced by the simulator cannot be excluded. More interesting is the specific receiver-type behaviour of the UCDs. Some receiver types show almost stable biases, both from day-to-day and between receivers of the same type, whereas others are considerably less stable and are more sensitive to a variety of effects and receiver settings, such as the activation of multipath mitigation techniques. The receivers B003 and B004 are examples of the impact of multipath mitigation techniques on the UCDs. With regard to these receivers, it became obvious that the UCD difference, L1 versus L2 (DCB), changes by about $3.9\,m$ as a response to this technique. However, the small number of samples for the different scenarios prevents the estimation of a reasonable standard deviation and the drawing of conclusive statements. It is clear that the small, day-to-day UCD variations at the level of one to ten centimetres indicate the significance of the demonstrated effects. The only exceptions are the UCDs on the L5 frequency band, which appeared to be significantly worse. However, due the missing calibration of the simulator, the results cannot be seen as representative of the individual receiver types. Nevertheless, the analyses demonstrated that, in the case of a constant setup, the daily mean of the UCDs can be assumed to be stable at the level of up-to-date pseudo-range accuracy ($\approx 0.3\,m$). Depending on the receiver type, the variations are at the level of one to ten centimetres.

For GNSS sites, this means that only in the case of a constant setup the UCDs can be assumed to be stable. A constant setup includes not only the antenna environment, installation, receiver, receiver settings, firmware and cables, but also various other effects, such as temperature, multipath and so on. The majority of these effects, including firmware changes or changes in the receiver settings, can be controlled by the operator and are generally predictable. Nevertheless, several years of IGS operations have demonstrated that even this is not an easy task for networks that operate on a "best-effort basis".

In addition to the least partially predictable long-term effects, there are also almost unpredictable short-term effects that cause sub-daily delay variations. One of the most significant effects for the temporal variability of signal delays is changes to the internal receiver temperature. A widespread opinion is that, in the case of temperature-stabilised locations, the internal receiver temperature also remains constant. In fact, the internal receiver temperature is not only affected by the external receiver temperature, but also by internal receiver heating. A major source of internal receiver heating is the Central Processing Unit (CPU). Thus, an increased CPU load can be expected to raise the internal receiver temperature. The reasons for differences in the CPU load are manifold. Examples are different amounts of visible and tracked satellites and administrative tasks like data downloads and so on being run on the receiver. Thus, it is almost impossible to stabilise the internal receiver temperature of common receivers completely. Figure 6.2 demonstrates the impact of a file download on the receiver temperature.

This shows the behaviour of the internal receiver temperature over three consecutive days. The vertical lines in magenta, green and cyan depict the scheduled beginning and end of the file downloads on receiver B003 and B004.

CPU effects on the receiver temperature
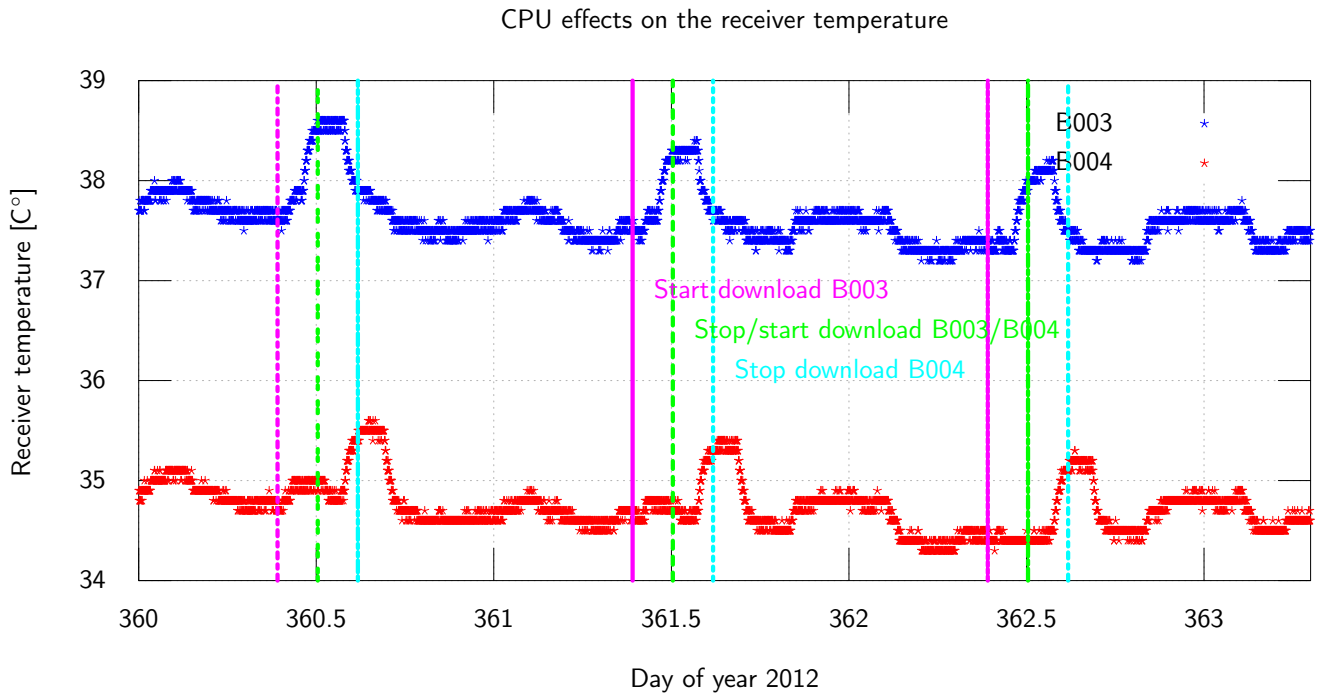
Figure 6.2: Impact of CPU load on the internal receiver temperature.

The file download from B004 starts when B003 finishes. It becomes obvious that the file download changes the receiver temperature significantly. In this specific case, the temperature increases by about $1°C°$ until the end of the file download. Afterwards, it remains briefly at that level and then reverts to the previous temperature level.

As is well known, most electrical components show significant temperature dependent behavior, particularly in the case of high-frequency signals. In order to study the temperature impact on the different signal components, the test receivers were exposed to a significant change in the environmental temperature, causing the internal receiver temperature to change. Since the observations of the artificial signals per se do not exhibit significant non-static delays, the impact of the temperate changes on the delays can be read directly from the respective code and phase residuals. In order to make the residuals of different runs comparable, the UCDs were fixed to a priori values that were derived from the previous code bias analyses and which were presented in table 6.6. The required changes to the parameter setup are described in table 6.7.

$trop$	STEC	δt_{rec}	ucd_{rec}	ucd^{sat}	N	CRD
modelled/estimated	estimated	estimated	estimated per link		estimated	estimated

Table 6.7: Modified parameter setup for temperature analysis.

In general, the residuals show no systematic behaviour in the absence of artificial temperature changes. However, the residuals do show significantly different characteristics during the period of the temperature experiments. As mentioned earlier, the scope of this analysis is the relative behaviour of observations on different carrier frequencies. For this purpose, the code and phase observations on L2 and L5 were compared to those on L1. The consideration of the residual differences (L1 - L2/L5) clearly reveals the effects. Nevertheless, it was not possible to characterise the temperature dependent systematics in this representation. One of the test receivers allowed the output of its internal temperature. Assuming similar behaviour of the internal temperature in all receivers allows the analysis of the residuals with regard to temperature. Figure 6.3 clearly shows the code and phase residual differences for the GPS satellites with PRN G03, G07 and G11.
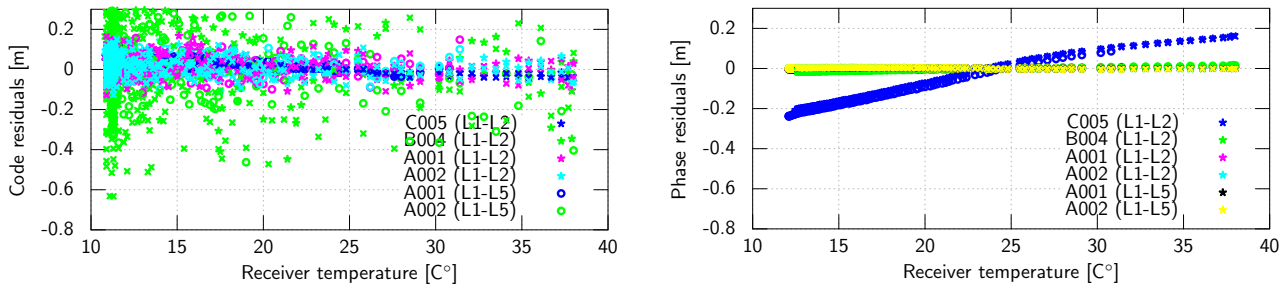
Figure 6.3: Temperature dependency of differential receiver code (left) and phase (right) delays for GPS (G03, G07, G11).

The high noise of the code observations prevents the detection of small drift rates. However, due to the accuracy and the subsequent weighting of the code observations, these drifts are insignificant in terms of processing. The situation is different for the carrier phase observations. Figure 6.3 shows a clear drift between the phase observations on L1 and L2/L5. The almost linear temperature-dependent behaviour in the receiver most affected (C005) confirms the validity of the assumption of comparable behaviour of the internal receiver temperatures. Comparing the different receiver types, it becomes apparent that some receivers have almost stable biases, whereas others show drift rates of up to $17\,mm/^\circ C$. Figure 6.4 demonstrates that the same is true for the Galileo signals.
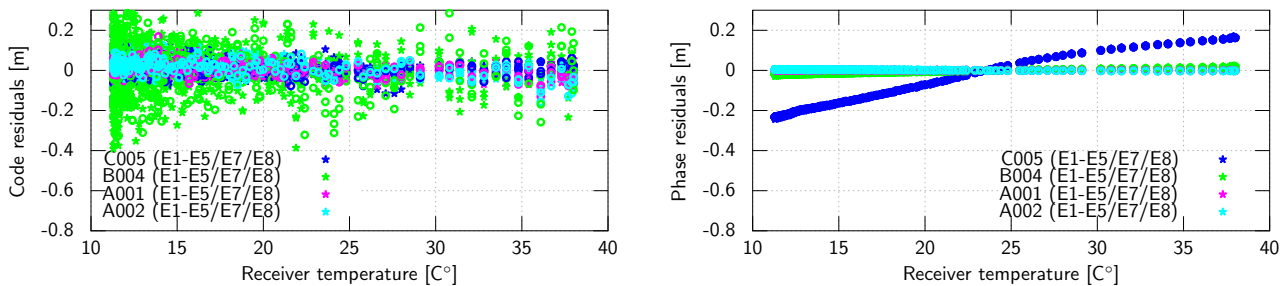
Figure 6.4: Temperature dependency of differential receiver code (left) and phase (right) delays for Galileo (E03, E18).

Table 6.8 shows the mean drift rate of the different signal components relative to L1/E1 and the standard deviation of the estimates between the different satellites.

Sys.	Receiver	Frequency	Code drift	Std.	Phase drift	Std.
GPS	A001	L1-L2	-2.4	0.3	0.1	0.1
	A001	L1-L5	-6.2	0.7	0.1	0.1
	A002	L1-L2	-2.1	0.1	-0.1	0.1
	A002	L1-L5	-5.9	1.2	-0.1	0.1
	C005	L1-L2	-4.4	0.3	16.6	1.4
	B004	L1-L2	-6.1	5.9	1.1	0.1
Galileo	A001	E1-E5	-5.0	0.2	0.0	0.3
	A001	E1-E7	-0.4	0.5	0.0	0.2
	A001	E1-E8	-1.0	1.4	-0.2	0.1
	A002	E1-E5	-4.5	0.5	-0.1	0.3
	A002	E1-E7	-1.0	0.4	-0.2	0.2
	A002	E1-E8	-2.2	0.4	-0.1	0.2
	C005	E1-E5	2.7	0.1	16.7	0.3
	C005	E1-E7	-2.3	0.0	16.5	0.2
	C005	E1-E8	0.9	0.2	16.6	0.3
	B004	E1-E5	6.5	0.4	1.6	0.3
	B004	E1-E7	-4.1	0.5	1.4	0.2
	B004	E1-E8	-2.8	0.3	1.5	0.2

Table 6.8: Differential drift of code and phase delays for the test receivers relative to L1/E1 [mm/C°].

It becomes obvious that the drift rates for code observations are negligible for all tested receivers. However, the situation is different for phase observations. Here, some receivers such as C005 show L1 to L2 phase drift rates of up to $17\,mm/^\circ C$, still relying on the assumption of the similar behaviour of internal receiver temperatures.

Considering the impact of a file download on the internal receiver temperature (see figure 6.2), the significant impact of such effects in the processing cannot be excluded. However, there are also positive examples of being robust to temperature changes, such as that of A001/A002. Nonetheless, the reason that such effects did not show up in the common GNSS analyses remains to be explained. With reference to this, it is worth recalling that common GNSS processing is carried out using dual-frequency, ionosphere-free linear combination observations. To demonstrate the impact of such drifts on dual-frequency PPP solutions, different PPP runs were conducted, one based on ionosphere-free linear combination observations (PAI), and two based on raw observations. The first raw observation PPP run was designed to expose the original effects (RER), whereas the second run (PAR) was set up to be comparable to the PAI scenario. Table 6.9 gives an overview of the different parameterisations compared to the respective initial setups.

Scenario	$trop$	STEC	δt^{rec}	ucd_{rec}	ucd^{sat}	N	CRD
RER	modelled/estimated	estimated	estimated	estimated per link		estimated	estimated
PAI	modelled/estimated	LC	estimated	ISB		estimated	estimated
PAR	modelled/estimated	estimated	estimated	estimated per link		estimated	estimated

Table 6.9: Modified parameter setups for temperature analysis.

The resulting code (left) and phase (right) residuals are shown in figure 6.5. In addition to the different residuals, the impact of the ionosphere as estimated in PAR is depicted in addition.
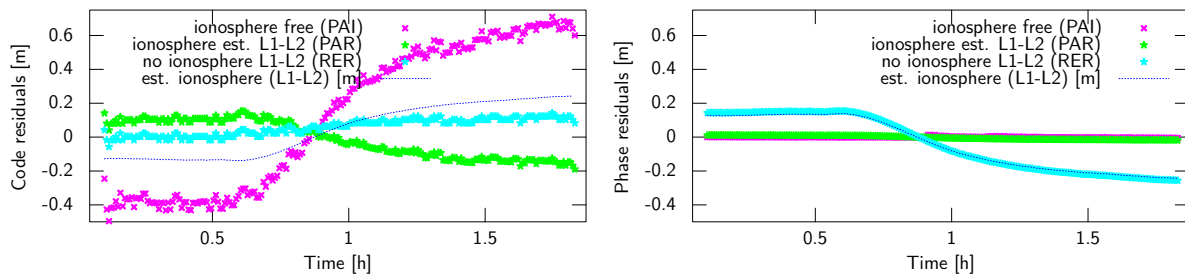
Figure 6.5: Impact of phase drifts (L1 versus L2) on ionosphere-free linear combination and raw PPP residuals (G07 at C005).

This shows that the estimated ionospheric delay matches the original phase residual (RER) exactly. Consequently, the phase residuals of PAR, corrected by the estimated delay, no longer show the phase drift. It becomes obvious that, in the case of ionosphere estimation (PAR), the code residuals absorb the phase-induced effects. Again, the effect on the code residuals is even magnified for the ionosphere-free linear combination. Due to the minor weight of the code observations in the LSQ process and in the case of dual-frequency observations, phase drifts do not significantly affect the coordinate solution. However, as soon as the third frequency comes into play, as demonstrated in section 4.2, a complete absorption of phase drifts is no longer possible. With the third frequency, the ionospheric estimate (first-order) is overdetermined for the first time, at least with observations being equally weighted (three phase observations). This complicates or even prevents the absorption of inter-frequency biases. Consequently, these effects show up as variations in the phase measurement. Such variations can be mitigated by observation differences, whereas the effects remain in the equation for undifferentiated observations. A more detailed discussion of this topic can be found in section 7.3.2. The presented effects are an extreme example and will probably never occur in normal operations. Nevertheless, they underline the importance of bias stability and of potential error sources.

6.1.3 Analyses based on real observations

The previous section demonstrated the sensitivity of UCDs and UPDs according to different parameters, such as receiver settings, temperature and so on. Taking into account that the GNSS simulator was not calibrated, a true assignment of the different effects to the test receivers was not possible. Furthermore, it is clear that the observation system cannot be seen merely as a standalone receiver. It is instead a rather complex system that includes numerous components like GNSS antennae, cables, splitters and so on. Hence, the observations are also

influenced by various effects and their interactions. This section aims to confirm the results from the previous section and to expose the impact of various different error sources like the antenna and the environment. It is clear that time and satellite-elevation-dependent delay variations can only be decoupled from atmospheric delays with difficulty. The main objective of this analysis is the characterisation of constant (daily) code delays. Again, as in the simulator analyses, the zero-baseline setup was found to be optimal. However, contrary to the simulator tests, the synthetic signal source was replaced by a real GNSS antenna that received true GNSS signals. The zero-baseline setup ensures comparable effects on the observations recorded by the four test receivers (A001, A002, B003 and B004).

The simulator analyses demonstrated the similar performance of Galileo- and GPS-related UCDs. For this reason, as well as to simplify the analyses, the following study concentrates exclusively on GPS-related UCDs. Furthermore, the selection of GPS-only analyses allows the utilisation of external satellite orbit and clock estimates, ensuring the highest accuracy. The analyses were performed by making use of the raw observation PPP setup, described in table 5.1. It is well known that the IGS final orbits and clocks do not contain the epoch at midnight. Therefore, the decision was made to use the "internal" ESA final orbit and clock (30-second) solution that still contains this epoch. Table 5.1 describes two parameter setups for raw observations, one making use of satellite-receiver pair specific UCDs and a second using UCD constraints. Since a comparison of satellite-receiver pair related UCDs is not reasonable, the following analysis makes use of a priori UCDs. The a priori values for the receiver UCDs were derived from the simulator analysis. The application of satellite UCDs is not required for the following analysis, which concentrates on inter-receiver bias differences. However, in order to make the results more realistic, the DCBs provided by CODE were transformed and applied as satellite UCDs. The transformation equation from DCBs to UCDs is as follows:

$$DCB = UCD_{L1} - UCD_{L2} \tag{6.4}$$

for $UCD_{L1} = 0$, the equation can be rewritten as:

$$UCD_{L2} = -DCB \tag{6.5}$$

The strong constraints on the UCDs prevent straightforward comparison. However, due to the correlation of STEC estimates and UCDs (see section 4.2), STEC estimates are optimally suited to be a quality indicator for a priori UCDs. In case of zero-baselines or nearby stations with identical or comparable ionospheric delays, the conformity of the applied UCDs is given by the accordance of the estimated STEC parameters. For reasons of clarity, assuming the UCDs on L1 to be zero, in the following section the term DCB is used for the UCDs on L2 (UCD_{L2}), whereas the UCDs on L1 are always zero. Consequently, in the following section, the term UCD is universally replaced by DCB. As the first example, figure 6.6 shows the epoch-wise STEC differences to the mean of all four receivers for a single pass of G10.
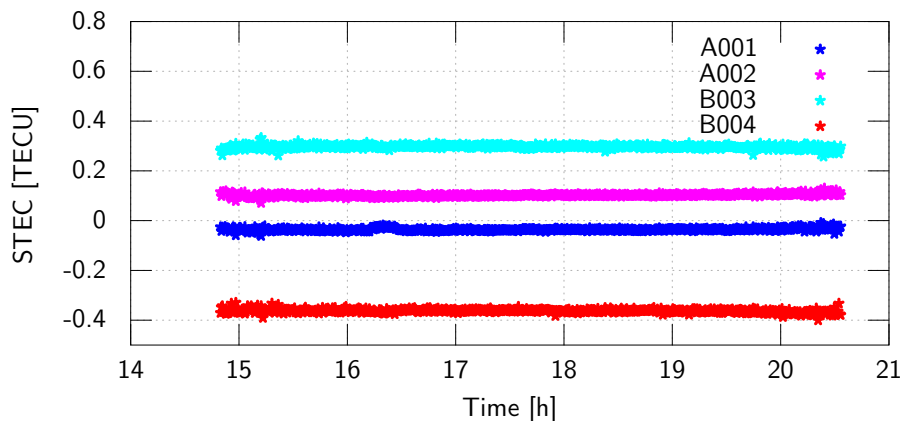
Figure 6.6: Comparison of receiver STEC estimates versus the mean for G10 (day 355 in 2012).

At first glance, it becomes obvious that the different STEC estimates show the same behaviour, cancelling out the differences. However, it is clear that the different time series are offset by a constant value. Since the time variable differences between the STEC estimates were found to be negligible, the following analysis concentrates on the

mean STEC offsets per satellite-receiver pair. The left part of figure 6.7 shows the satellite-receiver pair dependent STEC differences from the mean.

While it is apparent that some satellites behave differently, in general, most satellites belonging to a receiver were affected in a similar way. The existence of such receiver-dependent offsets demonstrates that the a priori applied DCB values do not fully represent the delay between the code observations on L1 and L2. In order to derive more realistic DCB values, the satellite-receiver pair dependent DCB corrections (ΔDCB), required to align the corresponding ionospheric estimates with the mean, were computed. This was done by transformation of the STEC difference ($\Delta STEC$), as expressed in the following equation:

$$\Delta DCB = \Delta TEC \frac{A}{f_{L2}^2}$$

(6.6)

By using this formula, the mean ΔDCB per receiver was computed and then applied to the a priori DCBs. Based on the corrected DCBs, the PPP analysis was repeated. The resulting STEC differences ($\Delta STEC$) are displayed in the right-hand section of figure 6.7.
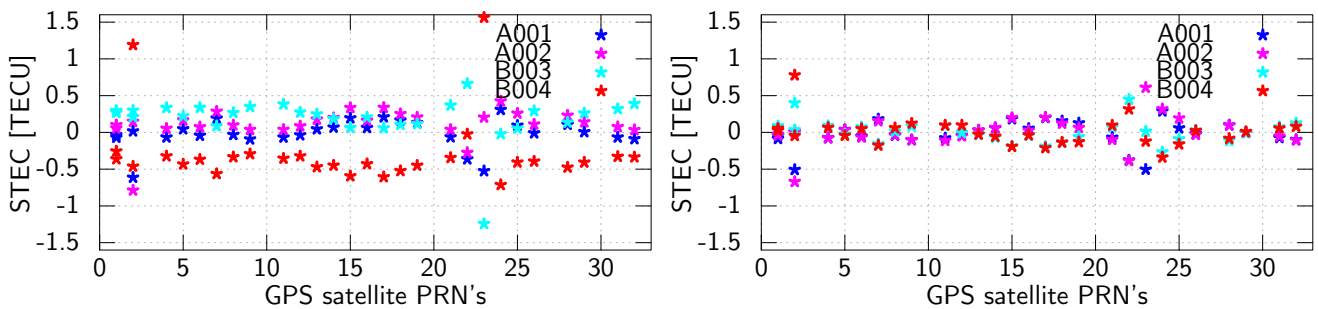
Figure 6.7: Individual unadjusted (left) and the adjusted (right) $\Delta STEC$ estimates of all GPS satellite-receiver pairs (day 355 in 2012).

It becomes obvious that the STEC estimates resulting from the second PPP and making use of the corrected DCBs are significantly better aligned. This shows that the presented procedure can be used to relatively calibrate DCBs between different receiver systems. However, in order to achieve a reasonable calibration of DCBs it is important to know their characteristics. Therefore, the main concern of the analysis presented in the following section was the day-to-day stability of receiver system DCBs and their sensitivity to receiver settings, the environment and antenna changes. For this purpose, different test scenarios (SCs) were set up and run for several days. This procedure not only allows for the analysis of the DCB stability within a dedicated setup, but also exposes the differences between the different setups. Scenarios one and three are the basic or reference scenarios. Scenario two was set up to show the impact of multipath mitigation techniques on the DCBs. The first three scenarios were run by making use of a zero-baseline setup. All other scenarios require different antennae in different locations. For this purpose, two antennae were mounted in different locations, displaced by approximately $23\,m$, and two receivers were connected to each of them. The scenarios SC4 - SC8 were set up to show the impact of the environment and of different antennae. An overview on the different scenarios is given in table 6.10. A brief description of the different scenarios is given in the subsequent analyses.

Scenario	Description	A001/B004			A002/B003		
		Point	Antenna	Settings	Point	Antenna	Settings
SC1	baseline scenario	P I	BI	mp m. off	P I	BI	mp m. off
SC2	mp mitigation	P I	BI	mp m. on/off	P I	BI	mp m. off/on
SC3	baseline scenario	P I	BI	mp m. off	P I	BI	mp m. off
SC4	environment	P I	BI	mp m. off	P II	BII	mp m. off
SC5	antenna	P I	BI	mp m. off	P II	AI + ext.	mp m. off
SC6	antenna	P I	BI	mp m. off	P II	BII + ext.	mp m. off
SC7	antenna	P I	AI	mp m. off	P II	BII + ext.	mp m. off
SC8	antenna	P I	AI	mp m. off	P II	BI + ext.	mp m. off

Table 6.10: Scenarios run to analyse the DCBs.

The evaluation of the recorded observations was again carried out using the raw observation PPP setup. In contrast to the previous run, the receiver DCBs were fixed to the adjusted values resulting from the previous step. Note the DCB adjustment was intentionally based on observations data of a single day in order to allow an independent analysis of the DCB stability for the following days. In the following analyses, the STEC differences are mapped to DCBs. It is clear that a change in a single DCB affects the mean of all receivers and consequently causes all values to change. Therefore, to make this clearer, the different offsets are no longer referred to the mean of all receivers. Instead, A001 was used as a reference. The decision in favour of A001 as a reference was firstly taken because the two A001/A002 receivers appeared to be more stable than were the two B003/B004 receivers. Secondly, following the setup of A001, most of the scenarios had remained unchanged. Figure 6.8 shows the mean daily $\Delta DCBs$ for the remaining three receivers (A002/B003/B004).
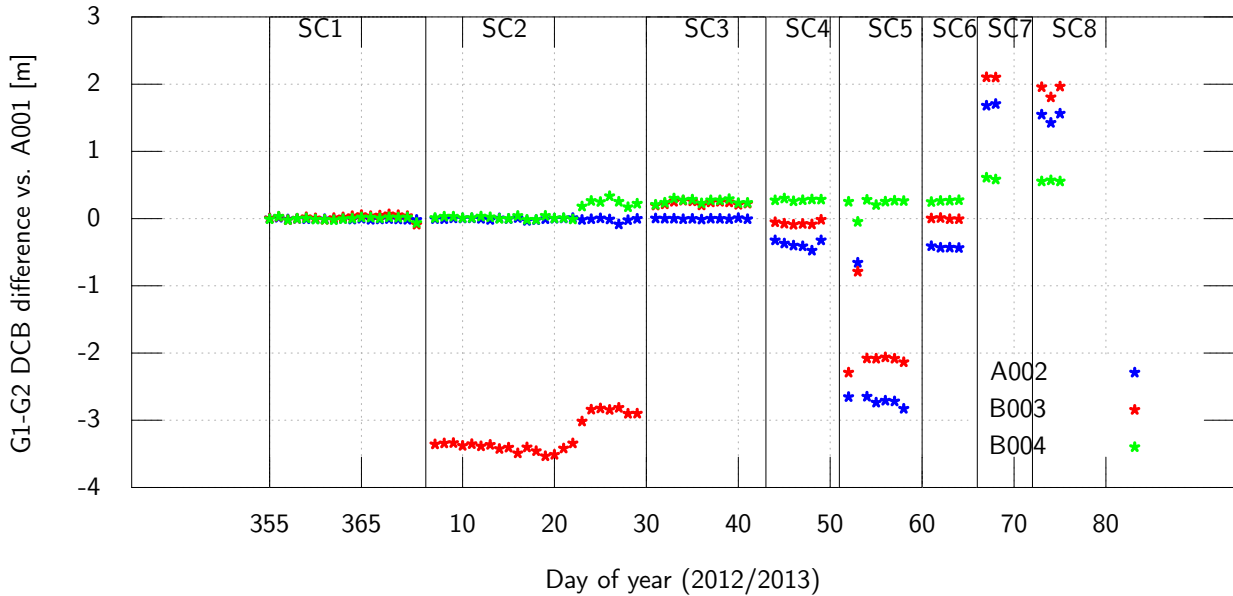
Figure 6.8: Stability and sensitivity of receiver dependent DCBs.

It is obvious that the receiver DCBs are relatively stable within an scenario. However, it becomes clear that the use of multipath mitigation techniques, different environmental conditions or antennae causes the receiver DCBs to change. The meaning of the different scenarios for the DCBs is described in the following section.

Baseline scenarios (SC1/SC3)

The baseline scenarios SC1 and SC3 were set up to adjust the receiver DCBs as described previously, as well as to demonstrate the stability of the DCBs regarding unchanged receiver settings, environmental factors and antennae. This setup applies identical receiver configurations to all receivers of the same type and comparable settings between the receivers of different types. Furthermore, all receivers are connected to the same antenna. This ensures equal input signals for all four receivers. Figure 6.8 shows almost constant bias behaviour within SC1, as well as within SC3. For the receivers B003 and B004, it is obvious that something occurred between SC1 and SC3, causing the biases to change. This can also be confirmed by inspecting the mean ΔDCB values of the respective receivers. Table 6.11 shows the mean and the standard deviation of daily ΔDCB estimates for the different test receivers for SC1.

Receiver	Mean	Std
A001	ref.	0.02
A002	-0.01	0.01
B003	0.02	0.02
B004	-0.00	0.01

Table 6.11: Mean and standard deviation of Δ DCBs (SC1) [m].

The presented values confirm the first impression from figure 6.8 and show the day-to-day stability of the delays at a centimetre level. When comparing the two identical setups SC1 versus SC3 (table 6.11 versus table 6.12), B003 and B004 receivers show similar behaviour in that they are displaced by 0.23 m/0.26 m compared to A001. At this point, it remained unclear if the change appeared in the two A or the two B receivers.

Receiver	Mean	Std
A001	ref.	0.01
A002	-0.00	0.02
B003	0.23	0.01
B004	0.26	0.02

Table 6.12: Mean and standard deviation of Δ DCBs (SC3) [m].

Impact of multipath mitigation techniques (SC2)

This setup was designed to demonstrate the impact of multipath mitigation techniques on the receiver DCBs. For this purpose and in contrast to the baseline scenario, two receivers (A001/B003), one of each type, were configured to apply multipath mitigation techniques. Table 6.13 shows the mean and the standard deviation of the ΔDCBs for the test receivers.

Receiver	Mean	Std
A001	ref.	0.09
A002	-0.01	0.10
B003 I	-3.33	0.02
B003 II	-2.99	0.03
B004 I	0.06	0.01
B004 II	0.11	0.04

Table 6.13: Mean and standard deviation of Δ DCBs (SC2) [m].

Table 6.13 confirms what was already obvious in figure 6.8, namely that something happened to the DCBs of the two B003/B004 receivers. For this reason, the ΔDCBs for these two receivers were estimated once before (I) and once after (II) the change. Considering the DCBs before the change (I) confirms the findings from figure 6.8. It clearly indicates a change of the DCB by -3.33 m for B003 as a response to the use of the multipath mitigation technique. Considering the DCBs after the change, it is very likely that the change appeared in both B003 and B004, rather than in the A001 and A002 receivers. Thus, the DCBs of the two A receivers remain comparable, whereas B003 (-0.34 m) and B004 (0.05 m) are affected differently. Figure 6.9 gives a deeper insight into the behaviour of the individual estimates. It shows the ΔDCBs of B003 per satellite and per day.
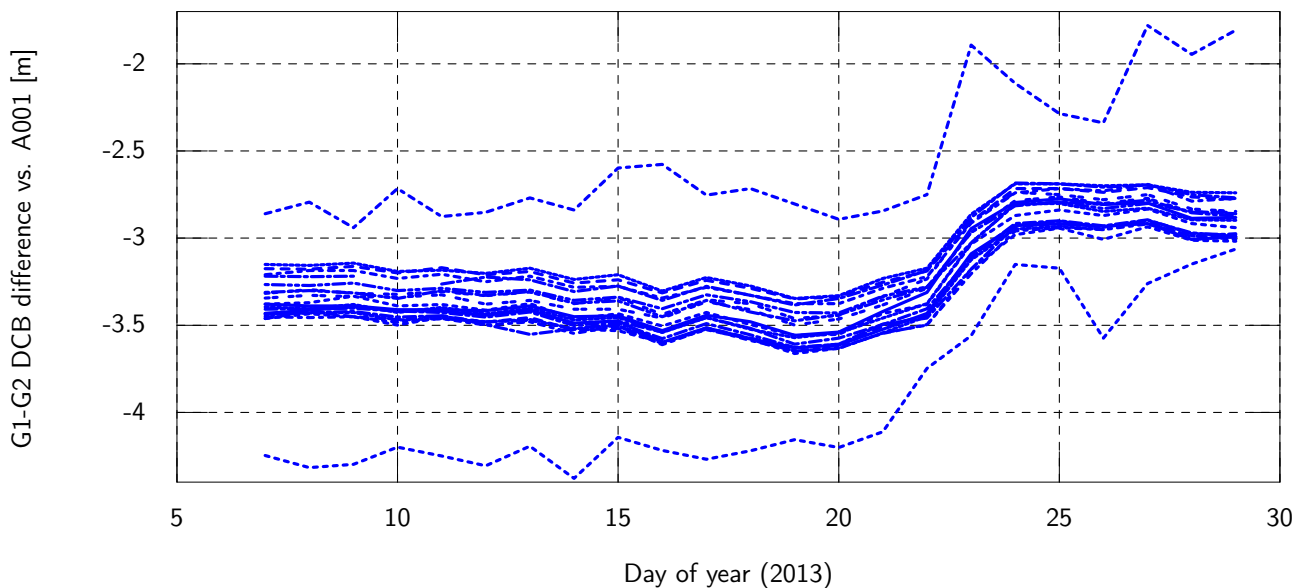
Figure 6.9: Unexpected change in the receiver DCBs, visible for all satellites (B003).

It becomes obvious that the change is not a problem caused by a single satellite, but is instead an effect affecting all satellites equally. Another interesting aspect of figure 6.9 is the behaviour of the different satellites. It has to be noted that, due to chosen zoom options, not all satellites are visible. It becomes obvious as was explained in section 3.1.2 that different satellites, depending on their PRN, have different DCBs. Admittedly, the receiver DCBs for most satellites are within a range of a few centimetres and are therefore insignificant compared to the pseudo-range accuracy. Nonetheless, there are also satellites that show offsets of several decimetres from the mean. However, since the code observations are significantly down-weighted in the processing, this does not significantly affect the positioning solution. Another option for overcoming this issue is the estimation of satellite-receiver-pair (link) specific DCBs. Since this entails with the loss of separability of clock, signal and ionospheric delays, this strategy is not suitable for all applications.

Impact of antennae and environment (SC4-SC8)

Several scenarios were set up in order to analyse the impact of different environments and antennae. Thus, the zero-baseline setup is no longer applicable for this research. Furthermore, the use of different antennae in different environments entails different observations. As a result, the assignment of bias variations to their initial sources also becomes more difficult. The test receivers A002 and B003 were installed at two separate locations. In scenario SC4, in order to keep the changes to the previous scenarios as small as possible, test sites PI and PII were equipped with antennae of the same type.

Setup SC6 aims to enable a separation of effects caused by the antenna mounting and by the antenna itself. For this purpose, the antenna in point P II was raised by $0.049\,m$ (SC5), whereas all other components remained untouched. The next point of interest was the impact of different antenna types on the DCBs. For this analysis, antenna BI that was mounted at location P II, was replaced by an antenna of type AI. Further antenna changes became necessary (SC7 - SC8) in order to decouple the different effects and to allow for a clear assignment of the effects to the respective antenna change. A summary of the different setups can be found in table 6.10.

Even though the sample of test cases is limited, comparing the scenarios' typical offsets (up to several metres) with the respective standard deviation of the daily solutions (few centimetres), it can be seen that the offsets found are representative of their respective setups. Based on the differences between the different setups and their typical values, the impact of the individual components can be derived. A summary of the different analyses and their respective effects is given in table 6.14. For the original tables, see tables 6.11, 6.13 and 6.12, as well as tables 9.6, 9.7, 9.8, 9.9 and 9.10 in the appendix.

Scenario	Receiver	Mean	Std
Multipath mitigation (SC1 vs. SC2)	A002	0.01	0.03
Multipath mitigation (SC1 vs. SC2)	B003	3.33	0.05
Extension of 49 mm (SC4 vs. SC6)	A002	0.05	0.05
Extension of 49 mm (SC4 vs. SC6)	B003	-0.02	0.07
Antenna AI - BII (SC5 vs. SC6)	A002	-2.29	0.05
Antenna AI - BII (SC5 vs. SC6)	B003	-2.12	0.07
Antenna BI - AI (SC6 vs. SC7)	A001	2.12	0.0
Antenna BI - AI (SC6 vs. SC7)	B004	1.26	0.01
Antenna BII - BI (SC7 vs. SC8)	A002	0.18	0.05
Antenna BII - BI (SC7 vs. SC8)	B003	0.19	0.06
Environment (SC3 vs. SC4; SC7 vs. SC8)	A002	0.20	0.07
Environment (SC3 vs. SC4; SC7 vs. SC8)	B003	0.11	0.07

Table 6.14: Summary of analysed DCB sources and their impact [m].

The results show that almost every change in the setup affects the DCBs, no matter whether this change involves the receiver setting, mounting, obstruction or installed antenna type. Fortunately, the day-to-day variability shows that the biases are in most cases representative of the respective setups. Once again, this allows the assignment of biases to dedicated sources, such as antennae or receiver settings. Therefore, for example, it can be seen that the change from the BI antenna to the AI antenna causes DCB differences in the range of $2.2\,m$ and that changes in the environment cause delays at the decimetre level, whereas the lifting of the antenna by $0.049\,m$ did not show a significant impact. A further point of interest in the analysis is the impact of the multipath mitigation technique, where some receivers, such as A002, showed no observable impacts, but in the B003 receiver, in accordance with the simulator analysis, the DCB changed by about $3.3\,m$.

6.1.4 Summary of receiver-related delay analysis

In the frame of this analysis, the newly implemented, raw observation-based PPP approach was used to analyse the performance of uncalibrated signal delays. The comparison of these results with the results of direct observation differences demonstrated an accordance at the centimetre level. Therefore, this confirms the correctness of the implementation and the applicability of this approach for signal analyses. The analyses presented give some idea of the potential of raw observation processing. In contrast to the commonly used ionosphere-free processing strategy, this approach allows a detailed analysis of all individual components and parameters, as well as the relationships among them.

The performed analyses were split into two parts, the first part making use of artificial GNSS signals in a controlled environment, and the second part making use of real GNSS signals. This split not only allowed for a detailed analysis of the individual components in a controlled environment, but also addressed the pathlessness of real observations. Nonetheless, both analyses produced comparable results. The analyses showed significant performance differences among the different receiver types. For phase observations, two of the three tested receiver types showed a significant sensitivity to temperature variations, whereas the receivers of the other receiver type remained unaffected. In addition to the temperature variability, numerous other effects, such as model errors, affects the uncalibrated phase delays. Consequently, in the case of undifferentiated observations, these cannot be assumed to be stable at the accuracy level required for reasonable ambiguity fixing.

With regard to code observations, it was shown that almost every change in the station, receiver setup and configuration affects the DCBs. For one type of test receiver, it was shown that the activation of multipath mitigation techniques caused the DCBs to change by about $3.3\,m$, whereas the others remained unaffected. A further example demonstrated within the analyses showed the impact of antenna changes. For the test antennae, it was shown that the change from one antenna type to another caused a change of about $2.2\,m$ in the DCBs. Nevertheless, in most cases where the setups were unchanged for several days, the experiments demonstrated DCB stability at the centimetre level. The established stability of the code delays indicates that it might be possible to calibrate receiver site UCDs in situ and in a real environment. Admittedly, the impact of numerous error sources for such a calibration, such as antenna, cable, mounting and so on needs to be considered, either in terms of elements or with regard to the full system. However, any change in the environment needs to be regarded with caution and possibly involves a new calibration. It has to be mentioned that, within the test period, two of the test receivers changed their DCBs permanently for some reason. This again demonstrates that a definitive statement on this topic requires further tests that cover longer time periods, additional scenarios and different receiver types. Furthermore, according to the theory and as explained in section 3.1.2, the analyses demonstrated that different PRNs are tracked differently by different receivers or, to be more precise, by different correlator types and their settings.

6.2 Satellite-related signal delays

The complement of the receiver-dependent signal delays are the signal delays in the satellites. In fact, the situation for the satellite delays is quite similar to delays in the receivers. Thus, several publications, such as that by Schaer (2008), demonstrated the almost constant behaviour of the satellite dependent DCBs (UCDs). Again, with regard to the phase delays, strong phase variations have been observed for some satellites like GPS-62 (Montenbruck et al., 2010), although this is not the case for all satellites. Schönemann et al. (2011) demonstrated that there are no significant variations of the phase delays on GIOVE-B.

6.3 Summary of analyses of uncalibrated signal delays

It was demonstrated that neither the receiver- nor the satellite-dependent uncalibrated phase delays can be assumed to be stable. In both cases, for at least some satellites as well as for some receiver types, the differential UPDs are stable and for others they are not stable. Since both components need to be considered jointly, it is somewhat unlikely that the sum thereof is stable. Moreover, numerous model inaccuracies, such as inappropriate PCO/PCV values acting in a similar way complicate the situation. However, in the case of float-valued carrier phase ambiguities, constant phase delays are insignificant. The impact of ambiguity fixing for raw observations is discussed in section 7.3.2.

For geodetic analyses, the less stringent accuracy requirement for code observations permits the assumption of stable differential UCDs (DCBs) for both satellites and receivers. Nevertheless, it has been shown that the receiver UCDs depend on a number of different parameters, such as receiver type, settings, cable, antennae, environmental factors and the like. In order to calibrate the receiver-dependent UCDs, all these effects need to be considered. Moreover, in the event of any change in the setup, it might become necessary to recalibrate the system. The analyses performed are not sufficient for a final statement. Nevertheless, it has been demonstrated that raw observation PPP allows detailed analyses of individual signal components and their relationships, also in the case of real GNSS observations. Consequently, a relative calibration of receiver UCDs with real GNSS signals is imaginable.

7 Applicability of raw observation processing

The previous section demonstrated the applicability of the raw processing approach for bias analyses. The aim of this section is to demonstrate the applicability and the comparability of the results of raw observation processing compared to the commonly used processing of ionosphere-free LC observations in terms of both network and standalone PPP solutions. Moreover, this section intends to highlight the advantages of an equivalent handling of any arbitrary GNSS observation. Because standalone PPP solutions require precise satellite orbit and clock estimates derived from a global network solution, the first point of interest is the network analysis. As outlined in the previous section, the utilisation of undifferentiated raw integer-ambiguities is neither feasible nor rational. For this reason, both analyses concentrate on the comparison of solutions based on float ambiguities. Integer-ambiguity constraints are renowned for stabilising common, ionosphere-free LC GNSS solutions; accordingly, the application of this technique and alternative ways of stabilising raw observation-based PPP approaches are discussed separately in section 7.3.

The raw processing approach was developed to optimally combine and process different GNSS, arbitrary observation types on multiple (more than two) carrier frequencies. Therefore, in order to demonstrate its maximum benefits, the test case is expected to examine these features. At present, GNSS satellites from GPS and GLONASS, as well as validation and experimental satellites from Galileo, QZSS and BeiDou are in orbit and are available for testing. Test and validation satellites are not always usable and, if they are, they do not always fulfil the specified requirements. Therefore, in order to keep the burden of new implementations, testing and optimisation within reasonable bounds, the test case concentrates on two GNSS, one operational GNSS, namely GPS, and one GNSS, Galileo, which is still under construction. The decision in favour of GPS was made because GPS operates dual-frequency satellites, as well as modernised triple-frequency satellites. The modernised satellites transmit both old and new signals on three instead of two frequencies. Another criterion for the decision in favour of GPS was that up-to-date GLONASS dual-frequency satellites still suffer from the problems related to FDMA. As a result, the benefit of processing up-to-date GLONASS dual-frequency observations using the raw processing approach is somewhat negligible. The final argument for the restriction to two GNSS is the intention to use the same tracking network for all GNSS. Because some of the receivers only track GPS, others track GPS and GLONASS or Galileo and still others track all three GNSS, it is particularly laborious to select a global network with an optimal distribution that is compatible with all three GNSS. When concentrating on two GNSS, the situation is significantly simpler.

7.1 Applicability for global networks

The aim of this section is the demonstration of the applicability of the raw processing approach for global network analyses. This was conducted by means of a quality analysis of the orbit and the clock offset estimates. The quality was assessed in an absolute sense with respect to an external reference solution and, internally, by a stability analysis. As outlined in section 1.2, IGS final orbit and clock products are the reference of choice for any type of GNSS analysis. However, it has to be taken into account that all products are computed by making use of ionosphere-free linear combinations. Consequently, these products are, strictly speaking, only valid for the same kind of processing and are not necessarily applicable for other processing approaches, such as the processing of raw observations. However, for reasons of consistency, any new upcoming approach needs to be able to reproduce the IGS products, at least within certain limits. Furthermore, since there is no existing reference solution for raw observations at present, the IGS finals are the best reference. Global GNSS network PPP estimates a number of different parameters, such as ERPs, satellite, station, clock and atmospheric parameters. The parameters that are mainly affected by the choice of the processing approach are satellite orbits, clock offsets, UCDs and the atmospheric parameters. For this reason, the following analysis concentrates on these parameters. Furthermore, it is clear that the remaining parameters, such as ERPs and satellite parameters like SRPs, are at least indirectly compared when comparing orbit and clock products.

The network PPP analyses were based on observation data, freely available at the main IGS and on the MGEX repositories. The decisive point for the station selection was the tracking capability of GPS and Galileo observations. The limited number of available GNSS stations did not allow for a selection of geometrical points of view. It is well known that the stations accepted as "IGS" stations, for which data are distributed via the main IGS server, have to fulfil a minimum set of requirements (IGS, 2013). By contrast, the requirements for the stations participating in the MGEX are rather lax in terms of station setup, information provided on the receivers, their settings, the antennae and, finally, the data quality. Even so, the data quality is not the best and the continuous operation of all stations cannot be guaranteed, the available data set is sufficient for performing a global network analysis. The observation pre-processing was performed according to the description in section 5.2. It has to be mentioned that, due to the changing availability of stations and their data quality, the station network differs from day-to-day. A first set of analyses was run for a period of five months (November 1, 2012 to March 18, 2013). However, due to numerous changes in the tracking network and different satellite tests performed on the new Galileo satellites, the product quality was not as stable as expected. For this reason, the results presented in the following concentrate on a test period of two weeks from May 10 to May 23, 2013. However, as demonstrated within the orbit analyses, both test periods sent out the same message. Figure 7.1 exemplarily shows all stations available between May 10 and May 24, 2013.
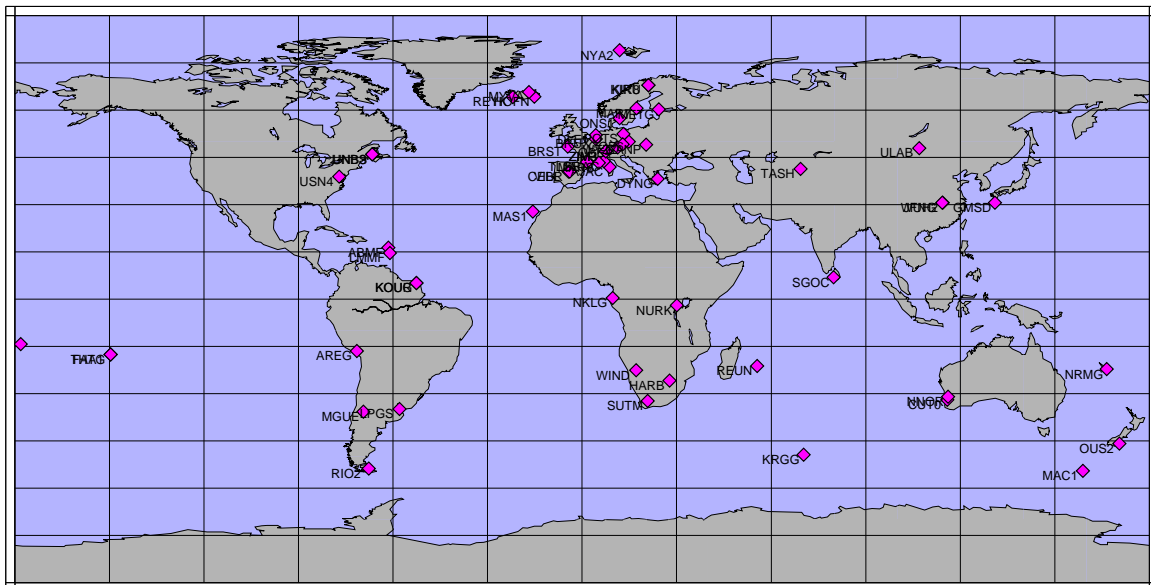
Figure 7.1: Map of the global GNSS tracking network used for the tests.

Different parameter setups are feasible for network PPP, as explained in section 5.3 and as shown in table 5.2. For the following analyses, one ionosphere-free standard (FREE_I) setup, settings comparable to ESOC's IGS processing and two scenarios based on raw observations were set up. The only difference between the two raw observation-based setups is the handling of the UCDs. The first setup applies a zero mean condition (FREE_R), whereas the second setup (FREI_R) makes use of a priori UCDs. In the second case, it is imaginable that the UCDs are either fixed to zero, comparable to the ionosphere-free processing or, alternatively, to a priori values. Table 7.1 summarises the differences in the parameter setups.

With the exception of parameters that are different by design, all the setups are identical. In addition to the parametrisation, the observation screening and weighting properties are also important for the quality of the final results. At this point, due to a lack of knowledge regarding the actual measurement accuracy, it is significantly more difficult to ensure comparable setups between the two approaches. Finally, as described in section 5.4, the ionosphere-free setup applies the standard values from ESOCs's IGS processing whereas, for the raw observation setups, the values are based on assumptions and empirical tests. The values applied are given in table 5.3.

Parameter	FREE_I	FREI_R	FREE_R
ISBs	1/Galileo/link	-	-
STECs	-	1/link	1/link
Satellite UCDs	-	zero/a priori	$\begin{cases} L1/E1 : UCDs = zero \\ L2/E5a : \sum UCDs = zero \\ other : UCDs = estimated \end{cases}$
Receiver UCDs	-	zero/a priori	

Table 7.1: Differences in the parametrisation of the analysed network PPP setups.

7.1.2 Quality assessment of satellite orbit estimates

The first point of interest was the orbit accuracy of the different approaches. For this purpose, the different solutions were compared to the external reference solution. Figure 7.2 shows the mean of the daily 1D orbit rms with reference to the IGS final products. The comparison was performed per satellite and per setup. In addition to the three scenarios mentioned and based on MGEX data, two further scenarios are shown in figure 7.2. The intention behind the additional scenarios is to demonstrate that the raw approach is equivalent to the ionosphere-free (IF) processing, even when the highest precision is required. Since the highest precision cannot be obtained by the sub-optimally balanced MGEX network, these scenarios are based on 110 well-distributed IGS stations and GPS-only data. Accordingly, these scenarios are referenced as IGS-like (IGSL) setups. The parameter setups for the ionosphere-free and the raw scenario are identical to FREE_I and FREE_R.
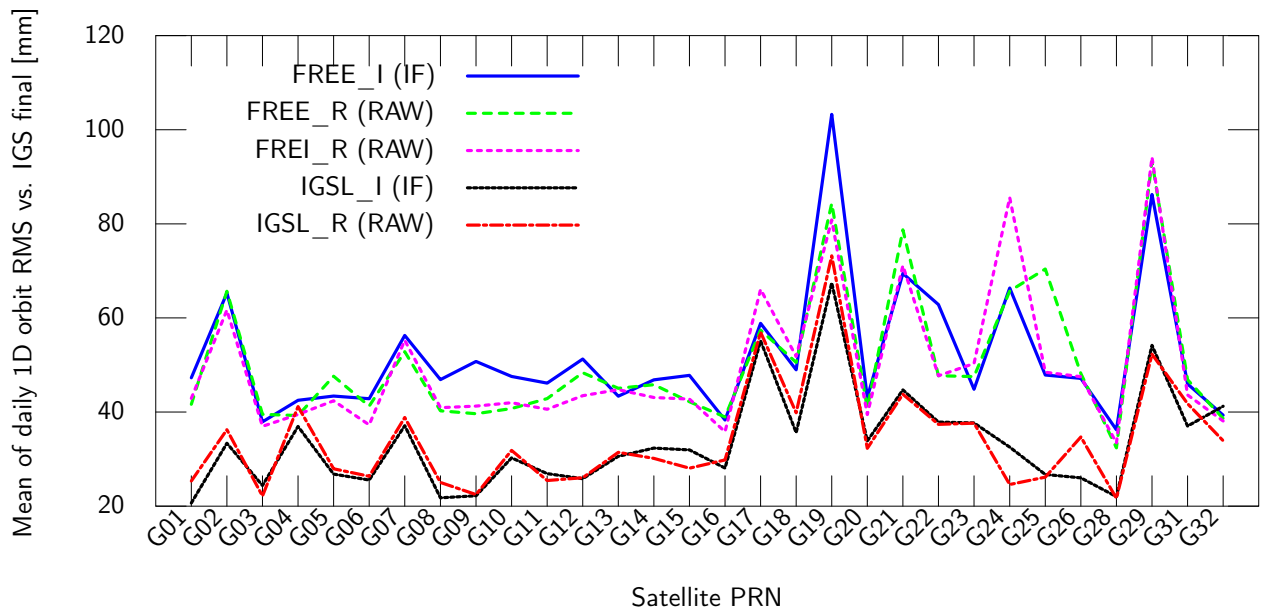
Figure 7.2: Mean 1D orbit rms w.r.t. IGS final orbits [mm].

In comparison to the IGS final orbits, the two approaches do not show a significant difference, neither for the MGEX network nor for the precise solution with the IGS-like network. The overall rms for the different float scenarios are given in table 7.2. The full tables are given in the appendix (see tables 9.11 and 9.12).

Network	FREE_I	FREE_R	FREI_R
MGEX	52	50	50
IGSL	33	34	34

Table 7.2: Mean 1D orbit rms w.r.t. IGS final orbits [mm].

In addition to the accordance with the external reference solution, the internal orbit consistency was also analysed. The quality assessment of the internal orbit consistency is usually done by means of an orbit overlap analysis. An orbit overlap analysis compares satellite orbits within a common period. In many cases, this denotes the comparison of the last and the first orbit point of two consecutive orbit arcs (midnight). However, the result of this implementation depends strongly on the geographical satellite position at the time. Since the orbit accuracy differs significantly along the path, particularly for the sparse MGEX tracking network, the following analysis compares orbit periods of 24 hours. For this purpose, two-day orbit arcs are fitted through two 24-hour orbit solutions. Consequently, the resultant consecutive two-day orbit arcs have one day in common. A better fit of the satellite orbits for the day in common indicates a better consistency between the different daily orbit solutions. Figure 7.3 shows the 1D rms of the orbit overlaps per satellite and per scenario.
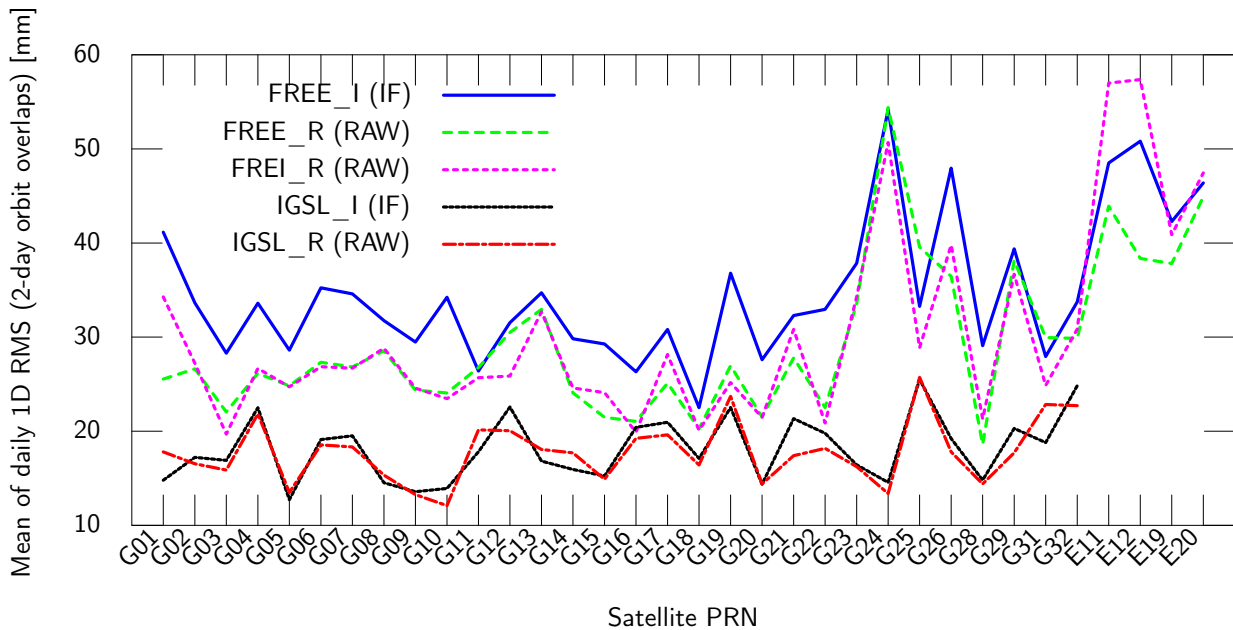
Figure 7.3: Mean 1D rms of two-day orbit overlaps [mm].

The raw observation approach appeared to be significantly more consistent with regard to the solutions based on MGEX stations. This finding is also confirmed by the overall rms, shown in table 7.3. The complete set of results is given in the appendix (see tables 9.13 and 9.14).

Network	FREE_I	FREI_R	FREE_R
MGEX	35	30	29
IGSL	18	18	18

Table 7.3: Mean 1D rms of two-day orbit overlaps [mm].

Because of the differences in the observation weighting and screening settings that are not one-to-one transferable, it is difficult to trace the improvement back to the new implementation exclusively. A closer inspection of the results showed that all scenarios used exactly the same stations. In fact, the only differences were the input observations (LC versus raw) and their screening and weighting settings. Considering the number of rejected observations, the raw observation-based scenarios reject slightly more observations (2.5%) compared to the ionosphere free setup (1%). However, the impact of the screening and weighting settings seems negligible for the IGSL solutions. In this case, both approaches are equivalent. For the MGEX based ionosphere-free scenario, a trial was made to adjust the observation weighting and screening settings in such a way as to obtain the same results. The different setups demonstrated that it was possible to bring the results closer together for individual cases, but it was not possible to achieve the same orbit consistency in effect. Indeed, this is not completely surprising since the raw processing approach provides considerably more flexibility for observation weighting and screening. Thus, it is not possible to transfer all settings to the common ionosphere-free approach. Nevertheless, it showed that the raw processing approach is "at least" equivalent to ionosphere-free processing.

In contrast to the quality assessment compared to IGS finals, orbit overlaps also enable the analysis of the Galileo orbit accuracies. At first sight, the Galileo orbits appear to be less accurate. However, a closer inspection reveals strong variations in the accuracy of the daily estimates (24-70 mm). The renouncement of the screening of daily rms values leads to increased mean values. It should be mentioned that the Galileo satellites are still affected by satellite performance tests. Furthermore, with regard to the heterogeneous signal tracking, different signals are tracked differently at different stations. In addition, models that are not yet fully optimised and the processing procedure for Galileo may affect the orbit accuracy. Finally, it has to be mentioned that due to different orbit repeat cycles (GPS: 1 day, Galileo: 10 days) the results of the orbit overlap analyses cannot be seen as one-to-one comparable. Rather the analysis benefits GPS, since station-dependent errors as multipath, antenna near-field effects, antenna phase centre errors repeat almost every sidereal day and their impact on the orbit trajectory is about the same and thus cancels out in the overlaps. In the case of Galileo with its 10-day ground track repeat cycle, however, station-dependent errors do not repeat after one day and, therefore, do not cancel out in the overlaps.

At this point, the question that arises is whether or not the conclusions drawn from two weeks of data processing are representative. As mentioned earlier, a period of five months was processed. In order to demonstrate that the statement drawn from the full period corresponds to the one presented previously, the 1D rms of the orbit overlaps of E11 for the complete test period is shown in figure 7.4.
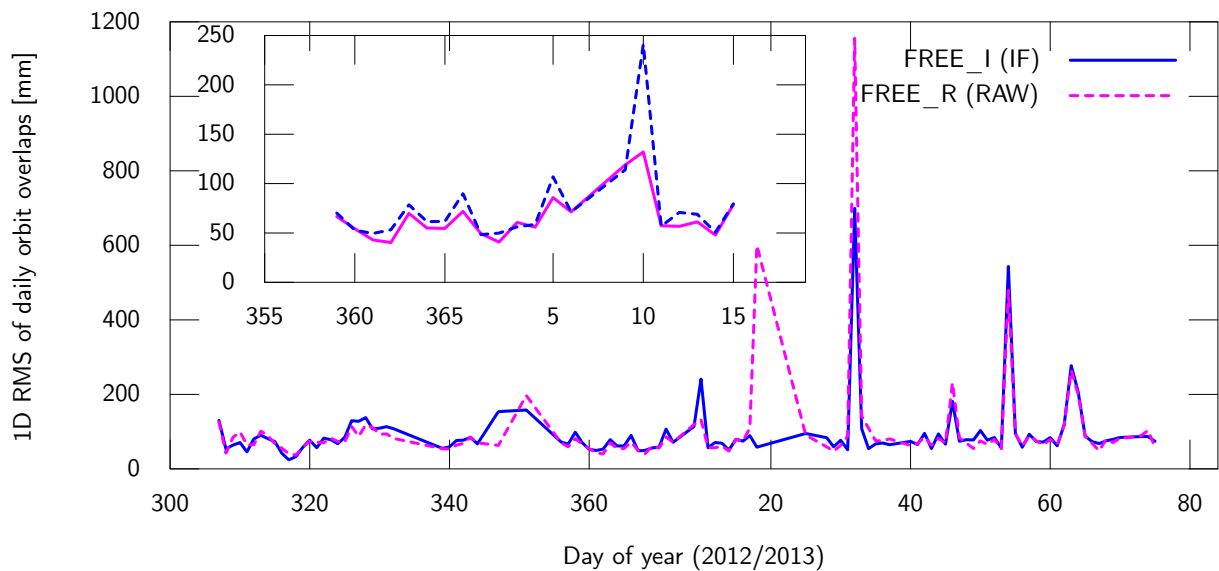
Figure 7.4: 1D rms of two-day orbit overlaps for GAL-101 (E11) [mm].

The first obvious concern is the problem of interpreting the total period, which shows significant variations in the orbit quality. This issue was the basis of the decision to focus on the analysis of two representative weeks. In agreement with the analysis presented so far, it can be seen that in the case of a sparse tracking network, the raw processing approach performs slightly better. This statement is confirmed by table 7.4, which shows the outlier-cleaned values of the enlargement in figure 7.4.

	FREE_I	FREE_R
Test period (two weeks)	59	44
Enlargement	63	59

Table 7.4: Comparison 1D rms of two-day orbit overlaps of GAL-101 (E11) [mm].

It shows that even though the rms of the test period is less than those in the enlarged period (day 359 in 2012 to day 008 2013), the final outcome remains the same, emphasising the raw observation-based solution as the best. This emphasises that the decision regarding the analysis period as discussed previously was reasonable and that the presented results are representative.

The next point of interest is the quality of the satellite clock estimates. Admittedly, the processing of different signals affected by different signal delays (UCDs, UPDs) and the application of different weighting schemes, in other words different clock definitions, results in different clock estimates. As a result, clock estimates of different processing approaches are not necessarily one-to-one comparable. Depending on the selected signal or signal combination and the related variable delays caused not only by atmosphere, multipath, UCDs and UPDs but also by model inaccuracies, for example, in the case of PCOs and PCVs, the clock estimates differ. It can be expected that the clock estimates of the different approaches differ in both their magnitude and in their characteristics. Accordingly, it is clear that, technically speaking, a quality assessment of estimated satellite clock offsets based on a direct comparison with the external reference solution is not correct. Keeping this in mind, a direct comparison is a suitable tool for the precise analysis of clock differences. Thus, in order to get a feeling for such differences, the clock estimates of the different scenarios are compared to the IGS final clocks. Figure 7.5 shows a comparison of the different epoch-wise clock estimates for GPS-61 (G02) on day 133 2013. In order to account for orbit differences, the radial orbit displacements between the different solutions were removed prior to this comparison.
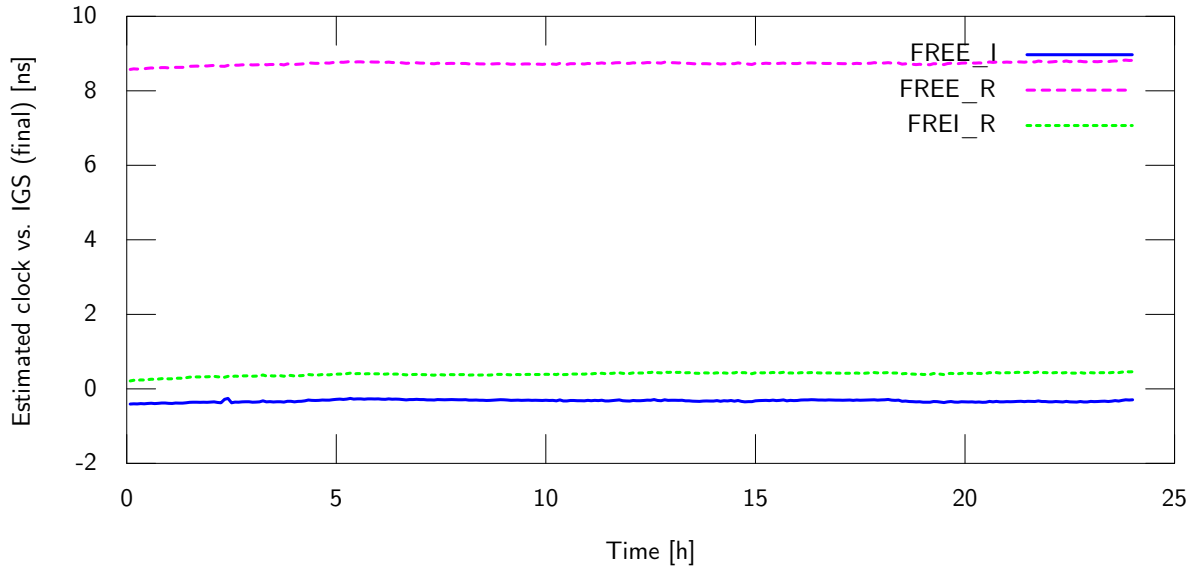
Figure 7.5: Comparison of epoch-wise clock estimates for GPS-61 (G02) for day 133 2013 [ns].

It shows, as expected, that the ionosphere-free solution (FREE_I) has the best agreement with the IGS final clocks. This is closely followed by the raw observation scenario that makes use of a comparable assumption on the a priori UCDs, namely that UCDs on L1 and L2 are equal to zero. Even though the solution based on raw observations applies the same assumption to the UCDs and uses an equal basis of observations, the clock estimate is different. However, this is not surprising when recalling the impact of UCDs on the clock offset estimates. In the following presentation, the term UCD covers both the receiver and satellite portions. If the assumption regarding UCDs is correct, both clock estimates are identical. However, if the actual UCDs differ from the assumption by ΔUCD, the impact on the clock estimate ($\Delta_{UCD} \delta t$) can be expressed as:

$$(IF) \quad \Delta_{UCD} \delta t = \frac{1}{f_1^2 + f_2^2} \left(f_1^2 \Delta UCD_1 + f_2^2 \Delta UCD_2 \right)$$

$$(raw) \quad \Delta_{UCD} \delta t = p_1 \Delta UCD_1 + p_2 \Delta UCD_2 + p_n \Delta UCD_n + \ldots$$

(7.1)

This shows that, in the case of ionosphere-free observations, the offset is defined by the frequency of the observations, whereas in the case of raw observations, the observation weight (p) is the decisive parameter. It becomes clear that the use of different or additional observation types with different UCDs affects the absolute clock level. Differences in the absolute level of the global clock offset estimates do not affect the user, since common offsets are absorbed by the receiver clock estimates. As a result, all the individual satellite clocks are correctly aligned with each other. For this reason, the relevant quality measure for clock estimates is the standard deviation versus the external reference solutions. Figure 7.6 clearly shows the different clock behaviours with reference to the IGS final clock (mean offset removed) for GPS-61 (G02) on day 133 2013.
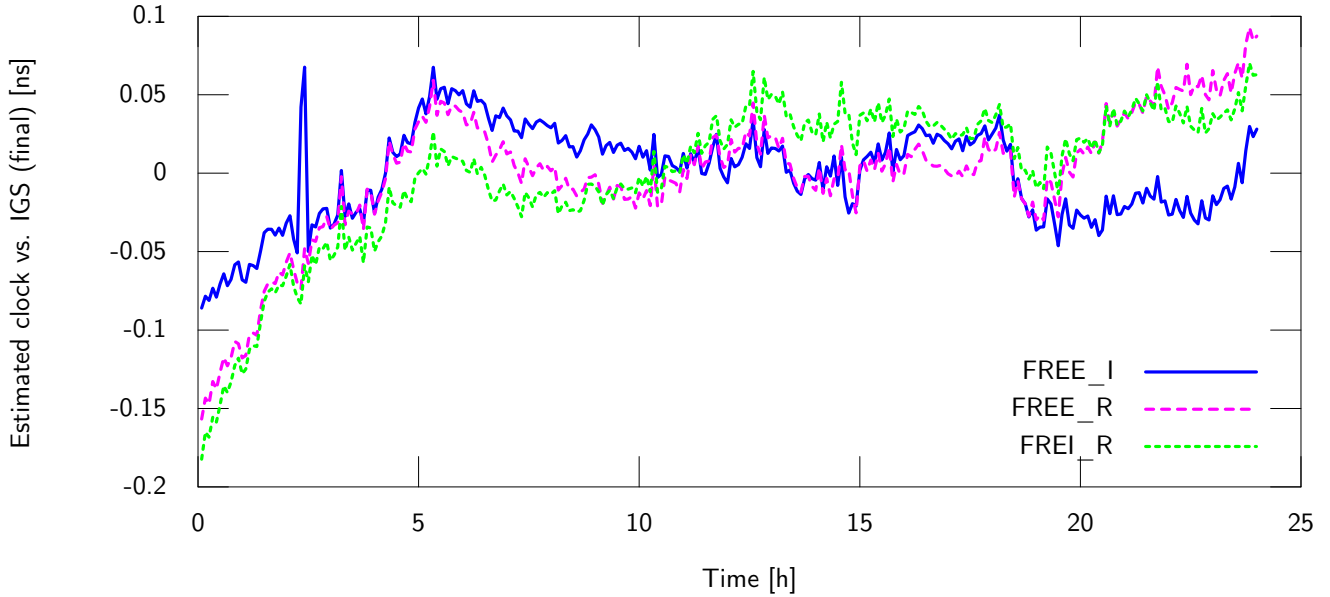
Figure 7.6: Adjusted comparison of epoch-wise clock estimates for GPS-61 (G02) for day 363 in 2012.

At first sight, all clock estimates appear to show similar behaviour. However, a closer look reveals a drift between the clock solutions in the different approaches. As a result of the minor weight of code in comparison to phase observations, the code observations have almost no impact on the relative behaviour of the clock estimates. Consequently, the time variable differences of the clock estimates are caused by variations in the phase observations. This means that the clock estimates are affected by UPD instabilities. In the following representation, these are expressed as the difference from the constant UPDs (Δ_{UPD}). Thus, the time-dependent clock variations as a response to UPD instabilities ($\Delta_{UPD}\dot{\delta t}$) can be written as follows:

$$(IF) \quad \Delta_{UPD}\dot{\delta t} = \frac{1}{f_1^2 + f_2^2}\left(f_1^2 \Delta\dot{UPD}_1 + f_2^2 \Delta\dot{UPD}_2\right)$$

(7.2)

$$(raw) \quad \Delta_{UPD}\dot{\delta t} = p_1 \Delta\dot{UPD}_1 + p_2 \Delta\dot{UPD}_2 + p_n \Delta\dot{UPD}_n + \ldots$$

In order to get an idea of the stability of the UPDs and therefore the comparability of the different clock products, the standard deviation of the different satellite clock estimates with reference to the IGS final clocks were computed and is depicted in figure 7.7.
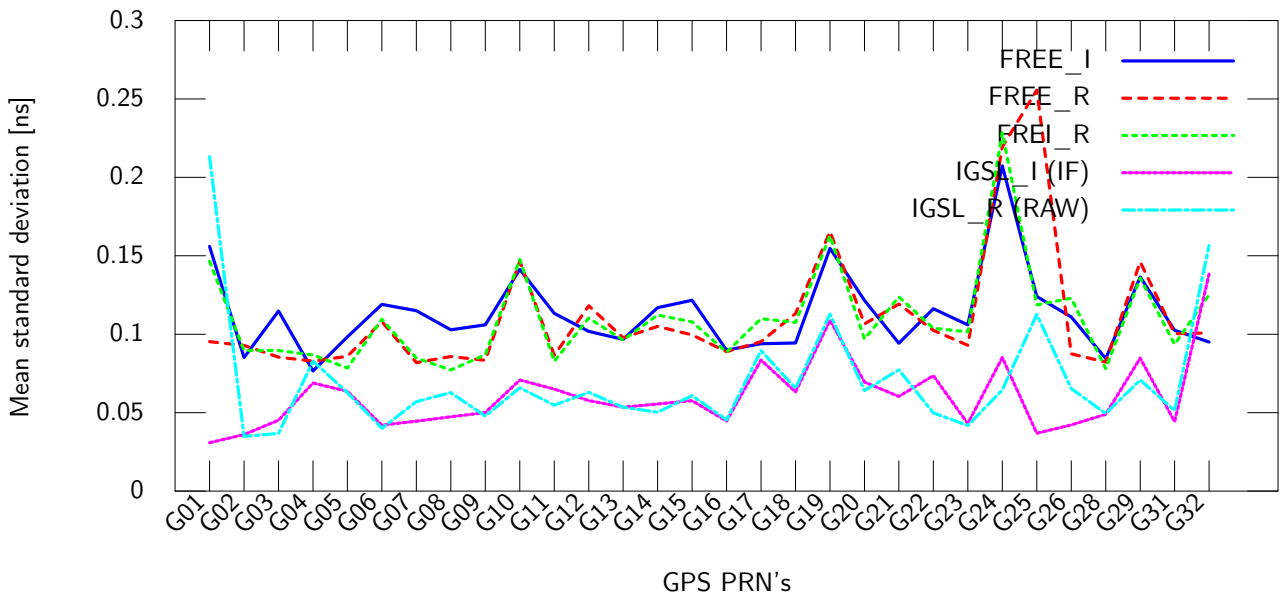
Figure 7.7: Mean standard deviation of satellite clock estimates w.r.t. IGS final clocks [ns].

This shows that, apart from the absolute clock offsets, the clock behaviour is absolutely comparable. This finding is confirmed by the summarised comparisons for the different scenarios, as shown in table 7.5.

	FREE_I	FREE_R	FREI_R
MGEX	0.11	0.11	0.11
IGSL	0.06	0.07	0.07

Table 7.5: Mean satellite-specific standard deviation of satellite clock estimates w.r.t. IGS final clocks [ns].

7.1.4 Quality assessment of ionospheric delay estimates

As outlined in chapter 4 and demonstrated in section 6.1.3, the STEC estimates are linked directly to the clocks and the UCDs. Consequently, a direct comparison of STEC estimates, without considering UCD and clock estimates is, strictly speaking, not possible. This also means that the absolute TEC level can easily be adjusted by changes to UCD and clock estimates. Accordingly, the separation of clock offset, signal and ionospheric delays are not necessary for applications exclusively interested in coordinates. In the case of timing applications, it is of primary importance to be aware of the characteristics of the station setups and to estimate consistent STEC values. In this context, "consistent" means a uniform global TEC level. In order to obtain a first impression of the accordance of the "absolute" TEC estimates from the different solutions, the individual STEC estimates were compared to an external reference solution. This approach is not primarily a global comparison, since it compares the satellite-receiver pair related estimates and concludes with global models on a station-specific accordance. However, in the case of a good agreement of the local parameters, the global parameters can also be assumed to be consistent with the reference.

For this test, the STEC estimates of the two-week test period for the different scenarios were analysed. The external reference values were derived from the IONEX maps provided by CODE. Figure 7.8 compares the estimates for the two raw observation scenarios (FREI_R/FREE_R) and a third scenario with a priori UCD constraint (FREC_R), which is explained later. It shows the mean STEC difference per station in metres on L1. The respective error bars depict the mean of the relative TEC variations (standard deviation per satellite path). The corresponding table is given in the appendix (see table 9.15).
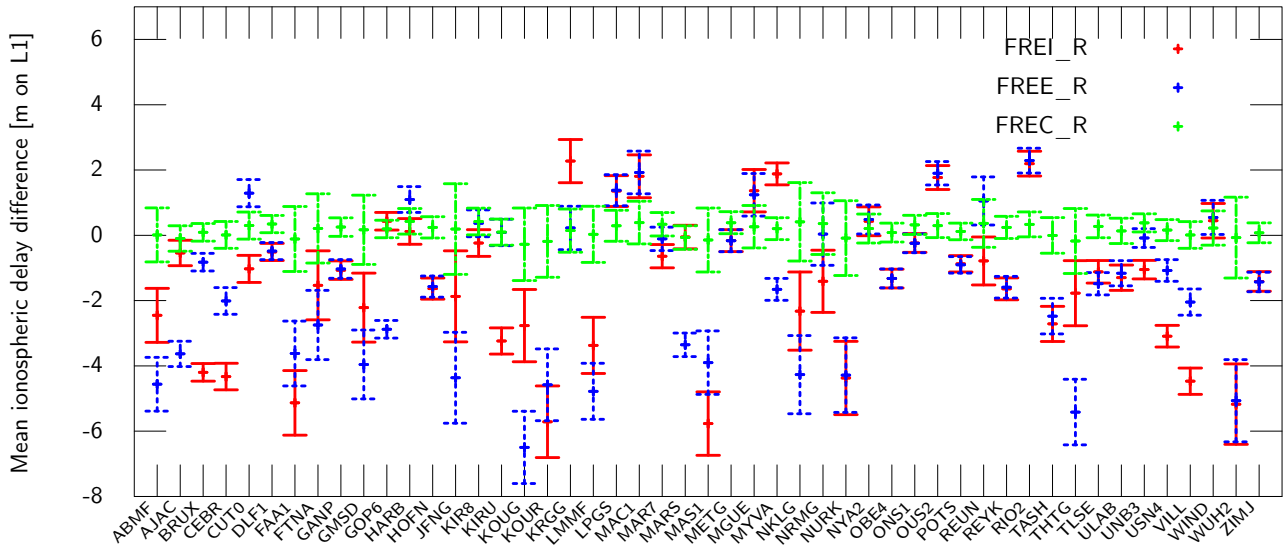
Figure 7.8: Mean site-specific ionospheric delay difference over the two week test period [m on L1].

At first glance at the presented STEC differences reveals obvious that none of the scenarios produces completely un-realistic values. In most cases, the differences are within a range of ±4 m (±25 TECU) from the external reference. This is far too much for timing applications and ambiguity resolution, but can be considered to be a satisfactory result for processing that waives external information. The question remains as to whether it is possible to calibrate or constrain the solution in order to allow for an estimation of comparable STEC values for all stations. For this purpose, as well as to show the full comparability of the two approaches, a third raw processing scenario (FREC_R) was set up. This scenario makes use of a priori UCD constraints. The a priori UCDs were estimated using a sin-gle day of observation data and the corresponding IONEX maps. It has to be mentioned that the a priori UCDs, derived from a single 24-hour run, were applied to data processing covering a period of two weeks. The absence of a gradual degradation once again confirms the assumption of stable UCDs on one hand, but also strengthens the assumption of the possibility of the a priori calibration of UCDs. Over the complete test period, the estimated ionospheric delay shows good accordance (below 1 m) with the reference solution. This again confirms that it is possible to estimate the ionospheric delay on a comparable level with appropriate a priori values, regardless of whether these are for the ionosphere (global models) or for the UCDs. Bearing this in mind and recalling the results from the UCD analysis (see chapter 6), it is very likely that a reasonable calibration of satellite and receiver UCD is possible and, furthermore, that the raw processing approach is capable of performing this action. With regard to global network analysis, it is also conceivable to estimate a constraint global TEC function instead of using a priori information concerning the UCDs. This approach has the advantage of significantly reducing the number of required a priori constraints.

Another point of interest is the relative behaviour of the STEC estimates compared to the external reference. The agreement is depicted by the error bars in figure 7.8. The comparison of the error bars shows accordance between the different scenarios at centimetre level. It clearly shows that, in some cases, the error bars do not fully agree. The main cause of this is differences in the observation selection and in the rejection procedures. This good agreement is not surprising since, as explained earlier, the UCDs responsible for the absolute TEC level have almost no impact on the relative behaviour of the STEC estimates. Furthermore, the good accordance of the relative STEC estimates with the external reference solution (about 48 cm) shows that, in the case of ionosphere estimation, the raw processing approach is comparable to proven setups. In addition, there is the advantage that the raw processing approach does not require a separate step for the estimation of TEC values.

7.1.5 Quality assessment of tropospheric delay estimates

It is well known that the impact of the troposphere is a local phenomenon. Consequently, a comparison on the global level is not expedient. For this reason, the hourly troposphere estimates for the raw processing scenarios FREI_R and FREE_R were station-wise compared to the ones from the ionosphere-free (FREE_I) scenario in order to demonstrate the accordance of the troposphere estimates of the different approaches. Table 7.6 shows the mean difference and standard deviation summarised from all the stations used in the network analyses.

Scenario	Mean	Std
FREE_R	0	2
FREI_R	0	2
FREC_R	0	2

Table 7.6: Summary of the mean difference in the tropospheric estimates versus FREE_I [mm].

This shows that the troposphere parameters derived from the standard ionosphere-free processing (FREE_I) are fully comparable at a millimetre level to the ones from the raw processing scenarios.

7.1.6 Summary of network PPP analyses

The analyses presented so far have neglected the topic of integer-ambiguity resolution. They compared the results of a global GNSS network analysis using the common ionosphere-free approach to the results of the raw observation-based approach. The analyses showed that the raw observation-approach provides results that are at least equivalent. For sparse tracking networks like the up-to-date MGEX network, the raw processing approach showed an improved agreement with the reference. Because the weighting and screening settings of the two scenarios are not one-to-one transferable, it is difficult to trace the improvements unequivocally to the raw approach. However, it is clear that raw observations offering the most flexible observation-weighting and screening capabilities will definitely benefit from this.

For the current GNSS environment, which is still dominated by dual-frequency GPS satellites, the true advantages, such as the combination of all available signals, could not yet be fully utilised. Moreover, in order to show the advantages of the third frequency and the new signal modulations on a global scale requires an acceptable number of new satellites and stations that are capable of tracking these. Since this requirement is not yet fulfilled, a conclusive statement regarding the global product quality of the raw processing approach cannot yet be provided.

The fact that the raw processing approach allows the estimation of all parameters in a single process has to be seen as the most beneficial capability for global network analyses and for providers of global GNSS products like the IGS or commercial companies that are interested in a variety of different signal-related parameters in particular.

7.2 Applicability for standalone PPP

This section aims to demonstrate the applicability of the raw processing approach for standalone PPP solutions. The implementation of the NAPEOS adjustment module limits the processing to a batch least squares adjustment. For this reason, the presented analysis concentrates on 24-hour batch runs. This, in turn, means that the coordinate and parameter estimates do not show convergence behaviour. Nevertheless, the estimation of epoch-wise coordinate offsets is possible. Furthermore, since the discussion in the previous section included the analysis of atmospheric parameters such as the troposphere and STEC estimates at station level, a further analysis explicitly for standalone PPP solutions was declined. Therefore, this section concentrates on the analysis of the station coordinates.

7.2.1 Parameter setups and station selection

As in the case of the network setups, different parameterisations are also imaginable for standalone PPP implementations. Depending on the application, the a priori knowledge regarding the biases (UCDs) and the available input orbits and clocks, the parameter setup might differ. In the first scenario, it is imaginable that no code bias information, neither for the stations (receiver, antenna) nor for the satellites, is available. In this case, the UCDs need to be handled within the estimation procedure. Since a separation of satellite and receiver biases for a single receiver is not possible, the estimation has to be performed per satellite-receiver pair (link). Admittedly, this is at the cost of non-representative STEC estimates. The corresponding PPP setup is called PPL_R, where L stands for link and R for raw. The next scenario covers the case of a priori known UCDs, either for satellites, for stations or for both. In this case, the bias parameter can be fixed or constraint to the a priori values. To account for the uncertainty in the a priori estimated UCDs, the following analysis constrains the UCDs by the standard deviation of the estimates (approximately $0.1 - 0.2\,m$). This scenario is referred to as the PPP raw setup (PPP_R). For reasons of comparison, a common PPP run based on ionosphere-free LC observations (PPP_I) was performed, in which _I stands for "ionosphere-free". Finally, to allow for a direct comparison of the two approaches a third ionosphere-free like raw scenario (PPI_R) was set up. This scenario made use of the same observations (dual-frequency only) and assumptions regarding the UCDs (L1 and L2 are equal to zero) as in the ionosphere-free (PPP_I) scenario. The most relevant parameters of the different scenarios are compared in table 7.7.

Parameter	PPP_I	PPI_R	PPL_R	PPP_R
ISBs	estimated 1/signal/link	-	-	-
Satellite UCDs	-	$\begin{cases} L1: UCDs = zero \\ L2: UCDs = zero \end{cases}$	$\begin{cases} estimated \\ 1/signal/link \end{cases}$	$\begin{cases} estimated\,1/signal \\ constr.\,(\approx 0.1\,m) \end{cases}$
Receiver UCDs	-			

Table 7.7: Scenarios applied for the PPP analyses and their most important parameters.

The parameter setups of PPI_R and PPP_R are similar. PPI_R assumes the UCDs to be zero, whereas in the case of PPP_R, these are constrained to a priori values. For the test receivers (A001, A002, B003 and B004), both satellite and receiver and, for the other stations, only satellite UCDs were constrained. It is well known that the modelling capability of atmospheric effects depends heavily on the receiver location. For this reason, a set of globally distributed test stations was selected. The main advantage of the raw observation approach is the combination of different signals on more than just the two most common frequencies. The station selection was again restricted to receivers that tracked GPS and Galileo. The selected test stations are shown in figure 7.9.
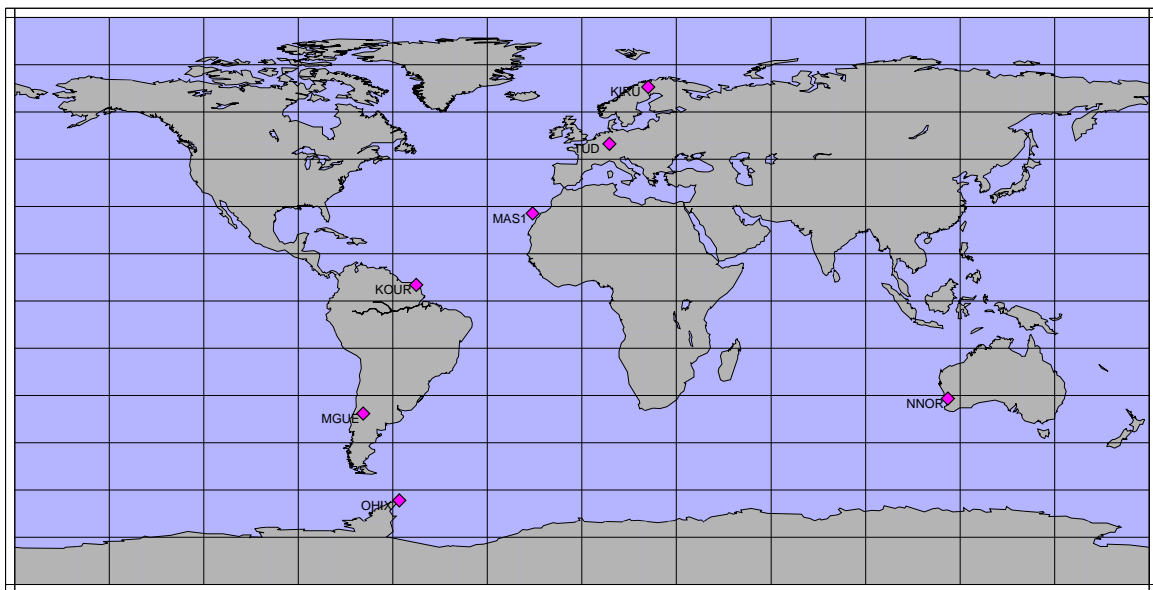
Figure 7.9: Global distribution of PPP test stations.

The fact that only four "validation" satellites of the Galileo system are currently in orbit and all of them are affected by satellite performance tests complicates the selection of a suitable set of stations and a suitable observation period. Therefore, in the first step, the analysis concentrates on a general evaluation and comparison of the different scenarios, mainly driven by GPS dual-frequency observations. In the second step, the advantages of multiple signals and GNSS are explicitly analysed. For the first tests, a period of ten days (December 25, 2012 to January 3, 2013) was selected. All analyses were performed with a sampling rate of 30 seconds; even so, not all satellite clocks were sampled within 30 seconds. This again means that, for the MGEX based clock estimates (300 s), an interpolation became necessary.

7.2.2 Quality assessment of static receiver coordinate estimates

The first point of interest is the coordinate stability. Most conventional geodetic applications are interested in static coordinate solutions, whereas for deformation monitoring, kinematic positions are also of interest. For this purpose, the following analysis covers both types of coordinates, namely static (24 hours) and kinematic (epoch-wise, 30 seconds). The starting point is the stability analysis of the static coordinates. For this analysis, the orbit and clock products from the network analysis (FREE_R) were used as input. The resulting standard deviations of the different daily coordinate solutions are presented in table 7.8.

Station		PPP_I			PPI_R			PPL_R			PPP_R		
		East	North	Up	East	North	Up	East	North	Up	East	North	Up
TUD	A001	6	3	14	4	3	16	3	3	9	3	3	10
	B004	5	4	19	5	3	18	5	3	13	5	3	13
IGS / MGEX	KIRU	5	4	27	5	4	27	5	4	24	5	4	24
	KOUR	8	7	9	9	7	8	9	7	10	9	7	8
	MAS1	7	5	7	8	5	6	6	5	3	6	5	4
	MGUE	15	5	12	17	5	11	17	5	9	17	5	9
	NNOR	23	18	15	24	17	15	23	17	17	24	17	17
	OHIX	18	7	17	17	7	16	16	6	15	17	6	15

Table 7.8: Day-to-day repeatability of static coordinates (Std [mm]) for the different PPP scenarios (FREE_R orbits and clocks).

It can be seen that the horizontal coordinates of all scenarios are determined with comparable accuracy. However, the height component seems to benefit from additional observations. No significant difference between the two dual-frequency scenarios, PPP_I and PPI_R, was found. The two others, even though they were mainly driven by dual-frequency observations, show improved stability of two to three millimetres. Another interesting aspect is the performance comparison of the scenarios with constraints (PPP_R) and link-wise estimated UCDs. It becomes obvious that the handling of the UCDs has no significant impact on the coordinate results.

The input orbits and clocks used for this test were generated using the raw processing approach. As outlined in section 7.1, the orbit and clocks differ depending on the processing approach. However, it is expected that the differences are negligible for float solutions. Therefore, in order to demonstrate the applicability of ionosphere-free orbit and clock solutions for raw PPP with float-valued ambiguities, the experiment is repeated, making use of ESA's IGS products. The results are summarised in table 7.9.

Station		PPP_I			PPI_R			PPL_R			PPP_R		
		East	North	Up	East	North	Up	East	North	Up	East	North	Up
TUD	A001	2	2	12	4	2	10	4	2	10	4	2	10
	B004	3	2	12	4	2	10	5	2	10	5	2	10
IGS / MGEX	KIRU	4	1	26	4	1	26	5	1	25	5	1	25
	KOUR	4	4	7	4	3	8	4	3	6	4	3	6
	MAS1	3	3	3	4	3	3	4	3	3	4	3	3
	MGUE	3	3	5	3	3	4	3	3	4	3	3	4
	NNOR	4	2	5	5	2	5	5	3	6	5	3	6
	OHIX	2	1	5	2	1	5	2	2	5	2	2	5

Table 7.9: Day-to-day repeatability of static coordinates (Std [mm]) for the different PPP scenarios (ESA orbits and clocks).

This second analysis confirms the results of the previous analysis. It shows no significant difference between the different approaches. Furthermore, it proves that ionosphere-free orbit and clock products, in the case of float ambiguities, are completely suitable for the processing of raw observations. It is clear that the performance improves significantly when using the highly accurate ESA products instead of the FREE_R orbit and clock estimates. However, for the analyses presented in the following section, the FREE_R orbits and clocks are sufficient. As already demonstrated in the first analyses, the two multi-frequency raw scenarios show the same behaviour. As a result, the PPL_R is no longer considered in the following analyses.

7.2.3 Quality assessment of kinematic receiver coordinate estimates

It is well known that numerous effects, like short periodic multipath averaging out for longer observation periods, significantly impacts the epoch-wise coordinate solutions. Therefore, epoch-wise coordinates are the next point of interest. For this analysis, the PPP scenarios were re-run with the difference that epoch-wise (30-second) coordinate offsets, instead of static 24-hour coordinates, were estimated. Figure 7.10 shows the kinematic position offset for the different scenarios and the test receiver A001 on day 360 in 2012.
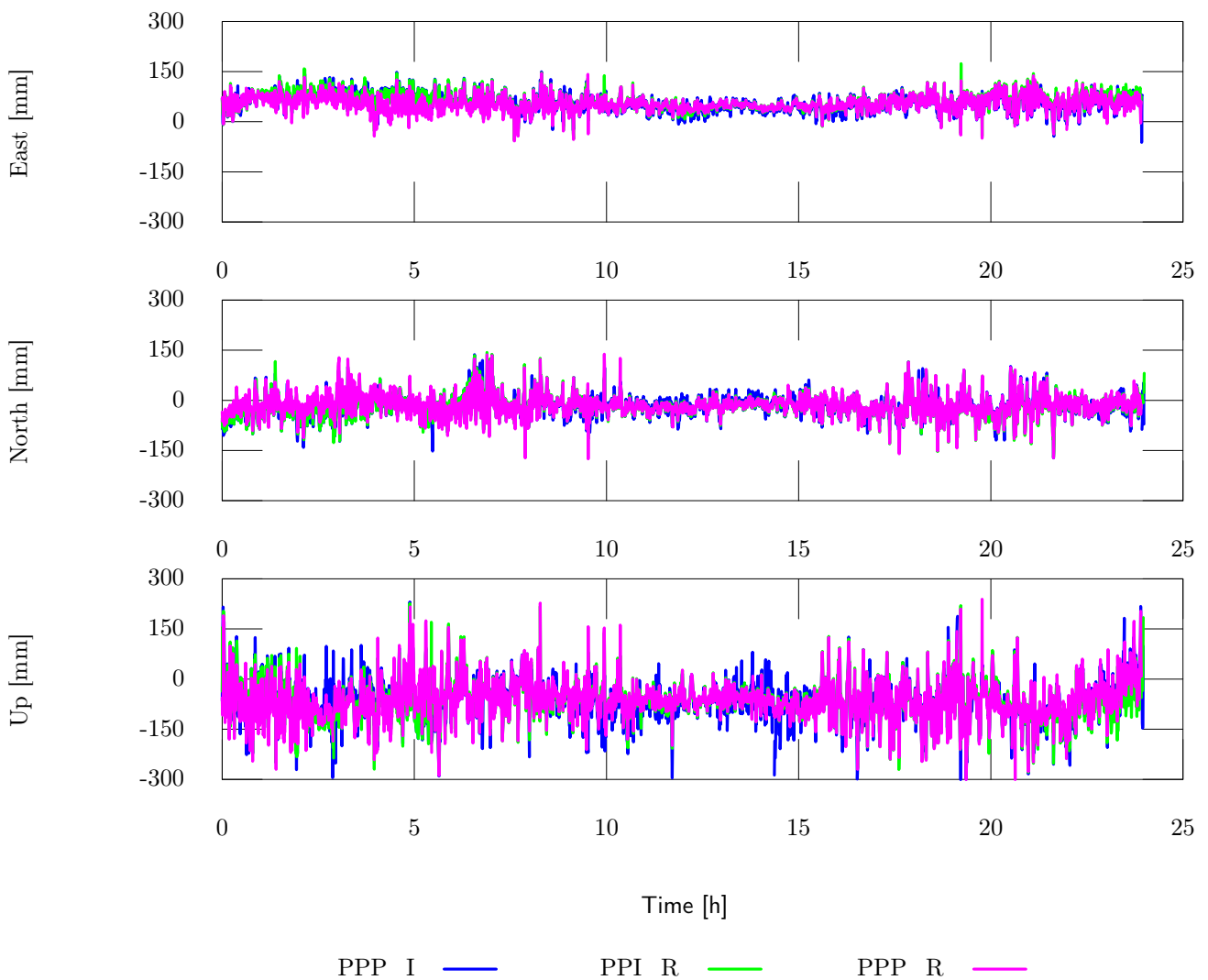
Figure 7.10: Residuals of different 24-hour kinematic coordinate solutions for receiver A001 (day 360 in 2012).

At first glance, the ionosphere-free (PPP_I) and the two raw processing scenarios provide comparable kinematic coordinate estimates. However, it is conspicuous that all coordinate solutions show periods with more and less accurate estimates. A closer inspection shows that the improvement correlates with the appearance of the Galileo

IOV satellites. Figure 7.11 depicts the situation for the PPP_R scenario and the receiver A001 on day 360 in 2012 (left) and day 67 2013 (right). It compares the epoch-wise differences for the east and north coordinate components and the number of GPS and Galileo satellites.
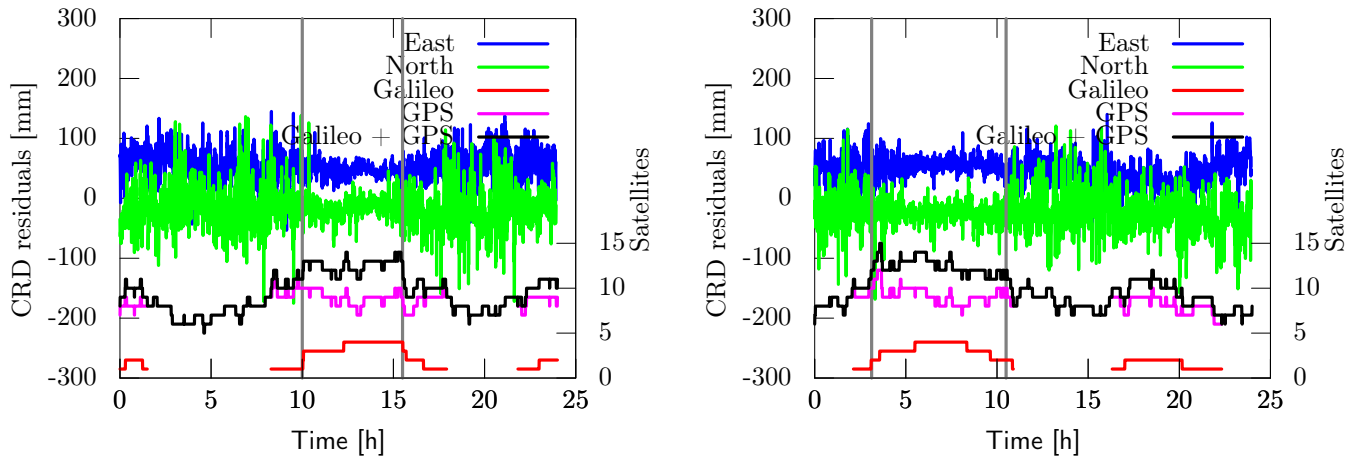
Figure 7.11: Kinematic coordinate differences (east/north), A001 day 360 2012 (left) and day 67 2013 (right) (PPP_R).

The relevant period in the respective figures is enclosed by two vertical lines. The correlation with the number of satellites and, in this case, the appearance of the Galileo satellites, is clearly visible. Certainly, similar effects can be observed when using GLONASS satellites in addition to GPS. Since the benefit of an individual satellite on the positioning depends on its relative position, or rather the overall satellite geometry for the respective time and location, a direct comparison of the contribution of GLONASS, Galileo or other GNSS satellites is not possible. Consequently, this graphic can only confirm the well-known fact that a greater number of satellites significantly improves the PPP solution. Nevertheless, it is worth having a final look at the standard deviation for the different periods and scenarios. Table 7.10 shows the standard deviation of the kinematic coordinate solutions with/without the four Galileo IOV satellites.

Scen.	Year doy	East	North	Up
PPP_I	12 360	16/26	22/33	45/64
	13 067	26/32	24/32	75/91
PPI_R	12 360	12/23	16/33	31/59
	13 067	14/23	17/30	61/74
PPP_R	12 360	12/23	16/33	29/61
	13 067	14/23	17/30	42/67

Table 7.10: Coordinate std (kinematic) for different scenarios, with/without four Galileo IOV satellites [mm].

This clearly indicates the improvement resulting from the additional Galileo satellites. It should be noted that, with the on-going development of GLONASS and the new, upcoming GNSS like Galileo such performance improvements will become regular in the near future. Furthermore, when thinking about combining all available GNSS, the modernised GPS and GLONASS, the currently developing Galileo, BeiDou and other upcoming global and regional navigation satellite systems, the kinematic positioning can be assumed be significantly improved. However, optimally combining observations from all these systems is of major importance, although this is not an easy task when using system-specific linear combinations.

Another interesting point in table 7.10 is the improved coordinate stability for the raw processing scenarios. When comparing the two raw processing scenarios to each other, the horizontal coordinate components seem to be almost identical. When inspecting the height component, it shows that the PPP_R scenario, which makes use of all the available signals, gives the most accurate results. At present, the improvement resulting from the utilisation of more than two frequencies is still small. This is not truly surprising, since the number of triple-frequency satellites is still limited. Furthermore, the triple carrier GPS satellites still suffer from problems with phase stability on different frequencies and the Galileo IOV satellites do not always provide their final (operational) performance.

Therefore, further tests were conducted in order to highlight the impact of additional (more than two) signals on the analysis results. The tests were based on the PPP_R setup. For these tests, only periods with more than four and usually with five multi-frequency satellites were selected. Matching test data sets are very limited for the current, freely available GNSS observation data and the up-to-date satellite constellations. One issue is the availability of the four Galileo IOV satellites, which are neither simultaneously visible nor usable on all days. Hence, the following examination concentrates on an analysis of individual stations on selected days. In the following section, the results for A001, located at the Technische Universität Darmstadt (TUD) and Kiruna (KIRU) are discussed in depth. The left-hand side of figure 7.12 shows the satellite paths and the behaviour of the positional dilution of precision (PDOP) during the test period (receiver A001, day 363 in 2012). The right-hand side of the figure compares the residuals of the kinematic position in the east, north and up components for dual frequency observations (DFO) versus multi-frequency observations (MFO).
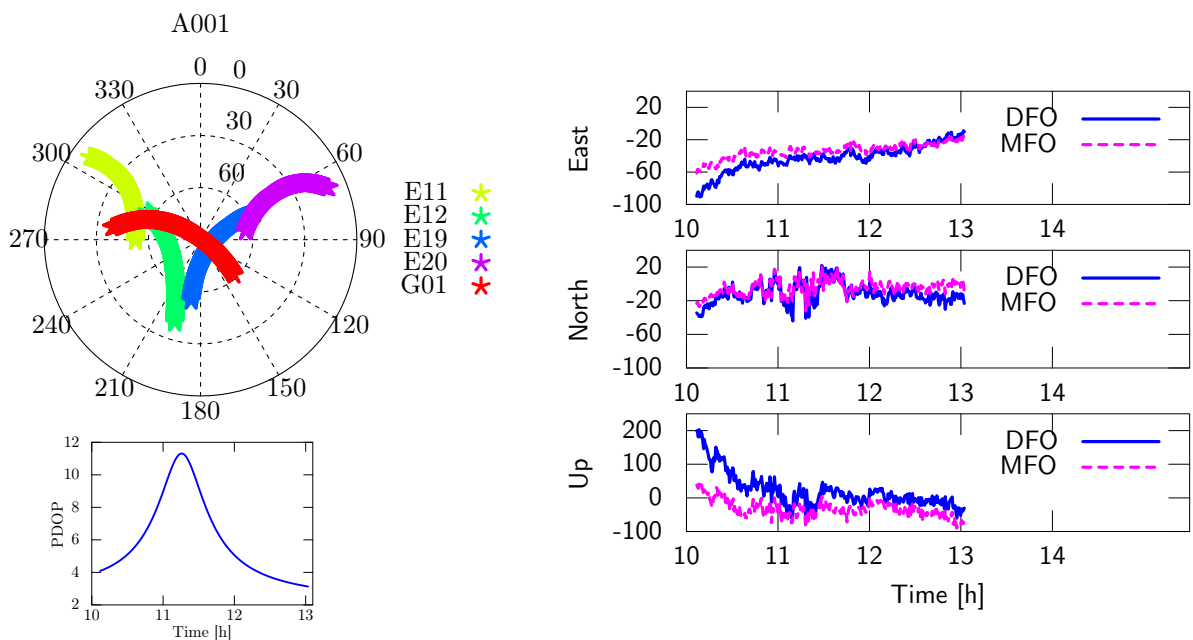
Figure 7.12: Comparison of kinematic coordinate estimates, dual-frequency (DFO) versus multi-frequency (MFO) [mm] (A001, December, 28 2012).

The satellite geometry, particularly in the middle of the observation period (PDOP > 5), appears to be somewhat less optimal. Nevertheless, the kinematic coordinate estimates are astonishingly good, even for this satellite geometry (see table 7.11). An interesting point is the performance difference of the results based on DFO versus MFO. For the north component, the MFO shows a rather small improvement. Indeed, this is not truly astonishing, because the additional signals do not contribute further to the geometry. For the east component, which benefits from improved observation accuracies, the MFO shows coordinate behaviour that is more stable. However, the most obvious improvement can be observed in the height component, which probably takes advantage of the improved separability of atmospheric effects and height.

Figure 7.13 shows the same analysis for Kiruna (KIRU) on day 67 2013. At first glance, the satellite geometry appears to be even better when compared to the previous example. When inspecting the behaviour of the coordinate estimates, a clear trend in all components becomes visible. As already shown in the previous example, the result based on MFO appears to be significantly more stable. This becomes particularly obvious when inspecting the height component. Here, the MFO results show a rather minor trend compared to the DFO coordinate estimates.
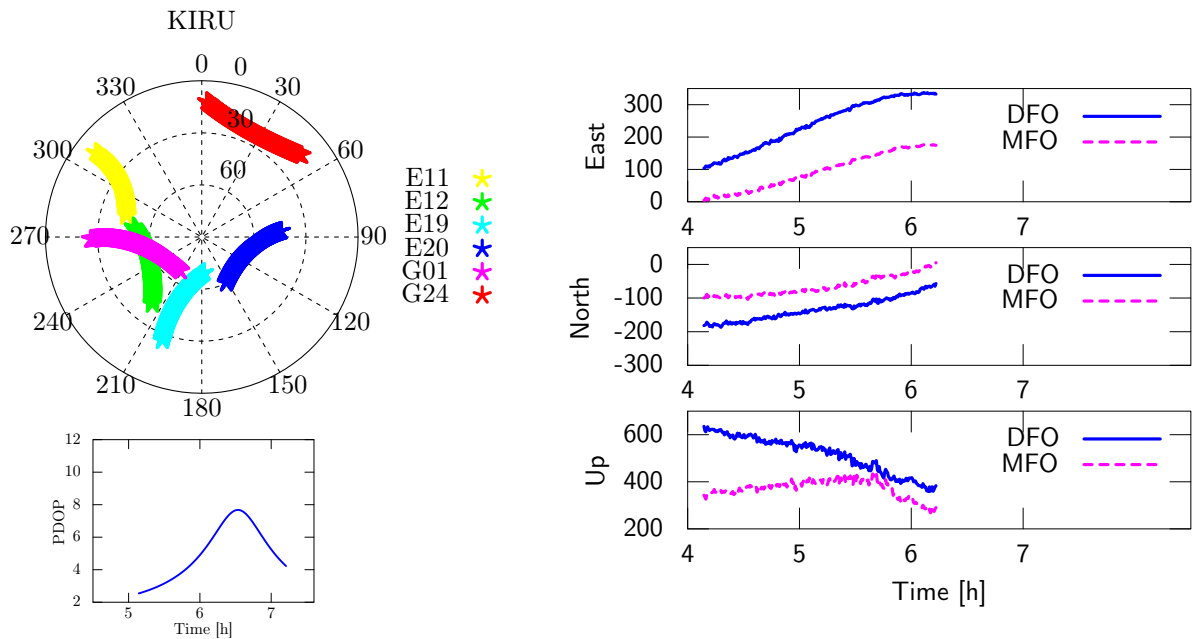
Figure 7.13: Comparison of kinematic coordinate estimates, dual-frequency (DFO) versus multi-frequency (MFO) [mm] (KIRU, March 8, 2013).

The same conclusion can be drawn for the other test receivers and for the arbitrarily selected test periods. Table 7.11 summarises the respective offsets and the standard deviation for the epoch-wise (30-second) coordinate estimates.

Station	yy doy	(Time)	East Mean dfo/mfo	East Std dfo/mfo	North Mean dfo/mfo	North Std dfo/mfo	Up Mean dfo/mfo	Up Std dfo/mfo
A001	12 363	(10:07-13:03)	-24/-15	16/9	-11/-4	12/9	85/31	51/24
A002	12 363	(10:07-13:03)	-24/-15	17/10	-11/-5	12/9	85/32	51/26
KIRU	13 067	(05:09-07:13)	241/95	76/56	-133/-65	34/29	516/372	78/38
NNOR	12 365	(09.42-11:49)	-16/-11	15/9	41/23	60/43	-370/-218	271/173

Table 7.11: Comparison of kinematic coordinate estimates, dual-frequency (DFO) versus multi-frequency (MFO) [mm].

This shows that, in all cases, the utilisation of additional signals (more than two) stabilises the coordinate solution and that the east and the height components particularly benefit from MFO. It is well known that the height component is strongly correlated with the receiver clock estimate. Thus, the next point of interest is the behaviour of the clock estimates.

7.2.5 Quality assessment of receiver clock

Since there is no existing external clock solution for the test receiver (A001/A002), the clock estimates are compared to the 24-hour, static ionosphere-free solution (PPP_I). In addition to the two kinematic solutions, the static raw run (PPP_R) was also considered. The results are summarised in table 7.12, which shows the respective offsets and standard deviations.

Scenario	A001 Mean	A001 Std	A002 Mean	A002 Std	KIRU Mean	KIRU Std	NNOR Mean	NNOR Std
DFO	-13.94	0.15	-13.58	0.14	7.41	0.15	3.10	1.17
MFO	-13.69	0.09	-16.38	0.09	5.92	0.10	-0.21	0.77
PPP_R	-8.32	0.04	-8.35	0.04	4.70	0.03	-10.03	0.06

Table 7.12: Comparison of DFO, MFO and PPP_R clock estimates w.r.t. 24 hour ionosphere-free clock solution [ns].

As expected, the utilisation of MFO also improved the clock solution. This shows that the standard deviation from the ionosphere-free based clock estimate reduced significantly for all test receivers and days. However, as expected, all raw clock estimates showed an offset against the ionosphere-free clock solution. This difference can be avoided by the utilisation of calibrated equipment.

Against the background of the limited number of available test data sets, it is clear that the results are more or less a snapshot. Nevertheless, all presented tests showed the same results, highlighting the MFO solutions as being the most accurate. It might be that with a sufficient number of satellites, the gain resulting from additional observations, which do not contribute to the geometry, is somewhat limited. Clearly, given the strong dependency of east, height and clock estimates on the measurement accuracy, it is not improbable that benefitting from additional observations will result in an improvement. In the future, it can be expected that a full constellation of multi-frequency satellites and the application of MFO will result in the significant improvement of the east, the height and the clock estimates.

7.2.6 Summary of PPP analyses

As has been demonstrated, the application of raw observations for dual-frequency PPP, in comparison with the common ionosphere-free processing, gives at least equivalent results. It was shown that additional observations on a third or any further frequency improves the coordinate and the clock solutions. The weaker east and the height components particularly profit from this improvement.

Moreover, the well-known fact that additional satellites from different GNSS strengthen the solution has been confirmed for both approaches. Remembering the fact that the presented approach is optimally suited to combining arbitrary observations, regardless of their GNSS, modulation and frequency, raises the prospect that raw observation PPP gains the most from the future heterogeneous GNSS environment.

In addition, it has been shown that, in the case of an application of the raw processing approach for positioning applications, it is neither essential to have dedicated raw observation orbit and clock products, nor to have a priori knowledge regarding the satellite and receiver UCDs. Although it is not possible to separate ionospheric delay, UCDs and clock estimates, the coordinates remain unaffected. Thus, it is possible to use the standard ionosphere-free orbit and clock products, for example the IGS finals, for positioning applications. The situation is different for timing applications, as here it is essential to apply consistent products, including satellite clocks, satellite and receiver UCDs.

7.3 Optimisation via bias calibration and ambiguity resolution

As explained earlier, one important measure of the accuracy of GNSS products, such as satellite orbit, clocks and station coordinates, is their repeatability. In addition, it is important to ensure a consistent separation of the different delays for timing and applications interested in the analysis of the ionosphere. The inseparability of different effects and the stability of the solution are directly linked to the parameter correlation. Hence, in order to allow for the proper separation of the different effects and to make the overall solution more repeatable, it becomes necessary to apply dedicated constraints to the parameter estimates. The most important constraint in common ionosphere-free processing is integer ambiguities. However, as explained in section 4.2, additional constraints are required to describe the relation between clocks, the ionosphere and the UCDs and UPDs for the processing of raw observations. The most straightforward approach to gaining information concerning the physical behaviour of the different biases is the calibration of the individually affected components.

7.3.1 Bias calibration

It is clear that the most efficient way to remove receiver, or rather receiver-system dependent biases, is a uniform setup resulting in equal biases in the network, as well as in the user processing. Since all positioning and timing solutions are in fact relative to the fixed orbits and clocks, the common biases remaining in these are mitigated. Such a setup is only theoretically realisable. However, in order to allow for a time transfer with sufficient accuracy, it is important to calibrate the different biases, of which the most important are the receiver-system related UCDs. For this purpose, different approaches that make use of artificially generated GNSS signals, as per Plumb et al. (2005);

Proia and Cibiel (2010), have been developed and demonstrated. The accuracy of the resulting UCDs depends on the signal modulation being between $0.6 - 1.1\,ns$ (Proia et al., 2011). Within this thesis (see section 6.1.3), it was to some extent demonstrated that relative calibrations of UCDs in a true environment can be performed with at least similar accuracy when using the raw processing approach. In addition, this analysis highlighted the effects of different receiver settings and therefore the need to handle changes in the station environment carefully. Besides the signal-specific calibration, the analysis also demonstrated the largely neglected aspect of PRN-specific correlator effects. The relation of receiver(-system) related UCDs and satellite-specific PRN codes, as previously demonstrated by Phelts (2004), has been confirmed.

In fact, the calibration of the receiver-system specific UCDs considers only one side of the problem. The counterpart is the satellite-dependent UCDs. In the case of a consistent processing scheme in all receivers, these UCDs are again mitigated. As demonstrated in the frame of the network analyses in section 7.1.3, the satellite-dependent UCDs and the receiver clock estimates are directly linked to the observation weighting. With regard to ionosphere-free processing with a fixed weighting scheme, this fact can be ignored. When processing raw observations, this is certainly a decisive point. Nevertheless, when applying the raw processing approach for global networks, particularly after introducing DD phase ambiguity constraints, satellite UCDs are in any case estimated within the least squares adjustment.

Apart from the pseudo-range related delays (UCDs), the carrier phases are also affected by frequency-dependent satellite and receiver-system delays. Aspects of these delays have already been considered, as in the case of antennae, by PCO and PCV corrections. It is clear that the high degree of accuracy of the phase observations (millimetres) places enormous accuracy requirements on the calibrations and on the actual stability of the UPDs. Because UPDs condense a number of different and variable delays (Montenbruck et al., 2010; Wübbena et al., 2012), chapter 6), a calibration of these is not expedient at present.

7.3.2 Recovery of integer nature of phase ambiguities

For all up-to-date, highly accurate GNSS applications, the recovery of the physical integer carrier-phase ambiguities is a regular feature, improving the stability and the consistency of the results. Nevertheless, it harbours the risk of incorrectly fixed ambiguities and, consequently, incorrect constraints on the estimated parameters. As demonstrated by Blewitt (1989) and recalled in section 3.4, the intention is the improvement of the carrier phase measurement accuracy, allowing for a better resolution of the east - west (receiver) and the along track (satellite) coordinates. Against the background of new and modernised GNSS that provide innovative and advanced signal modulations on additional frequencies, the question arises as to whether the same result can be gained by the utilisation of all available signals, as well as if the concept of ambiguity resolution is still the only way to stabilise the solution. A first, promising impression of the accuracy improvement when combining multiple signals on more than two frequencies is given in section 7.2. This, combined with the increasing number of available satellites, provides an optimistic prospect. However, this question cannot be answered on the basis of the available, up-to-date satellites and tracking networks. For this reason, and in order to demonstrate the full comparability of the implemented raw observation-based approach with the up-to-date ionosphere-free processing scheme, the application of raw observation-based DD constraints is demonstrated in the following section.

The DD ambiguities can either be formed based on narrow-lane observations as is the usual procedure or, as proposed in section 4.3, they can be based on raw observations. For reasons of consistency and in order to allow for unconditional combinations of carrier phase ambiguities, regardless of their GNSS and the availability of a second phase observation on a common frequency, the DDs have been formed using raw observations. It is well known that a sufficiently accurate float-valued ambiguity estimate (below a quarter cycle) is required to prevent the fixing of wrong ambiguities. However, this condition is not consistently achievable for MGEX based solutions; thus, in the first step, the analysis concentrates on the IGS-like (IGSL) solution (see section 7.1). Figure 7.14 compares the different orbit solutions for the (IGSL) network, with (FIX) and without (FREE) ambiguity fixing, to the final IGS orbits. The ionosphere-free solutions are denoted by IF.

As already demonstrated in section 7.1, in the case of equal input data, when waiving integer-ambiguity constraints, both approaches compare equally with the final IGS orbits. However, when applying DD integer-ambiguity constraints, the ionosphere-free solution shows the best agreement. It is clear that the new approach is not yet fully optimised and, consequently, still has the potential for improvement. Furthermore, it is clear that the different constraint models, raw observation versus narrow-lane DD, also affect the comparability. Consequently, it is not
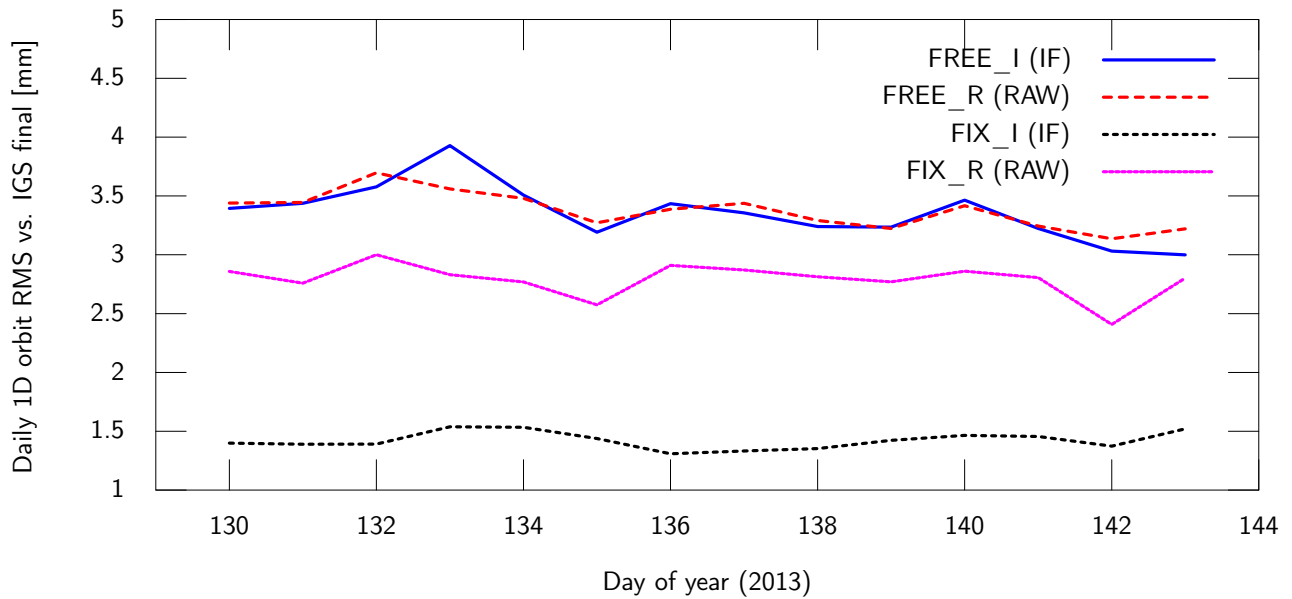
Figure 7.14: Comparison of 1D-orbit rms versus final IGS orbits for raw and ionosphere-free solutions, with and without DD ambiguity constraints.

surprising that the ionosphere-free approach shows a better accordance with the IGS finals. Nevertheless, the applicability of the new ambiguity-fixing approach is doubtlessly identifiable. As outlined in section 4.3, one of the main advantages of the proposed raw observation-based ambiguity-fixing is its system-independent applicability and the cross-system ambiguity-fixing. The proof of this feature requires an adequate multi-GNSS tracking network. The inhomogeneous and, in some areas, sparse MGEX network does not allow for the continuous application of ambiguity-fixing procedures. Thus, the analysis presented in the following section concentrates on selected time periods. The main point of interest for this analysis is the cross-system applicability of the proposed approach. Cross-system fixing means fixing DDs between different GNSS, such as GPS and Galileo. For this purpose, the ambiguity-fixing procedure is configured to form DD, regardless of their GNSS, by considering only the actual carrier frequency. This procedure, in the case of GPS and Galileo, allows for forming DD between L1 - L1, L1 - E1, L2 - L2, L5 - L5, L5 - E5a, E5a - E5a, E5b - E5b and E5 - E5. Therefore, as soon as two satellites have a common carrier frequency, ambiguity-fixing becomes possible. Figure 7.15 compares the orbit overlaps. At the top, it shows the ground tracks of the satellites. In the lower part of the figure, it compares the along-track rms with and without DD constraints for GAL-101 (left) and GAL-102 (right). In order to enlarge on the representation, the analysis shows different days for GAL-101 (day 131 2013) and GAL-102 (day 132 2013).
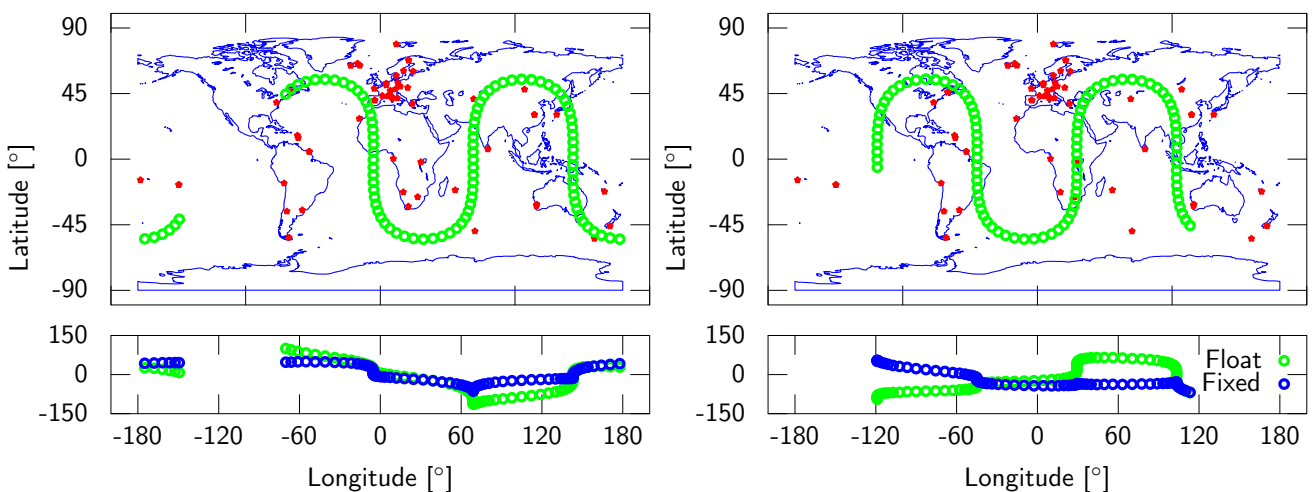
Figure 7.15: Along-track orbit rms [mm], GAL-101 (day 131, 2013) (left) and GAL-102 (day 132, 2013) (right).

When considering the location of the tracking stations, depicted by red markers, it becomes obvious that the tracking network is not optimally configured. This is again reflected in the orbit accuracy. Thus, the orbits based on the presented tracking network tend to be accurate for well-observed regions, causing errors to appear in regions with fewer observations. This becomes particularly obvious for the unconstrained solutions in the Asia-Pacific region. It is easy to imagine that this imbalance in the orbit accuracy on one hand and the baseline length for these regions on the other hand complicates DD ambiguity resolution. Furthermore, since common frequencies are required in order to form DD, the fact that different receivers track signals on different carrier frequencies also thins out the applicable network.

Despite the difficulties of ambiguity-fixing in the available network, the applicability can be demonstrated for selected time periods. Figure 7.15 shows the result of a cross-system fix, GPS - Galileo and Galileo - Galileo. Even though the total accuracy is not comparable to the IGS solution, it is obvious that the along-track component from consecutive orbit arcs can be significantly improved by the application of DD ambiguity constraints.

Thus far, the analysis did not consider the impact of the additional frequencies on the GNSS solution. Admittedly, on the basis of the available tracking network, this is not advisable. For this reason, one of the multi-signal test cases from section 7.2, in which the setup consisted of two receivers connected to the same antenna, is reused. The processing uses only those satellites with signals on more than two frequencies. Based on this requirement, a time period with four visible Galileo satellites and one visible GPS satellite is selected. Apart from the fact of there being only five visible satellites, in terms of satellite geometry all the satellites move similarly from south to north, which is a major issue for the accuracy. Regardless of this issue, the test case is optimally suited to comparing the impact of additional signals and ambiguity-fixing on the kinematic coordinate estimates. Figure 7.16 shows the behaviour of the kinematic coordinate offsets for the most affected coordinate components, namely east and height, for receiver A001.
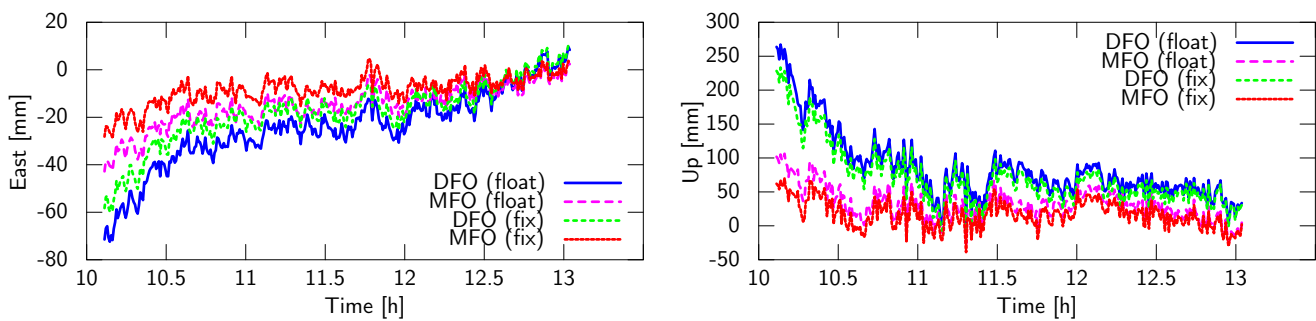
Figure 7.16: Comparison of kinematic coordinate variations, dual-frequency (DFO) versus multi-frequency (MFO), with and without DD constraints [mm] (A001, 28/12/2012).

Figure 7.16 shows a clear trend for all solutions in both east and height components. Even if the trend appears to be similar to a filter convergence, it is exclusively caused by the satellite geometry in conjunction with the selected time period. However, more interesting is the relationship of the different solutions. As expected, this shows that the dual-frequency (DFO) float solution has the worst performance. Somewhat more surprising is that the multi-frequency (MFO) solution outperforms the fixed dual-frequency solution. Nonetheless, the most stable solution in the east direction is the multi-frequency solution, which makes use of DD integer-ambiguity constraints. Although this analysis shows only a snapshot of a badly conditioned PPP, in principle, the results demonstrate the advantage of multiple frequencies and their joint processing. With up-to-date satellite observation data, an assessment of the true improvements resulting from additional satellites, frequencies, observation and ambiguity-fixing is not possible. In future, as indicated by the presented tests, it is expected that the accuracy, particularly of kinematic coordinates and poor observation conditions, will improve significantly.

8 Conclusions

The thesis discussed and demonstrated a flexible PPP analysis approach applicable for standalone PPP, regional and global networks. It is based on raw observations and renounces on any kind of linear combination and observation differences. Accordingly, it uses the observation equations in their original form. The complete renunciation of observation differences and linear combinations entails a number of advantages and simplifications, but also creates certain challenges.

8.1 Challenges of raw observation analysis

The greatest challenge for the processing of raw observations is the removal of rank defects in the normal equation system. The rank defects result from the strong correlation of various unknown parameters, such as clock offsets, uncalibrated signal delays and the ionospheric delay. In fact, there is no unique solution for the removal of these rank defects or for the implementation of the observation equation. Instead, the implementation depends strongly on the application, its characteristics and intention. Different implementations were demonstrated in the frame of this thesis. Amongst others, it is imaginable to renounce the complete separation of all individual disturbances and biases, and to concentrate on the desired parameters. A possible example of this is standalone PPP solutions, exclusively aimed at station coordinates. Here, it is irrelevant whether the ionospheric estimate represents the true physical properties of the ionosphere, or if it is used to absorb ionosphere and signal delays. Network PPP solutions offer further possibilities for solving rank defects. It is possible to imagine removing such singularities by global constraint models, for example by introducing or estimating global ionosphere parameters.

8.2 Benefits and capabilities of raw observation analysis

One of the most pre-eminent properties is the preservation of the original, physical observation characteristics. This feature allows a detailed analysis of all individual effects, biases and components. The on-going developments in the GNSS environment raise many questions and define numerous requirements, which need to be answered and validated in order to fully exploit the capabilities of the new systems. The ability of the proposed approach, which is to conserve the original characteristics of all individual components in the observations and to provide direct access to the raw observations, introduces a new dimension of analysis. The capabilities of signal-specific analyses are manifold, starting from simple quality analyses like multipath and noise behaviour, up to component calibrations for hardware (UCDs, UPDs) and antenna delays (PCOs/PCVs). It was rudimentarily demonstrated that the implemented approach is applicable for real observations in order to calibrate the relative UCDs of individual hardware components. Conversely, with a priori knowledge of the UCDs, the raw processing approach can be used to derive "absolute" ionospheric delays based on the observations of a single station. Admittedly, the presence of all the effects and biases in the observations entails the obligation for proper handling, but again there is the advantage of performing this using true physical models. One example is the highly stable clocks of future satellites, whereby it is possible to imagine stabilising the solution by means of functional clock models and, at the same time, significantly reduce the number of epoch parameters. The application of raw observations allows for a joint, flexible, unexceptional analysis of all available GNSS signals, regardless of belonging to a GNSS, their signal modulation or their frequency. It allows the renunciation of common workarounds like the misleadingly called intersystem biases (ISBs) and simultaneously ensures the equal treatment of all observations. The flexibility of this approach is reflected not only in the possibilities of observation selection, but also in the possibility of freely weighting and screening individual signal components in the processing. It has been demonstrated that a more realistic observation weighting and screening process improves the GNSS solution. Furthermore, the freedom of observation selection, weighting, screening and the ability to process any kind of signal in a single least squares adjustment or filter process enables access to the full capabilities of the future variety of GNSS.

Another advantage of the application of raw observations is the resulting simplification of the processing procedure. Comparing the standard ionosphere-free network processing strategy, as applied in the frame of the IGS and the proposed processing scheme for raw observations (see figure 8.1) it gives at least a hint on expected advantages.
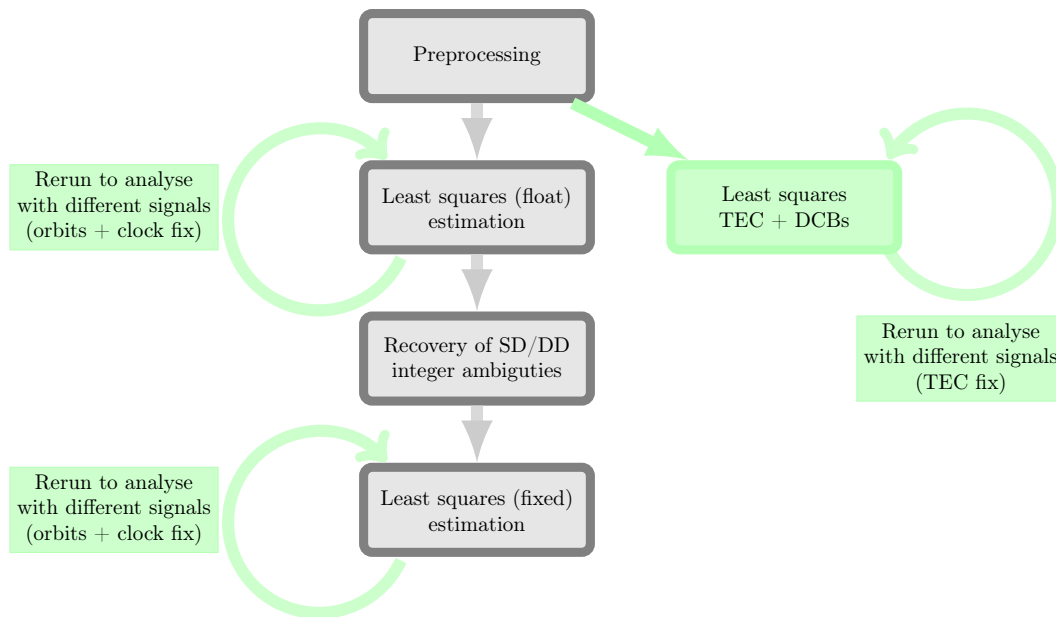
Figure 8.1: Ionosphere-free versus raw processing.

This shows that the raw observation analysis (grey) follows a straight line, consisting of either a single least squares estimation when waiving for double difference integer ambiguity constraints, or of three steps, including an additional step for DD ambiguity resolution and a final least squares estimation applying the DD constraints. After each of the two least squares estimations, the full spectrum of parameters is estimated. However, in the case of constrained UCDs, these cannot be freely estimated in the first least squares run. If the constraints are realised by global models or, in the case of DD integer-ambiguity constraints as in the second least squares estimation, even these parameters can be estimated. The same analysis is significantly more elaborate for the common ionosphere-free linear combination. At a reasonable cost and in the event of more than two signals per satellite, a setup with an equal contribution by all signals is cumbersome. Moreover, since ionosphere-free observations are used, the ionospheric and UCD information cannot be directly derived. In order to gain information concerning the ionosphere and the UCDs, or in this case the DCBs, a further, separate least squares estimation is required. Furthermore, it has to be noted that the common ionosphere-free linear combinations are restricted to a single pair of each, phase and code observations per satellite-receiver link and thus to two signals. The situation becomes confusing as soon as more than two signals need to be analysed. Usually the initial analysis is performed with two signals, whereby the different least squares runs are repeated for the additional signals. In order to ensure consistent results, the different parameters, such as coordinates, orbits and clocks or, in the case of DCBs the ionosphere, need to be fixed for all analyses except the first. The additional steps required are highlighted in green. However, it is clear that this strategy does not allow contributions from signals that were processed in the second run.

8.3 Ambiguity fixing in the case of raw observations

As outlined in figure 8.1, in addition to the complete renunciation of observation differences (first least squares estimation), the raw processing approach also offers the possibility of constraining the network or standalone PPP solutions by DD or SD integer-ambiguity constraints. Fixed integer-ambiguities or integer-ambiguity constraints are a common method used in high precision GNSS analyses to improve the solution. In the case of "correctly" fixed ambiguities, phase observations are strengthened, resulting in the improved repeatability of the east and up coordinates. However, in the case of incorrect ambiguity fixes, the solution is significantly degraded. This uncertainty leads to the desire to overcome this technique. The comparison of the results, dual- versus multi-frequency processing, has already shown a clear improvement in the east and up components. Combined with the greater number of satellites in the future, significant improvements to the coordinate accuracy can be expected. However, it is still an open question if the improvement will result in the same parameter stability as in the case of ambiguity-fixing. If the answer is yes, it is highly desirable to renounce ambiguity resolution. This decreases

the processing steps from three to one and it removes the risk of wrongly fixed ambiguities. However, in terms of the up-to-date GNSS environment, ambiguity-fixing is an integral feature for obtaining highest parameter stability. Hence, for reasons of comparability, a procedure to apply integer-ambiguity constraints to raw observations has been developed. In contrast to the usual approaches that make use of linear combinations such as wide-lane and narrow-lane, the presented approach continues the idea of raw observations. As explained in the analysis section of this thesis, a fixing of undifferentiated raw observation integer-ambiguities is not reasonable. The only observations that can be assumed to have integer characteristics after removing the atmospheric biases are double differences. Since the atmospheric biases have been estimated in the first least squares run and are no longer part of the ambiguity estimate, the ambiguity-fixing procedure can be significantly simplified. It has been demonstrated that, even for baselines of several thousand kilometres, an estimation of DD raw observations (L1/E1, L2, etc.) is possible. As a result, the detour via the narrow-lane observations and back conversion thereof is no longer required. The formation of DDs based on raw observations significantly enhances the cross-system ambiguity-fixing capabilities. Thus, belonging to a specific GNSS no longer matters, as the carrier frequency is the decisive point. This again allows for forming DDs between satellites and receivers with a single common signal.

8.4 Experiments and analyses

Within the frame of this thesis, different experiments and analyses were run in order to study the relevant bias characteristics and to confirm the implementation. The experiments demonstrated that a general statement regarding the performance of up-to-date hardware is not possible. Thus, some receiver types showed almost stable biases between the different observations, whereas others demonstrated variations as high as centimetres for carrier phase measurements. The outcome of these experiments was used to design an optimal parameter setup for the following tests.

Within these tests, it was demonstrated that the implemented raw processing approach, in the case of dual-frequency GNSS observations, is at least equivalent to the common ionosphere-free approach. Instead, and particularly under suboptimal network and observation conditions, this shows that the flexibility in observation selection, weighting and screening improves the solutions. However, due to different settings not directly transferrable between the two approaches, it is difficult to trace the improvement exclusively to the new implementation.

Moreover, the multi-frequency (more than two) performance of the new approach was rudimentarily demonstrated through the example of a PPP using Galileo and the block IIF GPS satellites exclusively. The limited number of samples makes it difficult to produce a definitive statement. However, all tests demonstrated the expected behaviour. Thus, it became apparent that the third frequency significantly improves the east and height components. This illustrates that it is not unreasonable to question the methodology of ambiguity-fixing. Nevertheless, it showed that up-to-date, also for raw observations, the fixing of integer-phase ambiguities gives the most consistent results.

In summary

The presented raw processing approach offers an "at least" equivalent alternative to the usual processing strategies, applicable for highly precise standalone, as well as regional and global network PPP solutions, allowing a simplified, consistent processing of different numbers of signals, suitable for an optimal, flexible, equivalent, joint processing of arbitrary GNSS observations, introducing a new dimension of analyses with direct access to all signal components.

8.5 Future work

Due to the limited availability of test data, the true capabilities of the newly implemented approach could not yet be fully utilised. This leaves a number of questions unanswered. Among others is the question of the necessity for ambiguity-fixing procedures in a fully developed GNSS environment. Furthermore, it remains to be confirmed that the proposed concept for an almost free parameter setup, estimating global ionosphere functions (spherical harmonics) instead of constraining the UCDs, is applicable. In addition to these open questions, the proposed approach offers a broad spectrum of possible analyses, which is required for the optimal incorporation of the new satellites and signals. One potential application is the estimation of native satellite PCOs/PCVs and UCDs. It is also conceivable that a relative, in situ calibration procedure for receiver UCDs could be developed. The number of further possible analyses is by far more diverse.

Bibliography

Agrotis, L. G. *Determination of satellite orbits and the Global Positioning System*. PhD thesis, University of Nottingham, 1984.

Altamimi, Z., Sillard, P., and Boucher, C. *ITRF2000: A new release of the International Terrestrial Reference Frame for earth science applications*. Journal of Geophysical Research: Solid Earth, 107(B10):ETG 2–1—-ETG 2–19, 2002. ISSN 2156-2202. doi: 10.1029/2001JB000561.

Altamimi, Z., Collilieux, X., and Métivier, L. *ITRF2008: An improved solution of the international terrestrial reference frame*. Journal of Geodesy, 85(8):457–473, 2011. ISSN 0949-7714. doi: 10.1007/s00190-011-0444-4.

Altamimi, Z., Métivier, L., and Collilieux, X. *ITRF2008 plate motion model*. Journal of Geophysical Research: Solid Earth, 117(B7), 2012. ISSN 2156-2202. doi: 10.1029/2011JB008930.

Ashby, N. *Relativity in the Global Positioning System*. Living Reviews in Relativity, 6(1), 2003. [Online] Available at: http://relativity.livingreviews.org/Articles/lrr-2003-1/. [Accessed 14 January 2014].

Avila-Rodriguez, J.-A., Hein, G. W., Irsigler, M., and Pany, T. *Combined Galileo/GPS frequency and signal performance analysis*. In Proceedings ION GNSS 2004, 632–649, 2004.

Avila-Rodriguez, J. A., Hein, G. W., Wallner, S., Issler, J.-L., Ries, L., Lestarquit, L., De Latour, A., Godet, J., Bastide, F., Pratt, T., and Owen, J. *The MBOC modulation, a final touch for the Galileo frequency and signal plan*. Inside GNSS, 2(6):43–58, 2007.

BeiDou. *BeiDou Navigation Satellite System signal in space interface control document*. Technical report, China Satellite Navigation Office, 2011. [Online] Available at: http://wenku.baidu.com/view/ec6d8748be1e650e52ea997d.html. [Accessed 14 January 2014].

Berg, H. *Allgemeine Meteorologie: Einführung in die Physik der Atmosphäre*. F. Dümmler, Bonn, 1948.

Beutler, G. *Methods of celestial mechanics volume II: application to planetary system, geodynamics and satellite geodesy*. Springer Berlin Heidelberg, 2005. ISBN 978-3-540-40750-8. doi: 10.1007/b137725.

Beutler, G., Rothacher, M., Schaer, S., Springer, T., Kouba, J., and Neilan, R. E. *The International GPS Service (IGS): An interdisciplinary service in support of Earth sciences*. Advances in Space Research, 23(4):631–653, 1999. doi: 10.1016/S0273-1177(99)00160-X.

Beutler, G., Bock, H., Dach, R., Fridez, P., Hugentobler, U., Jäggi, A., Meindl, M., Mervat, L., Prange, L., Schaer, S., Springer, T., Urschl, C., and Walser, P. *Bernese GPS software*. Technical report, Bern, Astronomical Institute, University of Bern, 2007.

Bhuiyan, M. Z. H. and Lohan, E. S. *Advanced multipath mitigation techniques for satellite-based positioning applications*. International Journal of Navigation and Observation, 2010:1–15, 2010. ISSN 1687-5990. doi: 10.1155/2010/412393.

Blewitt, G. *Carrier phase ambiguity resolution for the Global Positioning System applied to geodetic baselines up to 2000 km*. Journal of Geophysical Research, 94(B8):10187–10203, 1989. doi: 10.1029/JB094iB08p10187.

Boehm, J., Werl, B., and Schuh, H. *Troposphere mapping functions for GPS and very long baseline interferometry from European Centre for Medium-Range Weather Forecasts operational analysis data*. Journal of Geophysical Research: Solid Earth, 111(B2), 2006. ISSN 2156-2202. doi: 10.1029/2005JB003629.

Boucher, C., Feissel, M., and Lestrade, J.-F. *Concepts and methods of the Central Bureau of the International Earth Rotation Service*. Bulletin Geodesique, 62(4):511–519, 1988. ISSN 0007-4632. doi: 10.1007/BF02520241.

Boy, J. *A new and improved loading service for precise geodetic observations*, 2013. [Online] Available at: `http://loading.u-strasbg.fr/`. [Accessed 23 October 2013].

Boy, J. *A new and improved loading service for precise geodetic observations*. AGU Fall Meeting Abstracts, 906, 2011.

Braasch, M. S., Van Dierendonck, A. J., and Member, S. *GPS receiver architectures and measurements*. In Proceedings of the IEEE, 87:48–64, 1999.

Breuer, B., Campbell, J., Görres, B., Hawig, R., and Wohlleben, R. *Kalibrierung von GPS-Antennen für hochgenaue geodätische Anwendungen*. Zeitschrift für Satellitengestützte Positionierung, Navigation und Kommunikation (SPN), (2):49–59, 1995.

Burbidge, G. T. A. *Development of the navigation payload for the Galileo in-orbit validation (IOV) phase*. In International Global Navigation Satellite Systems Society IGNSS Symposium 2007, Sydney, Australia, 2007. The University of New South Wales.

Campbell, J., Görres, B., Siemes, M., Wirsch, J., and Becker, M. *Zur Genauigkeit der GPS Antennenkalibrierung auf der Grundlage von Labormessungen und deren Vergleich mit anderen Verfahren*. Allgemeine Vermessungsnachrichten, Nr.1, 111:2–11, 2004.

Collins, P. *Isolating and estimating undifferenced GPS integer ambiguities*. In Proceedings of the 2008 National Technical Meeting of The Institute of Navigation, 720 – 732, San Diego, CA, 2008.

De Jonge, P. J. *A processing strategy for the application of the GPS in networks*. PhD thesis, Netherlands Geodetic Commission, 1998. NGC-Publication No. 46, yellow series.

DeMets, C., Gordon, R. G., Argus, D. F., and Stein, S. *Effect of recent revisions to the geomagnetic reversal time scale on estimates of current plate motions*. Geophysical Research Letters, 21(20):2191–2194, 1994. ISSN 1944-8007. doi: 10.1029/94GL02118.

Dilssner, F., Wübbena, G., and Schmitz, M. *Impact of near-field effects on the GNSS position solution*. In International Technical Meeting, ION GNSS 2008, Savannah, Georgia, 2008.

Eissfeller, B., Ameres, G., V., K., and Sanroma, D. *Performance of GPS, GLONASS and Galileo*. In Photogrammetric Week, 185–199, Stuttgart, 2007. Wichmann.

ESOC. *NAPEOS mathematical models and algorithms*. Technical report, Darmstadt, Germany, Navigation Support Office, ESA/ESOC, 2009. DOPS-SYS-TN-0100-OPS-GN.

ESOC. *ESOC IGS analysis strategy summary*, 2011. [Online] Available at: `http://igs.org/igscb/center/analysis/esa.acn`. [Accessed 14 January 2014].

Fantino, M., Marucco, G., Mulassano, P., and Pini, M. *Performance analysis of MBOC, AltBOC and BOC modulations in terms of multipath effects on the carrier tracking loop within GNSS receivers*. In 2008 IEEE/ION Position, Location and Navigation Symposium, 369–376. Ieee, 2008. ISBN 978-1-4244-1536-6. doi: 10.1109/PLANS.2008.4570092.

Feng, Y. and Zheng, Y. *Efficient interpolations to GPS orbits for precise wide area applications*. GPS Solutions, 9(4):273–282, 2005. ISSN 1080-5370. doi: 10.1007/s10291-005-0133-y.

Fritsche, M., Dietrich, R., Knöfel, C., Rülke, A., Vey, S., Rothacher, M., and Steigenberger, P. *Impact of higher-order ionospheric terms on GPS estimates*. Geophysical Research Letters, 32(23), 2005. ISSN 0094-8276. doi: 10.1029/2005GL024342.

Galileo. *Mission high level definition*. Technical report, Brussels, Belgium, Commission, European, 2002. [Online] Available at: `http://ec.europa.eu/dgs/energy_transport/galileo/doc/galileo_hld_v3_23_09_02.pdf`. [Accessed 14 January 2014].

Galileo. *European GNSS (Galileo) open service signal in space interface control document*. Commission, European, September 2010. [Online] Available at: `http://www.gsa.europa.eu/sites/default/files/galileo_os_sis_icd_revised_2_en.pdf`. [Accessed 14 January 2014].

Ge, M., Gendt, G., Rothacher, M., Shi, C., and Liu, J. *Resolution of GPS carrier-phase ambiguities in precise point positioning (PPP) with daily observations*. Journal of Geodesy, 82(7):389–399, 2008. ISSN 0949-7714. doi: 10.1007/s00190-007-0187-4.

Gendt, G. *[IGSMAIL-5438]: IGS switch to absolute antenna model and ITRF2005*, IGS Central Bureau, 2006.

Geng, J., Meng, X., Dodson, A. H., and Teferle, F. N. *Integer ambiguity resolution in precise point positioning: method comparison*. Journal of Geodesy, 84(9):569–581, 2010. ISSN 0949-7714. doi: 10.1007/s00190-010-0399-x.

GLONASS. *Interface control document navigation radio signal in bands L1, L2*. Technical report, Moscow, Russia, Russian Institute of Space Device Engineering, 2008.

GPS. *Interface specifications IS-GPS-200G*. Technical report, Global Positioning Systems Directorate Systems Engineering & Integration, 2012a. [Online] Available at: `http://www.navcen.uscg.gov/pdf/gps/IS-GPS-200G.pdf`. [Accessed 14 January 2014].

GPS. *Interface specifications IS-GPS-705*. Technical report, Global Positioning Systems Directorate Systems Engineering & Integration, 2012b. [Online] Available at: `http://www.navcen.uscg.gov/pdf/gps/IS-GPS-705C.pdf`. [Accessed 14 January 2014].

GPS. *Interface specifications IS-GPS-800*. Technical report, Global Positioning Systems Directorate Systems Engineering & Integration, 2012c. [Online] Available at: `http://www.navcen.uscg.gov/pdf/gps/IS-GPS-800C.pdf`. [Accessed 14 January 2014].

Gurtner, W. and Estey, L. *RINEX the receiver independent exchange format version 3.01*. Technical report, 2009. [Online] Available at: `http://igscb.jpl.nasa.gov/igscb/data/format/rinex301.pdf`. [Accessed 14 January 2014].

Hall, M. P. M., Barclay, L. W., Hewitt, T., and of Electrical Engineers, T. I. *Propagation of radiowaves*. Institution of Electrical Engineers, 1996. ISBN 9780852968192.

Han, S. and Rizos, C. *The impact of two additional civilian GPS frequencies on ambiguity resolution strategies*. In 55th National Meeting U.S. Institute of Navigation, Cambridge, Massachusetts, 315–321, 1999.

Hein, G. and Pany, T. *Architecture and Signal Design of the European Satellite Navigation System Galileo - Status Dec. 2002*. Positioning, 1(2):73–84, 2002.

Hein, G., Avila-Rodriguez, J.-A., and Wallner, S. *The Galileo code and others*. Inside GNSS, 1(6):62–74, 2006a.

Hein, G. W., Godet, J., Issler, J.-L., Martin, J.-C., Erhard, P., Lucas-Rodriguez, R., and Pratt, T. *Status of Galileo frequency and signal design*. In Proceedings ION GNSS 2002, 266—-277, 2002.

Hein, G. W., Avila-Rodriguez, J.-A., Wallner, S., Pratt, A. R., Owen, J., Issler, J.-L., Betz, J. W., Hegarty, C. J., Lenahan, S., Rushanan, J. J., Kraay, A. L., and Stansell, T. A. *MBOC : The new optimized spreading modulation recommended for Galileo L1 OS and GPS L1C*. Inside GNSS, 57–66, 2006b.

Héroux, P. and Kouba, J. *GPS precise point positioning using IGS orbit products*. In Proceedings of the First COST Action 716 Workshop Towards Operational GPS Meteorology and the Second Network Workshop of the International GPS Service (IGS), 26:573–578, 2001. doi: 10.1016/S1464-1895(01)00103-X.

Herring, T. *Modelling atmospheric delays in the analysis of space geodetic data*. In Proceedings of the Symposium on Refraction of Transatmospheric Signals in Geodesy, number 36, 157–164, The Hague, 1992. Netherlands Geodetic Commission Series.

Hilla, S. *The extended standard product 3 orbit format (SP3-c)*. Technical report, Silver Spring, USA, National Geodetic Survey, National Ocean Service, NOAA, August 2010.

Hofmann-Wellenhof, B., Lichtenegger, H., and Wasle, E. *GNSS - Global Navigation Satellite Systems*. Springer, 2008.

Hopfield, H. S. ***Two-quartic tropospheric refractivity profile for correcting satellite data***. Journal of Geophysical Research, 74(18):4487–4499, 1969. doi: 10.1029/JC074i018p04487.

Horemuž, M. and Andersson, J. ***Polynomial interpolation of GPS satellite coordinates***. GPS Solutions, 10(1): 67–72, 2006. ISSN 1080-5370. doi: 10.1007/s10291-005-0018-0.

Hugentobler, U., Steigenberger, P, Montenbruck, O., Hauschild, A., Weber, G., and Hessels, U. ***Evaluation of GIOVE satellite clocks using the CONGO Network***, 24th European Frequency and Time Forum, 2010. Noordwijk, Netherlands.

IERS. ***International Earth Rotation and Reference Systems Service***, 2013. [Online] Available at: `http://www.iers.org/`. [Accessed 23 Oktober 2013].

IGS. ***Strategic plan 2008-2012***. Pasadena, California, IGS Central Bureau, Jet Propulsion Laboratory, 2008. [Online] Available at: `http://igscb.jpl.nasa.gov/igscb/resource/pubs/IGS_StrategicPlan_proof5.pdf`. [Accessed 14 January 2014].

IGS. ***IGS site guidelines***. Technical report, Pasadena, California, IGS Central Bureau, Jet Propulsion Laboratory, April 2013. [Online] Available at: `http://igs.org/network/guidelines/IGS_Site_Guidelines.pdf`. [Accessed 14 January 2014].

IGS. ***International GNSS service***, 2014. [Online] Available at: `http://igscb.jpl.nasa.gov`. [Accessed 14 January 2014].

Irsigler, M. and Eissfeller, B. ***Comparison of multipath mitigation techniques with consideration of future signal structures***. In Proceedings of the International Technical Meeting of the Institute of Navigation, ION-GPS 2003, September 9-12, 7, Portland, Oregon, 2003. Institute of Navigation.

Joosten, P. and Tiberius, C. ***Fixing the ambiguities: Are you sure they're right?*** GPS World, 11(5):46–51, 2000.

Kaplan, E. ***Understanding GPS - principles and applications***. Artech House, 2 edition, 2005.

Kedar, S., Hajj, G. A., Wilson, B. D., and Heflin, M. B. ***The effect of the second order GPS ionospheric correction on receiver positions***. Geophysical Reseach Letters, 30(16):1829, 2003. doi: 10.1029/2003GL017639.

Kersten, T., Schön, S., and Weinbach, U. ***On the impact of group delay variations on GNSS time and frequency transfer***. In European Frequency and Time Forum (EFTF), 2012, 514–521, 2012. doi: 10.1109/EFTF.2012. 6502435.

Klobuchar, J. A. ***Ionospheric effects on GPS***. GPS World, 2(4):48–51, 1991.

Koch, K.-R. ***Parameter estimation and hypothesis testing in linear models***. Springer, Berlin, Heidelberg, New York, 2nd update edition, 1999. ISBN 3540652574.

Kouba, J. ***A guide to using International GPS Service (IGS) products***. Geodetic Survey Division, Natural Resources Canada, 615 Booth Street, Ottawa, Ontari K1A 0E9, 2009.

Laurichesse, D., Mercier, F., Berthias, J.-P, Broca, P., and Cerr, L. ***Integer ambiguity resolution on undifferenced GPS phase measurements and its application to PPP and satellite precise orbit determination***. In NAVIGATION, 56:135–149, 2009.

Lestarquit, L., Artaud, G., and Issler, J.-L. ***AltBOC for dummies or everything you always wanted to know about AltBOC***. In Proceedings of the 21st International Technical Meeting of the Satellite Division of The Institute of Navigation (ION GNSS 2008), 961–970, Savannah International Convention Center Savannah, GA, September 2008.

Li, X., Ge, M., Zhang, H., and Wickert, J. ***A method for improving uncalibrated phase delay estimation and ambiguity-fixing in real-time precise point positioning***. Journal of Geodesy, 87(5):405–416, 2013. ISSN 0949-7714. doi: 10.1007/s00190-013-0611-x.

Loyer, S., Perosanz, F., Mercier, F., Capdeville, H., and Marty, J.-C. *Zero-difference GPS ambiguity resolution at CNES-CLS IGS Analysis Center*. Journal of Geodesy, 86(11):991–1003, 2012. ISSN 0949-7714. doi: 10.1007/s00190-012-0559-2.

Mader, G. L. *GPS antenna calibration at the National Geodetic Survey*. GPS Solutions, 3(1):50–58, 1999. ISSN 1080-5370. doi: 10.1007/PL00012780.

Mader, G. L. and Czopek, F. M. *The Block IIA satellite calibrating antenna phase centers*. GPS World, 13(5):40, 2002. ISSN 10485104.

Maral, G., Bousquet, M., and Sun, Z. *Satellite communications systems: systems, techniques and technology*. Wiley, 2009. ISBN 9780470660881.

Melbourne, W. G. *The case for ranging in GPS based geodetic systems*. In Goad, C., editor, *Proceedings of the 1st International Symposium on Precise Positioning with the Global Positioning System*, 373–386, Rockville, Maryland, 1985. US Department of Commerce.

Misra, P. and Enge, P. *Global Positioning System signals, measurements, and performance*. Ganga-Jamuna Press, Lincoln MA, second edition, 2006.

Montenbruck, O., Hauschild, A., Steigenberger, P., and Langley, R. B. *Three's the challenge: A close look at GPS SVN62 triple-frequency signal combinations finds carrier-phase variations on the new L5*. GPS World, 21 (8):8–19, 2010. ISSN 1048-5104.

Montenbruck, O., Hugentobler, U., Dach, R., Steigenberger, P., and Hauschild, A. *Apparent clock variations of the Block IIF-1 (SVN62) GPS satellite*. GPS Solutions, 2011. ISSN 1080-5370. doi: 10.1007/s10291-011-0232-x.

Montenbruck, O., Steigenberger, P., Schönemann, E., Hauschild, A., Hugentobler, U., Dach, R., and Becker, M. *Flight characterization of new generation GNSS satellite clocks*. Navigation, Journal of the Institute of Navigation, 59(4):291–302, 2012.

Mueller, I. I. *Planning an international service using the Global Positioning System (GPS) for geodynamic applications*. In Mader, G. L., editor, *Permanent Satellite Tracking Networks for Geodesy and Geodynamics*, 109 of *International Association of Geodesy Symposia*, 1–22. Springer Berlin Heidelberg, 1993. ISBN 978-3-540-55827-9. doi: 10.1007/978-3-642-77726-4_1.

Niell, A. E. *Global mapping functions for the atmosphere delay at radio wavelengths*. Journal of Geophysical Research: Solid Earth, 101(B2):3227–3246, 1996. ISSN 2156-2202. doi: 10.1029/95JB03048.

Niell, A. E. *Improved atmospheric mapping functions for VLBI and GPS*. Earth, Planets, and Space, 52:699–702, 2000.

Niemeier, W. *Ausgleichungsrechnung: eine Einführung für Studierende und Praktiker des Vermessungs- und Geoinformationswesens*. De Gruyter. Berlin, Boston, 2002. ISBN 9783110140804.

Odijk, D. *Fast precise GPS positioning in the presence of ionospheric delays*. PhD thesis, Delft University of Technology, Netherlands Geodetic Commission, 2002.

Odijk, D., Teunissen, P. J. G., and Tiberius, C. C. J. M. *Triple-frequency ionosphere-free phase combinations for ambiguity resolution*. In Proceedings of the European Navigation Conference ENC-GNSS 2002, 1–10, Copenhagen, Denmark, 2002.

Office of the Assistant Secretary of Defense (Public Affairs). *DoD permanently discontinues procurement of Global Positioning System selective availability*, September 2007. News Release.

Ohm, J. R. and Lüke, H. D. *Signalübertragung: Grundlagen der digitalen und analogen Nachrichtenübertragungssysteme*. Springer-Lehrbuch. Springer, Berlin, Heidelberg, 2010. ISBN 9783642102004.

Petit, G. and Luzum, B. *IERS conventions (2010)*. Technical Report 36, Frankfurt am Main, 2010.

Phelts, R. E. *Nominal signal deformations: limits on GPS range accuracy*. In the 2004 International Symposium on GPS/GNSS, Sydney, Australia, 2004.

Phelts, R. E. ***Range biases on modernized GNSS codes***. In European Navigation Conference GNSS/TimeNav 2007, Geneva, Switzerland, 2007.

Phelts, R. E. and Akos, D. M. ***Effects of signal deformations on modernized GNSS signals***. Journal of Global Positioning Systems, 5:1-2, 2006.

Plumb, J., Larson, K. M., White, J., and Powers, E. ***Absolute calibration of a geodetic time transfer system.*** IEEE transactions on ultrasonics, ferroelectrics, and frequency control, 52(11):1904–1911, 2005. ISSN 0885-3010. doi: 10.1109/TUFFC.2005.1561658.

Proia, A. and Cibiel, G. ***Progress report of CNES activities regarding the Centre National d ' Etudes Spatiales***. In 42nd Annual Precise Time and Time Interval (PTTI) Meeting, 541–556, Reston, VA, 2010.

Proia, A., Cibiel, G., White, J., Wilson, D., and Senior, K. ***Absolute calibration of GNSS time transfer systems: NRL and CNES techniques comparison***. In IEEE International Frequency Control Symposium, 1–6, 2011. doi: 10.1109/FCS.2011.5977799.

Rebischung, P., Griffiths, J., Ray, J., Schmid, R., Collilieux, X., and Garayt, B. ***IGS08: the IGS realization of ITRF2008***. GPS Solutions, 16(4):483–494, 2012. ISSN 1080-5370. doi: 10.1007/s10291-011-0248-2.

Remondi, B. W. ***Global positioning system carrier phase: description and use***. Bulletin géodésique, 59(4): 361–377, 1985. ISSN 0007-4632. doi: 10.1007/BF02521069.

Richert, T. and El-Sheimy, N. ***Optimal linear combinations of triple frequency carrier phase data from future global navigation satellite systems***. GPS Solutions, 11(1):11–19, 2007. ISSN 1080-5370. doi: 10.1007/s10291-006-0024-x.

Ries, L., Lestarquit, L., Legrand, F., Vigneau, W., Bourga, C., Industries, A. S., Erhard, P., and Issler, J.-L. ***A software simulation tool for GNSS2 BOC signals analysis***. In Proceedings of the 15th International Technical Meeting of the Satellite Division of The Institute of Navigation (ION GPS 2002), 2225–2239, Oregon Convention Center Portland, OR, September 2002.

Rizos, C., Montenbruck, O., Weber, R., Weber, G., Neilan, R., and Hugentobler, U. ***The IGS MGEX Experiment as a milestone for a comprehensive multi-GNSS service***. In ION Pacific PNT Conference, 22-25 April 2013, Honolulu, Hawaii, 2013. Institute of Navigation.

Romero, N. ***[IGSMAIL-6542]: CC2NONCC update to handle more than 24 satellites per epoch***, IGS Central Bureau, 2012.

Rosen, J. S. and Center, G. C. M. S. F. ***The Runge-Kutta equations by quadrature methods***. NASA technical report. National Aeronautics and Space Administration, 1967.

Rothacher, M. and Schmid, R. ***ANTEX: The Antenna Exchange format, version 1.4***, Forschungseinrichtung Satellitengeodäsie, 2010. München.

Rothacher, M., Schaer, S., Mervart, L., and Beutler, G. ***Determination of antenna phase center variations using GPS data***. In Gendt G.; Dick, G., editor, ***Proceedings of the IGS Workshop "Special Topics and New Directions"***, 205–220. GeoForschungsZentrum Potsdam, 1996.

Rothacher, M., Beutler, G., Herring, T. A., and Weber, R. ***Estimation of nutation using the Global Positioning System***. Journal of Geophysical Research: Solid Earth, 104(B3):4835–4859, 1999. ISSN 2156-2202. doi: 10.1029/1998JB900078.

Saastamoinen, J. ***Contributions to the theory of atmospheric refraction. Part II. Refraction corrections in satellite geodesy.*** Bulletin geodesique, 107:13–34, 1973. doi: 10.1007/BF02522083.

Schaer, S. ***Mapping and predicting the Earth's ionosphere using the Global Positioning System***. French Studies of the Eighteenth and Nineteenth Centuries. Schweizerische Geodätische Kommission, 1999. ISBN 9783908440017.

Schaer, S. *Differential code biases (DCB) in GNSS analysis*. Presented at IGS Workshop, Miami Beach, Florida, 2nd June 2008 to 6th June 2008, IGS Analysis Center Workshop, 2008.

Schaer, S. and Dach, R. *Biases in GNSS analysis*. Presented at IGS Workshop 2010, Newcastle upon Tyne, England, IGS Workshop Newcastle, 2010.

Schenewerk, M. *A brief review of basic GPS orbit interpolation strategies*. GPS Solutions, 6(4):265–267, 2003. ISSN 2081-9919. doi: 10.1007/s10291-002-0036-0.

Scherneck, H.-G. *A parametrized solid earth tide model and ocean tide loading effects for global geodetic baseline measurements*. Geophysical Journal International, 106(3):677–694, 1991. ISSN 1365-246X. doi: 10.1111/j.1365-246X.1991.tb06339.x.

Schmid, R. and Rothacher, M. *Estimation of elevation-dependent satellite antenna phase center variations of GPS satellites*. Journal of Geodesy, 77(7-8):440–446, 2003. ISSN 0949-7714. doi: 10.1007/s00190-003-0339-0.

Schmid, R., Mader, G., and Herring, T. *From relative to absolute antenna phase center corrections*. In Meindl, M., editor, *Proceedings of the IGS Workshop and Symposium 2004, Bern*. Astronomical Institute, University of Bern, 2005.

Schmid, R., Steigenberger, P., Gendt, G., Ge, M., and Rothacher, M. *Generation of a consistent absolute phase-center correction model for GPS receiver and satellite antennas*. Journal of Geodesy, 81(12):781–798, 2007. ISSN 0949-7714. doi: 0.1007/s00190-007-0148-y.

Schmidt, R. *IGS Antenna Working Group*. In Dach, R. and Jean, Y., editors, *IGS Technical Report 2012*, 141–147, Bern, 2013. IGS Central Bureau, Astronomical Insitute, University of Bern.

Schönemann, E., Springer, T., Otten, M., Becker, M., and Dow, J. *GIOVE-A precise orbit determination from microwave and satellite laser ranging data - first perspectives for the Galileo constellation and its scientific use*. In Proceedings of the First Colloquium on Scientific and Fundamental Aspects of the Galileo Programme 2007, 1 October 2007 - 4 October 2007, Toulouse, France, 2007a.

Schönemann, E., Zeimetz, P., and Becker, M. *Antenna phase centre corrections (PCO/PCV) and near field effects in the scope of GPS, Glonass and Galileo*. Poster presented at the EGU General Assembly, Vienna, Austria, EGU General Assembly, 2007b.

Schönemann, E., Becker, M., and Springer, T. *A new approach for GNSS analysis in a multi-GNSS and multi-signal environment*. Journal of Geodetic Science, 1(3):204–214, 2011. ISSN 2081-9919. doi: 10.2478/v10156-010-0023-2.

Schupler, B. R. and Clark, T. A. *How different antennas affect the GPS observable*. GPS World, 32–36, 1991.

Seeber, G. *Satellite geodesy: Foundations, methods, and applications*. Mathematik gesamt. Walter de Gruyter, Berlin, New York, 2003. ISBN 9783110200089.

Simsky, A., Sleewaegen, J.-M., Hollreiser, M., and Crisci, M. *Performance assessment of Galileo ranging signals transmitted by GSTB-V2 satellites*. In Proceedings of ION GNSS, 25 September 2006 - 26 September 2006, Fort Worth, Texas, USA.

Simsky, A., Sleewaegen, J.-M., De Wild, W., and Wilms, F. *Overview of Septentrio's Galileo receiver development strategy*. In ION GNSS, Long Beach, California, U.S.A., 13 September 2005 - 16 September 2005 2005.

Simsky, A., Mertens, D., Sleewaegen, J.-M., De Wilde, W., Hollreiser, M., and Crisci, M. *MBOC vs BOC(1,1) multipath comparison based on GIOVE-B data*. Inside GNSS, 44:36–39, 2008a.

Simsky, A., Mertens, D., Sleewaegen, J.-M., De Wilde, W., Hollreiser, M., and Crisci, M. *Multipath and tracking performance of Galileo ranging signals transmitted by GIOVE-B*. In Proceedings of the 21st International Technical Meeting of the Satellite Division of the Institute of Navigation ION GNSS 2008, 1525–1536, 2008b.

Sleewaegen, J.-M., Simsky, A., De Wilde, W., Boon, F., and Willems, T. *Demystifying GLONASS Inter-Frequency Carrier Phase Biases*. Inside GNSS, 7(3):57–61, 2012.

Spilker Jr, J. J. *GPS navigation data*. In Spilker, Jr., J. J. and Parkinson, B. W., editors, *Global Positioning System: theory and applications volume I*, 121–217. American Institute of Aeronautics and Astronautics, Inc., 1996.

Spofford, P. R. and Remondi, B. W. *The National Geodetic Survey Standard GPS Format SP3*. Technical report, Silver Spring, USA, National Geodetic Survey, National Ocean Service, NOAA, 2010.

Springer, T. *Modelling and validating orbits and clocks using the Global Positioning System*. Phd thesis, Universität Bern, November 1999.

Svehla, D., Schönemann, E., Escobar, D., and Springer, T. *Complete relativistic modelling of the GIOVE-B clock parameters and its impact on POD, track-track ambiguity resolution and precise timing*, Presentation at IGS Workshop, 2 July 2010, Newcastle, England, UK, 2010.

Tapley, B. D., Watkins, M. M., Ries, J. C., Davis, G. W., Eanes, R. J., Poole, S. R., Rim, H. J., Schutz, B. E., Shum, C. K., Nerem, R. S., Lerch, F. J., Marshall, J. A., Klosko, S. M., Pavlis, N. K., and Williamson, R. G. *The joint gravity model 3*. Journal of Geophysical Research: Solid Earth, 101(B12):28029–28049, 1996. ISSN 2156-2202. doi: 10.1029/96JB01645.

Teunissen, P. J. G., Jonge, P. J. D., and Tiberius, C. *The LAMBDA-Method for fast GPS surveying*. In Proceedings of International Symposium GPS technology applications, 26–29, 1995.

Vallado, D. A. *Fundamentals of astrodynamics and applications*, 21 of *Space technology library*. Microcosm Press [u.a.], Hawthorne, Calif. [u.a.], 3. ed., 1. edition, 2007.

Van Dam, T. M. and Wahr, J. M. *Displacements of the Earth's surface due to atmospheric loading: effects on gravity and baseline measurements.* Journal of Geophysical Research, 92(B2):1281—-1286, 1987. doi: 10.1029/JB092iB02p01281.

Verhagen, A. A. *The GNSS integer ambiguities: estimation and validation*. PhD thesis, Delft University of Technology, 2005.

Vollath, U., Birnbach, S., Landau, H., Fraile-Ordoñez, J. M., and Martin-Neira, M. *Analysis of Three-Carrier Ambiguity Resolution (TCAR) technique for precise relative positioning in GNSS-2*. In Proceedings of ION 11th Annual Meeting 1998, 417–426, 1998.

Waller, P., Gonzalez, F., Binda, S., Rodriguez, D., Tobias, G., Cernigliaro, A., I., S., and Tavella, P. *Long-term performance analysis of Giove clocks*. In 42nd Annual Precise Time and Time Interval (PTTI) Meeting, 171–180, Reston, VA, 2010.

Wanninger, L. *Carrier-phase inter-frequency biases of GLONASS receivers*. Journal of Geodesy, 86:139–148, 2012. doi: 10.1007/s00190-011-0502-y.

Wong, G., Phelts, R. E., Walter, T., and Enge, P. *Alternative characterization of analog signal deformation for GNSS - GPS satellites*. In ION Institute of Navigation International Technical Meeting, San Diego, CA, 2011.

Wu, J.-T., Hajj, G. A., Wu, S.-C., Bertiger, W. I., and Lichten, S. M. *Effects of antenna orientation on GPS carrier phase*. Manuscripta Geodaetica, 18(2):91–98, 1993.

Wübbena, G. and Goad, C. C. *Software developments for geodetic positioning with GPS using TI 4100 code and carrier measurements*. In Proceedings of First Int Symposium on Precise Position with GPS Rockville Maryland, 403–412. U.S. Department of Commerce, 1985.

Wübbena, G., Schmitz, M., and Propp, M. *Antenna group delay calibration with the Geo++ robot extension to code observable*, Poster presented at the IGS Analysis Workshop, 2nd June 2008 to 6th June 2008, Miami Beach, Florida, US.

Wübbena, G., Menge, F., Schmitz, M., Seeber, G., and Völksen, C. *A new approach for field calibration of absolute antenna phase center variations*. In Proceedings of the International Technical Meeting, ION GPS-96, 1205–1214, Kansas City, Missouri, 1996.

Wübbena, G., Schmitz, M., and Boettcher, G. **Near-field effects on GNSS sites: Analysis using absolute robot calibrations and procedures to determine corrections**. In Proceedings of the IGS Workshop 2006 Perspectives and Visions for 2010 and beyond, 2006.

Wübbena, G., Schmitz, M., Garbsen, D., Mader, G., and Spring, S. **GPS Block II / IIA satellite antenna testing using the automated absolute field calibration with robot**. In ION GNSS 2007, 25 September 2007 - 28 September 2007, Fort Worth, Texas, 2007.

Wübbena, G., Schmitz, M., and Bagge, A. **Additional thoughts and findings on satellite induced GNSS phase shifts, receiver tracking and the impact on RINEX and RTCM**. White Paper, 2012.

Zeimetz, P. **Zur Entwicklung und Bewertung der absoluten GNSS-Antennenkalibrierung im HF-Labor**. PhD thesis, Rheinische Friedrich-Wilhelms-Universität Bonn, 2010.

Zhu, S. Y. and Groten, E. **Relativistic effects in GPS**. In Groten, E. and Strauß, R., editors, **Proceedings of the International GPS-Workshop**, 41–46, Darmstadt, Germany, 1988. Springer-Verlag Berlin Heidelberg New York London Paris Tokyo.

Zumberge, J. F., Heflin, M. B., Jefferson, D. C., Watkins, M. M., and Webb, F. H. **Precise point positioning for the efficient and robust analysis of GPS data from large networks**. Journal of Geophysical Research, 102(B3): 5005–5017, 1997. doi: 10.1029/96JB03860.

9 Appendix

A List of Figures

B List of Tables

C Definitions

baseline	baseline between two GNSS antennas.
chip	bit in a spreading code.
link	satellite-receiver pair.
receiver-system	"receiver system" is used for the entire system needed to receive, acquire and track the signals..
signal	signal is a composition of individual, trackable signal components, the code and carrier phases.

D Units and Constants

Constants

c	speed of light (c = 299,792,458 m/s).
GM_E	gravitational constant of the Earth ($GM_E = 398600.4415\,km^3/s^2$).
GM_S	gravitational constant of the Sun.
A	ionospheric constant ($A = 40.28\,m^3/s^2$).
π	Mathematical constant representing the ratio of a circle's circumference to its diameter.

Units

deg	degree.
mas	milliarcsecond.
km	kilometer.
m	meter.
cm	centimeter.
mm	millimeter.
h	hour.
min	minutes.
s	second.
ms	millisecond.
μs	microsecond.
ns	nanosecond.
ps	picosecond.
GHz	giga hertz.
MHz	mega hertz.
Hz	hertz.
$°C$	Celsius.
dB	dezibel.
TECU	total electron content unit ($1\,TECU = 10^{16}$ electrons/m^2).

ADC	Analog Digital Converter.
AltBOC	Alternative Binary Offset Carrier.
ANTEX	Antenna Exchange Format.
APC	Antenna Phase Centre.
ARP	Antenna Reference Point.
AS	Anti-Spoofing.
BDT	BeiDou Time.
BeiDou	BeiDou Navigation System.
BIPM	Bureau International des Poids et Mesures.
BOC	Binary Offset Carrier.
BPSK	Binary Phase Shift Keying.
C/A	Coarse/Acquisition Code.
CBOC	Composite Binary Offset Carrier.
CDMA	Code Division Multiple Access.
CGCS2000	China Geodetic Coordinate System 2000.
CMCU	Clock Monitoring and Control Unit.
CODE	Center for Orbit Determination in Europe.
COM	Centre of Mass.
CPR	Cycle-Per-Revolution.
CPU	Central Processing Unit.
CRD	Coordinates (ECEF).
CRS	Celestial Reference System.
DCB	Differential Code Bias.
DD	Double-Difference.
DFO	Dual Frequency Observations.
DLL	Delay-Lock Loop.
DoD	US Department of Defense.
DORIS	Doppler Orbitography and Radiopositioning Integrated by Satellite.
E1	Galileo E1 Frequency.
E5	Galileo E5 Frequency.
E5a	Galileo E5a Frequency.
E5b	Galileo E5b Frequency.
E6	Galileo E6 Frequency.
ECEF	Earth Centred Earth Fixed.
ECI	Earth Centred Inertial.
EGNOS	European Geostationary Navigation Overlay Service.
EM	Electromagnetic.
EOP	Earth Orientation Parameter.
ERP	Earth Rotation Parameter.
ESA	European Space Agency.
ESOC	European Space Operations Centre.
FCB	Fractional-Cycle-Bias.
FDMA	Frequency Division Multiple Access.
FGUU	Frequency Generator and Upconverter Unit.
FLL	Frequency-Lock Loop.
G1	GLONASS G1 Frequency.

G2	GLONASS G2 Frequency.
G3	GLONASS G3 Frequency.
Galileo	Galileo.
GCRS	Geocentric Celestial Reference System.
GIOVE	Galileo In-Orbit Validation Element.
GLONASS	Global Navigation Satellite System.
GLONASST	GLONASS Time.
GNSS	Global Navigation Satellite Systems.
GPS	Global Positioning System.
GPST	GPS Time.
GR	General Relativity.
GST	Galileo System Time.
GTRF	Galileo Terrestrial Reference Frame.
HEO	High Earth Orbit.
I	In-Phase (data signal).
ICD	Interface Control Document.
ICRF	International Celestial Reference Frame.
ICRS	International Celestial Reference System.
IDS	International DORIS Service.
IERS	International Earth Rotation and Reference Systems Service.
IF	Ionosphere-Free.
IGNSS	Indian Global Navigational Satellite System.
IGS	International GNSS Service.
ILRS	International Laser Ranging Service.
IONEX	Ionosphere Map Exchange.
IOV	In Orbit Validation.
IRC	Integer-Recovery-Clock.
IRNSS	Indian Regional Navigation Satellite System.
IS	Interface Specification.
ISB	Intersystem Bias.
ITRF	International Terrestrial Reference Frame.
ITRS	International Terrestrial Reference System.
L1	GPS L1 Frequency.
L2	GPS L2 Frequency.
L5	GPS L5 Frequency.
LAMBDA	Least-Squares Ambiguity Decorrelation Adjustment.
LC	Linear Combination.
LEO	Low Earth Orbit.
LLR	Lunar Laser Ranging.
LOD	Length of Day.
LOS	Line of Sight.
LSQ	Least Squares.
MBOC	Multiplexed Binary Offset Carrier.
MCAR	Multi Carrier Ambiguity Resolution.
MEO	Medium Earth Orbit.
MFO	Multi-Frequency Observations.
MGEX	IGS Multi-GNSS Experiment.
MP	Multipath.
MSAS	Multi-Functional Satellite Augmentation System.

NAPEOS	Navigation Package for Earth Observation Satellites.
NEQ	Normal Equation.
NSGU	Navigation Signal Generation Unit.
OPS-GN	Navigation Support Office.
OS	Open Service.
PCO	Phase Centre Offset.
PCV	Phase Centre Variation.
PDOP	Positional Dilution of Precision.
PHM	Passive Hydrogen Maser.
PLL	Phase-Lock Loop.
POD	Precise Orbit Determination.
PPP	Precise Point Positioning.
PRN	Pseudo Random Noise.
PSK	Phase Shift Keying.
PZ-90	Earth Parameters 1990 - Parametry Zemli 1990.
Q	Quadrature (pilot signal).
QZSS	Quasi-Zenith Satellite System.
RAFS	Rubidium Atomic Frequency Standard.
raw	Original Observations.
RCP	Right Circularly Polarised.
RF	Radio Frequency.
RHCP	Right Hand Circularly Polarised.
RINEX	Receiver Independent Exchange Format.
RNSS	Regional Navigation Satellite Systems.
SA	Selective Availability.
SBAS	Satellite Based Augmentation System.
SD	Single-Difference.
SDA	Signal Difference Analysis.
SDAO	Signal Difference Analysis Observation.
SLR	Satellite Laser Ranging.
SP3	Standard Product 3.
SR	Special Relativity.
SRP	Solar Radiation Pressure.
STEC	Slant Total Electron Content.
TAI	International Atomic Time.
TCAR	Three Carrier Ambiguity Resolution.
TEC	Total Electron Content.
TMBOC	Time-Multiplexed Binary Offset Carrier.
TRF	Terrestrial Reference Frame.
TRS	Terrestrial Reference System.
TUD	Technische Universität Darmstadt.
UCD	Uncalibrated Code Delay.
UPD	Uncalibrated Phase Delay.
USD	Uncalibrated Signal Delay.
UT	Universal Time.
UT1	Universal Time 1.
UTC	Universal Time Coordinated.

VLBI	Very Long Baseline Interferometry.
VTEC	Vertical Total Electron Content.
WAAS	Wide Area Augmentation System.
WGS84	World Geodetic System 84.
ZD	Zero-Difference.
ZPD	Zenith Path Delay.

F List of Functions

cos	cosine function.
D	discriminator function.
erfc	error function.
ln	logarithmus naturalis.
M	mapping function.
P_0	probability function.
R	autocorrelation function.
rms	root mean square.
S	power spectrum.
sin	sine function.
sinc	sinc function $sinc(x) = \frac{sin(x)}{x}$.
sign	signum function (-1 if arguments < 0, else 1).
std	standard deviation.
tan	tangens function.

Ph	carrier phase (in cycles).
L	carrier phase (in metres).
Pr	pseudo range.
L_{GF}	geometry free observation (carrier phase).
L_{IF}	ionosphere-free observation (carrier phase).
L_{MW}	Melbourne-Wübbena observation (carrier phase).
L_{WL}	widelane observation (carrier phase).
Pr_{GF}	geometry free observation (pseudo-range).
Pr_{IF}	ionosphere-free observation (pseudo-range).
N	carrier phase ambiguity.
Nf	float carrier phase ambiguity.
N_{wl}	widelane DD-ambiguity estimate in cycles.
ucd	uncalibrated code delays.
upd	uncalibrated phase delays.
pwu	phase wind-up.
λ	carriere phase wavelength.
δt	clock offset.
clk	clock errors.
orb	orbit errors.
e	epoch (RINEX).
t	reception time.
τ	time lag.
t^t	transmission time.
rel	relativistic effects.
$\vec{X}_{ecef}$	ECEF coordinates.
$\ddot{\vec{X}}_{gcrs}$	GCRS velocities.
$\vec{X}_{rec}$	receiver position (antenna reference point) (ECEF).
$\ddot{\vec{X}}^{sat}_{gcrs}$	satellite acceleration (centre of mass).
$\vec{X}^{sat}_{gcrs}$	satellite position (centre of mass) (GCRS).
$\dot{\vec{X}}^{sat}$	satellite velocity (centre of mass).
$\delta \vec{x}_{al}$	atmospheric loading.
$\delta \vec{x}_{oc}$	ocean loading.
$\delta \vec{x}_{pt}$	pole tide.
$\delta \vec{x}_{set}$	solid earth tide.
$site$	site displacements.
$\delta \vec{x}(t - t_0)$	tectonic movement.
ion	ionospheric delay.
trp	tropospheric delay.
ant	antenna dependent delays.
pco	phase centre offset.
pcv	phase centre variations.
mp	multipath.
n	refraction index.
atm	refraction of the earth's atmosphere.
pp	propagation-path.
$prop$	propagation path related effects.
f_0	nominal frequency.
f_c	spreading code frequency.
$f_{doppler}$	Doppler frequency.
f_{obs}	observed carrier frequency.
f	frequency.
f_s	square modulation frequency.

E	eccentric anomaly of the satellite orbit.
e	eccentricity of the satellite orbit.
$\vec{J}$	earth's angular momentum per unit mass.
$\vec{R}$	position of the earth with respect to the sun.
$\vec{a}$	total perturbing acceleration.
$\dot{\vec{R}}$	velocity of the earth with respect to the sun.
A	coefficient matrix.
Q	normal equation.
m	number of observations.
n	number of unknown parameter.
b	observations.
υ	observation corrections (residuals).
res	residuals.
w	observed - computed.
x	unknown parameter.
p	weigth.
P	weighting matrix.
$\vec{H}$	magnetic field.
$\vec{E}$	electric field.
g	spreading symbol.
$nInt$	nearest integer.
f	function.
isb	inter-system bias.
n_e	electron density.
ϵ	measurement error.
ψ	phase angle.
q	dynamical parameters.
R	geocentric distance.
rec	receiver.
sat	satellite.
sig	signal.
σ	sigma.
T_c	chip period.
T	temperature.
$track$	tracking mode.
$\rho(t)_{rec}^{sat}$	true geometric range.
T_s	half-period of a square wave ($T_s = 1/(2f_s)$).
v_{LOS}	relative velocity in the line of sight.
z	zenith angle.

H Additional Tables: uncalibrated signal delay analyses

Receiver	Mean	Std
A001	ref.	0.02
A002	-0.38	0.04
B003	-0.07	0.01
B004	0.28	0.02

Table 9.6: Mean and standard deviation of Δ DCBs (SC4) [m].

Receiver	Mean	Std
A001	ref.	0.03
A002	-2.72	0.05
B003	-2.12	0.07
B004	0.25	0.03

Table 9.7: Mean and standard deviation of Δ DCBs (SC5) [m].

Receiver	Mean	Std
A001	ref.	0.00
A002	-0.43	0.01
B003	-0.00	0.01
B004	0.26	0.01

Table 9.8: Mean and standard deviation of Δ DCBs (SC6) [m].

Receiver	Mean	Std
A001	ref.	0.00
A002	1.69	0.02
B003	2.10	0.00
B004	0.60	0.02

Table 9.9: Mean and standard deviation of Δ DCBs (SC7) [m].

Receiver	Mean	Std
A001	ref.	0.04
A002	1.51	0.03
B003	1.91	0.05
B004	0.56	0.05

Table 9.10: Mean and standard deviation of Δ DCBs (SC8) [m].

PRN	FREE_I	FREE_R	FREI_R
G01	47	42	43
G02	65	66	62
G03	38	40	37
G04	42	39	39
G05	43	48	42
G06	43	41	37
G07	56	53	55
G08	47	40	41
G09	51	40	41
G10	48	41	42
G11	46	43	41
G12	51	48	43
G13	43	45	45
G14	45	46	43
G15	48	42	43
G16	38	39	36
G17	59	57	66
G18	49	51	52
G19	103	84	81
G20	43	41	39
G21	69	79	71
G22	63	48	48
G23	45	48	50
G24	66	66	86
G25	48	70	48
G26	47	48	48
G28	36	32	33
G29	86	93	94
G31	46	47	44
G32	39	39	38
Total	52	50	50

Table 9.11: Mean 1D orbit rms versus IGS final orbits [mm] (MGEX network).

PRN	FREE_I	FREE_R	FREI_R
G01	21	25	22
G02	33	36	36
G03	24	22	22
G04	37	41	42
G05	27	28	28
G06	26	26	26
G07	37	39	38
G08	22	25	24
G09	22	22	22
G10	30	32	31
G11	27	25	26
G12	26	26	24
G13	31	31	31
G14	32	30	30
G15	32	28	28
G16	28	30	30
G17	55	57	59
G18	36	40	39
G19	67	73	73
G20	34	32	32
G21	42	44	44
G22	38	37	36
G23	38	38	37
G24	33	25	26
G25	27	26	24
G26	26	35	33
G28	22	22	21
G29	54	52	51
G31	37	42	41
G32	35	34	33
Total	33	34	34

Table 9.12: Mean 1D orbit rms versus IGS final orbits [mm] (IGSL network).

PRN	FREE_I	FREE_R	FREI_R
G01	41	26	34
G02	34	27	27
G03	28	22	20
G04	34	26	27
G05	29	25	25
G06	35	27	27
G07	35	27	27
G08	32	29	29
G09	29	24	25
G10	34	24	23
G11	26	27	26
G12	32	30	26
G13	35	33	33
G14	30	24	25
G15	29	21	24
G16	26	21	20
G17	31	25	28
G18	23	20	20
G19	37	27	25
G20	28	22	21
G21	32	28	31
G22	33	23	21
G23	38	34	34
G24	54	54	51
G25	33	40	29
G26	48	36	40
G28	29	19	21
G29	39	38	37
G31	28	30	25
G32	34	30	31
Total	33	28	28
E11	49	44	57
E12	51	38	57
E19	42	38	41
E10	46	45	47
Total	47	41	51

Table 9.13: Mean 1D rms of two-day orbit overlaps [mm] (MGEX network).

PRN	FREE_I	FREE_R	FREI_R
G01	15	18	17
G02	17	17	16
G03	17	16	16
G04	23	22	23
G05	13	14	13
G06	19	19	18
G07	20	18	17
G08	15	15	16
G09	14	13	13
G10	14	12	12
G11	18	20	20
G12	23	20	19
G13	17	18	18
G14	16	18	17
G15	15	15	15
G16	20	19	19
G17	21	20	20
G18	17	16	17
G19	23	24	24
G20	14	14	14
G21	21	17	18
G22	20	18	18
G23	16	16	16
G24	15	13	12
G25	26	26	24
G26	19	18	17
G28	15	14	15
G29	20	18	17
G31	19	23	23
G32	25	23	23
Total	18	18	18

Table 9.14: Mean 1D rms of two-day orbit overlaps [mm] (IGSL network).

Station	FREI_R Mean	FREI_R Std	FREI_R Mean	FREI_R Std	FREC_R Mean	FREC_R Std
ABMF	-2.45	0.83	-4.56	0.82	0.01	0.83
AJAC	-0.54	0.39	-3.63	0.39	-0.10	0.39
BRUX	-4.20	0.27	-0.82	0.27	0.09	0.27
CEBR	-4.33	0.41	-2.01	0.41	0.01	0.41
CUT0	-1.03	0.41	1.29	0.42	0.30	0.42
DLF1	-0.51	0.26	-0.48	0.26	0.35	0.26
FAA1	-5.13	0.99	-3.62	0.99	-0.11	0.99
FTNA	-1.53	1.06	-2.75	1.06	0.21	1.06
GANP	-1.07	0.28	-1.03	0.28	0.25	0.28
GMSD	-2.22	1.06	-3.96	1.06	0.17	1.06
GOP6	0.43	0.27	-2.88	0.27	0.19	0.27
HARB	0.12	0.39	1.10	0.40	0.43	0.39
HOFN	-1.63	0.33	-1.57	0.33	0.24	0.33
JFNG	-1.87	1.39	-4.36	1.39	0.19	1.39
KIR8	-0.23	0.41	0.37	0.41	0.42	0.41
KIRU	-3.23	0.40	0.09	0.40	0.10	0.40
KOUG	-2.77	1.11	-6.50	1.11	-0.28	1.11
KOUR	-5.71	1.10	-4.58	1.10	-0.19	1.10
KRGG	2.27	0.66	0.23	0.67	0.14	0.66
LMMF	-3.37	0.86	-4.78	0.86	0.03	0.86
LPGS	1.36	0.47	1.38	0.48	0.29	0.47
MAC1	1.81	0.66	1.93	0.65	0.39	0.65
MAR7	-0.64	0.36	-0.11	0.36	0.34	0.36
MARS	-0.05	0.36	-3.35	0.36	-0.07	0.36
MAS1	-5.77	0.97	-3.90	0.97	-0.14	0.98
METG	-0.16	0.34	-0.17	0.34	0.39	0.34
MGUE	1.36	0.65	1.24	0.65	0.26	0.65
MYVA	1.88	0.34	-1.66	0.33	0.20	0.34
NKLG	-2.32	1.20	-4.27	1.20	0.41	1.20
NRMG	-1.41	0.95	0.04	0.95	0.36	0.94
NURK	-4.37	1.12	-4.28	1.14	-0.09	1.14
NYA2	0.43	0.44	0.49	0.44	0.21	0.44
OBE4	-1.32	0.29	-1.32	0.29	0.09	0.29
ONS1	-0.23	0.29	-0.24	0.29	0.32	0.29
OUS2	1.77	0.37	1.90	0.36	0.30	0.37
POTS	-0.87	0.25	-0.90	0.25	0.12	0.25
REUN	-0.79	0.73	1.05	0.74	0.37	0.73
REYK	-1.64	0.33	-1.59	0.33	0.24	0.34
RIO2	2.20	0.38	2.29	0.38	0.33	0.38
TASH	-2.71	0.54	-2.48	0.55	-0.00	0.54
THTG	-1.77	1.00	-5.41	1.01	-0.17	1.00
TLSE	-1.12	0.35	-1.48	0.34	0.27	0.35
ULAB	-1.30	0.39	-1.16	0.39	0.14	0.39
UNB3	-1.05	0.28	-0.08	0.29	0.38	0.28
USN4	-3.09	0.33	-1.08	0.33	0.16	0.32
VILL	-4.47	0.40	-2.04	0.40	0.01	0.41
WIND	0.45	0.53	0.55	0.52	0.22	0.52
WUH2	-5.17	1.23	-5.07	1.26	-0.07	1.24
ZIMJ	-1.41	0.30	-1.43	0.30	0.08	0.30

Table 9.15: Difference of estimated STEC versus IONEX [m on L1].

Curriculum Vitae

Name	Erik Schönemann
Date of birth	3rd February 1978
Place of birth	Darmstadt, Germany
Nationality	German

Education

Aug. 1984 – Jul. 1988   **Grundschule**
Erich-Kästner-Schule, Pfungstadt, Germany

Sep. 1988 – Jul. 1994   **Gesamtschule**
Friedrich-Ebert-Schule, Pfungstadt, Germany

Aug. 1994 – Jul. 1997   **Oberstufe**
Schuldorf Bergstraße, Seeheim-Jugenheim, Germany
Graduated with Abitur

Apprenticeship

Aug. 1997 – Jan. 2000   **Ausbildung zum Vermessungstechniker (surveyor)**
Katasteramt Darmstadt-Dieburg, Dieburg, Germany
Graduated as surveyor

Military Service

Jan. 2000 – Oct. 2000   **Grundwehrdienst (basic military service)**
Germersheim / Mainz, Germany

Studies

Oct. 2000 – May 2005   **Studium des Vermessungswesens**
Technische Universität Darmstadt, Darmstadt, Germany
Graduated with a Dipl.-Ing. degree (M.Sc.)

Oct. 2004 – Mar. 2005   **Diplomarbeit** "Benefit of area correction parameters and similar network-based concepts for RTK-GPS"
The University of New South Wales, Sydney, Australia

Professional Positions

Since May 2005   **Wissenschaftlicher Mitarbeiter (research fellow)**
Institut für Geodäsie, Technische Universität Darmstadt, Darmstadt, Germany

Since Jan. 2007   **Contractor to Navigation Support Office, ESA/ESOC**

Since Jan. 2014   **Staff at Navigation Support Office, ESA/ESOC**